



Mohammad Ali Golkani, MSc

Higher-Order Sliding Mode Control Approaches for Systems with Saturating Actuators

Doctoral Thesis

to achieve the university degree of
Doktor der technischen Wissenschaften

submitted to

Graz University of Technology

Supervisor

Univ.-Prof. Dipl.-Ing. Dr.techn. Martin Horn

Co-Supervisor

Assoc.Prof. Dipl.-Ing. Dr.techn. Markus Reichhartinger

Institute of Automation and Control

Faculty of Electrical and Information Engineering

Graz, March 2020

This document is set in Palatino, compiled with pdfL^AT_EX2e and Biber.

The L^AT_EX template from Karl Voit is based on KOMA script and can be found online: <https://github.com/novoid/LaTeX-KOMA-template>

Affidavit

I declare that I have authored this thesis independently, that I have not used other than the declared sources/resources, and that I have explicitly indicated all material which has been quoted either literally or by content from the sources used. The text document uploaded to TUGRAZonline is identical to the present doctoral thesis.

Date

Signature

Abstract

The super-twisting and continuous twisting algorithms are well-known higher-order sliding mode methods that bring many benefits in the case they are applied respectively to perturbed first and second-order systems. However, for systems with saturating actuators, the windup effect may be produced and therefore, the closed-loop performance may degenerate. This thesis deals with the development of comprehensive higher-order sliding mode control approaches, in which anti-windup schemes are adopted. In order to lift additional constraints placed on the bound and class of addressed disturbances and uncertainties, the properties of the standard higher-order sliding mode algorithms are maintained. The performances of the standard ones are, however, significantly improved in the case that the initial conditions of the systems are far away from the origin. For the closed loops of the proposed techniques, global stability properties are investigated. This gives parameter settings for the controllers. Having employed numerical simulations, feasibility and effectiveness of the introduced strategies are indicated. Furthermore, exemplarily in a real-world application, it is illustrated how the windup effect is counteracted by applying the saturated feedback controls.

Kurzfassung

Die Super-Twisting und Continuous Twisting Algorithmen sind bekannte Gleitzustand Verfahren höherer Ordnung, die viele Vorteile bringen, falls sie auf gestörte Systeme erster und zweiter Ordnung angewendet werden. Bei Systemen mit sättigenden Stellgliedern kann jedoch der "Aufwickeleffekt" erzeugt werden, und daher kann die Leistung im geschlossenen Regelkreis degenerieren. Diese Dissertation befasst sich mit der Entwicklung umfassender Gleitzustand Regelungsansätze höherer Ordnung, bei denen Wicklungsschutz angewendet werden. Um zusätzliche Einschränkungen für die Grenze und Klasse der adressierten Störungen und Unsicherheiten aufzuheben, werden die Eigenschaften der Standard Gleitzustand Algorithmen höherer Ordnung beibehalten. Die Leistungen der Standardsysteme werden jedoch erheblich verbessert, wenn die Anfangsbedingungen der Systeme weit vom Ursprung entfernt sind. Für die Regelkreise der vorgeschlagenen Techniken werden globale Stabilitätseigenschaften untersucht. Dies gibt Parametereinstellungen für die Steuerungen. Durch numerische Simulationen werden Machbarkeit und Wirksamkeit der vorgestellten Strategien aufgezeigt. Weiterhin wird exemplarisch in einer realen Anwendung gezeigt, wie der Aufwicklungseffekt durch Anwenden der gesättigten Rückkopplungsregler entgegengewirkt wird.

Acknowledgements

This thesis was made during the time I was working as a project assistant at the Institute of Automation and Control within Graz University of Technology. Encouragement and inspiration of a number of individuals contributed to that.

I would like to express my gratitude to my supervisor, Prof. Martin Horn, whose encouragement, helpful advice, and support throughout my doctoral studies enabled me to work on this topic.

I would also like to appreciate my co-supervisor, Assoc. Prof. Markus Reichhartinger, for his patience answering my questions and his invaluable suggestions, which contributed significantly to the work documented here.

I take this opportunity to thank Prof. Johann Reger for reviewing my work and participating in the thesis committee.

Inspiration provided by Prof. Leonid Fridman, with whom I was in fruitful collaboration, is gratefully acknowledged.

Sincere thanks go to the colleagues at the Institute of Automation and Control, especially Drs. Stefan Koch and Richard Seeber for constructive discussions.

I dedicate my thesis to my family and my wife, who supported me unconditionally and sacrificed so much to make studying possible for me.

Mohammad Ali Golkani
March 2020, Graz

Nomenclature

Mathematical Symbols

\forall for all

\mathbb{R} the set of Real numbers

sup the supermum

Notations

$$\text{sgn}(\chi) = \begin{cases} 1 & \text{if } \chi > 0 \\ -1 & \text{if } \chi < 0 \end{cases}$$

$$\text{sgn}(0) \in [-1, 1]$$

$$[\chi]^\gamma = |\chi|^\gamma \text{sgn}(\chi)$$

$$[\chi]^0 = \text{sgn}(\chi)$$

$$\text{sat}_\eta(\chi) = \begin{cases} \chi & \text{for } |\chi| \leq \eta \\ \eta [\chi]^0 & \text{for } |\chi| > \eta \end{cases}$$

Abbreviations

CTA continuous twisting algorithm

RED robust exact differentiator

STA super-twisting algorithm

TA twisting algorithm

Contents

Abstract	v
List of Figures	xv
1. Introduction	1
1.1. State of the Art	1
1.2. Problem with Conventional Controllers	3
1.2.1. First-Order System	3
1.2.2. Second-Order System	6
1.3. Study Objective and Contribution	6
1.4. Thesis Structure	8
I. First-Order System	11
2. Saturated Super-Twisting Algorithm	13
2.1. Problem Statement	13
2.2. Saturated Super-Twisting Control	14
2.3. Stability Analysis	16
2.3.1. Nominal Case	16
2.3.2. Perturbed Case	18
2.4. Simulation Examples	23
2.4.1. Nominal Case	23
2.4.2. Perturbed Case	24
3. An Anti-Windup Strategy for the Super-Twisting Algorithm	27
3.1. Problem Statement	27
3.2. Proposed Scheme	28
3.3. Stability Analysis	29
3.4. Simulation Examples	33
3.4.1. First Case	33
3.4.2. Second Case	34
3.4.3. Third Case	35

II. Second-Order System	39
4. Saturated Continuous Twisting Algorithm	41
4.1. Problem Statement	41
4.2. Saturated Continuous Twisting Control	42
4.3. Stability Analysis	44
4.3.1. Full State Information	45
4.3.2. Output Feedback Control	52
4.4. Simulation Examples	53
4.5. Experimental Implementation	55
4.5.1. System Model	56
4.5.2. Control Design	57
5. Saturated Feedback Control Using the Twisting Algorithm	61
5.1. Problem Statement	61
5.1.1. Problem with Super-Twisting Controller	63
5.2. Saturated Output Feedback Control	65
5.3. Stability Analysis	66
5.4. Simulation Examples	68
5.4.1. Perturbed Double Integrator System	68
5.4.2. System with Uncertainties and Disturbances	69
6. Lyapunov-based Saturated Continuous Twisting Algorithm	73
6.1. Proposed Schemes	73
6.1.1. First Approach	73
6.1.2. Second Approach	74
6.2. Stability Analysis	75
6.3. Simulation Examples	81
6.3.1. First Case	82
6.3.2. Second Case	84
6.4. Experimental Implementation	86
7. Conclusion and Outlook	89
Appendices	91
A. Quadrant Analysis for the Saturated Super-Twisting Algorithm	93
B. Quadrant Analysis for the Saturated Continuous Twisting Algorithm	95
C. Quadrant Analysis for the Lyapunov-based Saturated Continuous Twisting Algorithm	99
Bibliography	103

List of Figures

1.1. Problem with the conventional super-twisting controller	5
1.2. Problem with the original super-twisting controller	5
1.3. Problem with the standard continuous twisting controller	7
2.1. The representation of the saturation function	14
2.2. Block diagrams of the conventional and saturated super-twisting algorithms	15
2.3. Saturated super-twisting control for unperturbed system (simulation results)	24
2.4. System trajectory of applying the saturated super-twisting algorithm	25
2.5. Saturated super-twisting control for perturbed system (simulation results)	26
3.1. Block diagram of the anti-windup strategy for the super-twisting algorithm	30
3.2. Anti-windup scheme for the super-twisting algorithm (first simulation case)	36
3.3. Anti-windup scheme for the super-twisting algorithm (second simulation case)	37
3.4. Anti-windup scheme for the super-twisting algorithm (third simulation case)	38
4.1. Block diagrams of the conventional and saturated continuous twisting algorithms	44
4.2. A majorant trajectory for the saturated continuous twisting algorithm	50
4.3. Saturated continuous twisting algorithm (simulation results)	54
4.4. First-order robust exact differentiator for the continuous twisting algorithm (simulation results)	55
4.5. A layout of the differential hydraulic cylinder	57
4.6. Saturated continuous twisting algorithm (experimental results)	58
5.1. Block diagram of the output feedback control using the twisting algorithm	66
5.2. Saturated feedback control using the twisting algorithm (simulation case of perturbed double integrator system)	70
5.3. Second-order robust exact differentiator for the twisting algorithm-based control (simulation results)	71

List of Figures

5.4.	A parameter plan for saturated feedback control using the twisting algorithm	71
5.5.	Saturated feedback control using the twisting algorithm (simulation case of system with uncertainties and disturbances)	72
6.1.	Block diagram of the Lyapunov-based saturated continuous twisting algorithm	76
6.2.	Lyapunov-based saturated continuous twisting algorithm (first simulation case)	83
6.3.	Difference between new versions of the saturated continuous twisting algorithm (in simulation)	85
6.4.	First-order robust exact differentiator for the twisting algorithm-based control (simulation results)	85
6.5.	Lyapunov-based saturated continuous twisting algorithm (second simulation case)	86
6.6.	Lyapunov-based saturated continuous twisting algorithm (experimental results)	87

1. Introduction

1.1. State of the Art

Sliding mode control approaches have been successfully applied to systems, which are subject to particular classes of plant uncertainties and external disturbances, see e.g. [RGH15; Li+17]. The closed-loops satisfactory robust performances have been demonstrated therein. Traditional sliding mode control, i.e. first-order sliding mode approach, can be just employed in the case that the relative degree of the system with respect to a defined sliding variable is one. It guarantees a saturated and discontinuous control input. A second-order sliding mode technique such as the twisting as well as super-twisting algorithm provides a continuous control signal in such a first-order system. These high-order sliding mode algorithms improve the sliding accuracy of the first-order sliding mode control under discrete-time measurements in the case that the sampling interval is small enough [Lev93; Sht+14]. They are able to counteract perturbations, which are Lipschitz continuous with respect to time, and recorded in the literature as the chattering reduction strategies if the actuator dynamics are fast enough [PF19]. It is noted that by using the super-twisting algorithm, unlike the other algorithms such as the twisting algorithm, the time derivative of the sliding variable is not incorporated into the control law design.

For a perturbed double integrator system, the twisting algorithm contributes to a finite-time convergence of the state variables to the origin. There is no need to design a sliding function. A saturated and discontinuous control signal is ensured [Lev93; PP09]. The continuous twisting controller introduced in [Tor+17] provides a continuous actuating signal for the aforementioned system. It also enjoys the advantage that both of the states converge to zero in a finite time. As a result of adopting this algorithm, perturbations, which are Lipschitz continuous with respect to time, can be theoretically exactly compensated. For systems with fast actuator dynamics, the chattering effect can be reduced. Furthermore, under discrete-time measurements with the small sampling interval, higher precision is achieved comparing to the standard twisting controller.

Due to the fact that unlimited control energy is unavailable, actuator saturation is a nonlinearity experienced frequently in industrial applications. Large tracking errors lead to large compensatory signals, which cannot be introduced to the system due to physical restrictions (e.g. a fully open or closed valve) or safety requirements.

As a result, the settling time is increased since the signal driving the system is smaller than the signal generated by the controller. Input saturation can also cause large overshoots or undershoots or both if the controller contains integral action. This undesired effect, which is produced through an overreaction of the integrator during that the controller works in an open loop situation, is called “integral windup” or “controller windup” in the literature [Hip06]. In this thesis, it is simply called “windup”. In order to prevent this effect, some methods such as the *observer technique* and the *conditioning technique* have been developed for classical linear controllers, see e.g. [Hip06; HKH87].

In the case that the control input is transferred to the system through a saturating actuator, applying the conventional super-twisting and continuous twisting controllers also poses a challenge. The control signals provided by them may exceed the given saturation bounds. The continuous element of the super-twisting algorithm (the square root of the sliding variable absolute value) as well as the continuous elements of the continuous twisting algorithm (the cube and square roots of the states absolute values) will not be within the bounds for every initial condition. As a result, the discontinuous integral actions of these controllers can give rise to the windup effect. In [BCB18], a domain of attraction for such a system under the conventional super-twisting control is computed and the finite-time stability within this domain is guaranteed. It is shown that in the case the initial condition of the closed-loop system belongs to this domain, the control signal remains within the bounds and windup does not occur. The satisfactory closed-loop performance, however, may be degenerated when the initial values are outside this domain.

A continuous non-singular terminal sliding mode control with an anti-windup scheme is applied to a practical application in [Wan+14]. The time derivative of a saturation function is included in the sliding surface therein, which is not working in a general case from the mathematical point of view. In order to attenuate the windup effect, a second-order sliding mode control scheme is introduced in [Lev93], which contributes to a continuous and bounded input. A sub-optimal second-order sliding mode controller is modified in [FR09] to ensure that the sliding variable converges to the origin in a finite time despite the fact that the actuator is saturated. In both of the control laws presented in [Lev93] and [FR09], switching between two control strategies based on the saturation bounds is included. This may result in high frequency switching on the bounds. Owing to the limitation on the switching frequency (e.g. by the discrete-time realization of the control law), some undesirable oscillations in the control signals as well as zigzag motions in the system trajectories appear.

A saturated super-twisting algorithm removing the aforementioned problem of high frequency switching is proposed in [Cas+16b; Cas+16a]. At most, one switch between two different sliding mode algorithms based on a predefined neighborhood of the origin exists therein. In [Cas+16b], the global finite-time stability of the closed-loop system

origin is ensured by means of a Lyapunov-based proof. It is given in [SH19b] how to choose an optimal Lyapunov function such that the magnitude of the discontinuity is minimized and the permissible bound of disturbances is maximized. However, in principle, the convergence for perturbations with the bound more than half of the saturation limit cannot be guaranteed based on this proof. Moreover, a continuous control signal is only produced if there is no disturbance. In order to deal with perturbations, whose bound is close to the saturation limit, a disturbance estimator is employed in [Cas+16a]. The convergence is speeded up removing the transient process of the super-twisting algorithm therein. However, this makes the sliding mode control law redundant since both the estimator and controller reconstruct disturbances. In [SH19a], by simplifying the control law designed in [Cas+16b] and imposing new conditions on the control parameters, a continuous control signal is introduced to the system and perturbations with any bound that is less than the saturation limit can be handled. It is noted that the aforementioned concept needs to be modified to be applicable to a system of order more than one.

1.2. Problem with Conventional Controllers

In the following, problem with conventional high-order sliding mode control methods in the case that the actuator is saturated is illustrated in simulation.

1.2.1. First-Order System

Consider a system described by

$$\frac{dz}{dt} = \text{sat}_\rho(u) + a(t), \quad (1.1)$$

where the output of the system is denoted by $z \in \mathbb{R}$. u is the scalar control input and the actuator is saturated if $|u| > \rho$, where ρ is a known constant. This saturation is realized from the definition

$$\text{sat}_\eta(\chi) = \begin{cases} \chi & \text{for } |\chi| \leq \eta, \\ \eta [\chi]^0 & \text{for } |\chi| > \eta, \end{cases} \quad (1.2)$$

where the notation

$$[\chi]^0 = \text{sgn}(\chi) \quad \text{as a particular case of} \quad [\chi]^\gamma = |\chi|^\gamma \text{sgn}(\chi)$$

1. Introduction

is used. The effect of perturbations is represented by the function a . The conventional super-twisting controller for the aforementioned system of relative degree one is designed as

$$u = -k_1 [z]^{\frac{1}{2}} + \nu, \quad (1.3a)$$

$$\frac{d\nu}{dt} = -k_2 [z]^0, \quad (1.3b)$$

where k_1 and k_2 are the positive constants to be tuned. Let's assume the system is subject to perturbations

$$a(t) = 2 + 0.6 \sin(t) + 0.4 \sin(5t). \quad (1.4)$$

It is noted that the absolute value of the time derivative of a is upper bounded by the constant $L_a = 2.6$. Therefore, the control constants $k_1 = 2.4$ and $k_2 = 2.7$ are selected such that the sufficient conditions set in [SH17] as $k_1 > \sqrt{k_2 + L_a}$ and $k_2 > L_a$ are satisfied. The numerical simulation is carried out through MATLAB/Simulink using the forward Euler method with the sampling step size of 1 ms and the initial values $z(t = 0) = z_0 = 20$ and $\nu(t = 0) = \nu_0 = 0$. The response curves of the system in the case that there is no saturating actuator ($\rho = \infty$) are compared in Figure 1.1 with the results obtained through that the actuator is saturated ($\rho = 5$). It is noted that the control signals introduced to the system through the actuator are depicted therein. In the case of the system with saturating actuator, this signal is different from that one generated by the controller. Since the initial condition is far away from the origin, the generated signal exceeds the saturation limits and therefore, the windup effect is produced.

The original super-twisting algorithm proposed in [Lev93] to retain the control input within a bound reads as

$$\begin{aligned} u &= \nu + \tilde{u}, \\ \frac{d\nu}{dt} &= \begin{cases} -u & \text{if } |u| > \rho \\ -k_2 [z]^0 & \text{if } |u| \leq \rho, \end{cases} \\ \tilde{u} &= \begin{cases} -k_1 c^{\frac{1}{2}} [z]^0 & \text{if } |z| > c \\ -k_1 [z]^{\frac{1}{2}} & \text{if } |z| \leq c, \end{cases} \end{aligned} \quad (1.5)$$

where the positive constant values k_1 , k_2 , and c are selected appropriately. For the nominal case of system (1.1), i.e. $a = 0$, $\forall t \geq 0$, with $\rho = 3$ and $z_0 = 20$, this control law with $k_1 = 1$, $k_2 = 0.5$, $c = 5$, and $\nu_0 = 0$ is implemented in simulation with the sampling time of 50 ms. As depicted in Figure 1.2, zigzag motions in the system trajectory, which is due to high frequency switching on the bound, can be seen. By increasing discretization step size, the amplitude of this oscillation increases.

1.2. Problem with Conventional Controllers

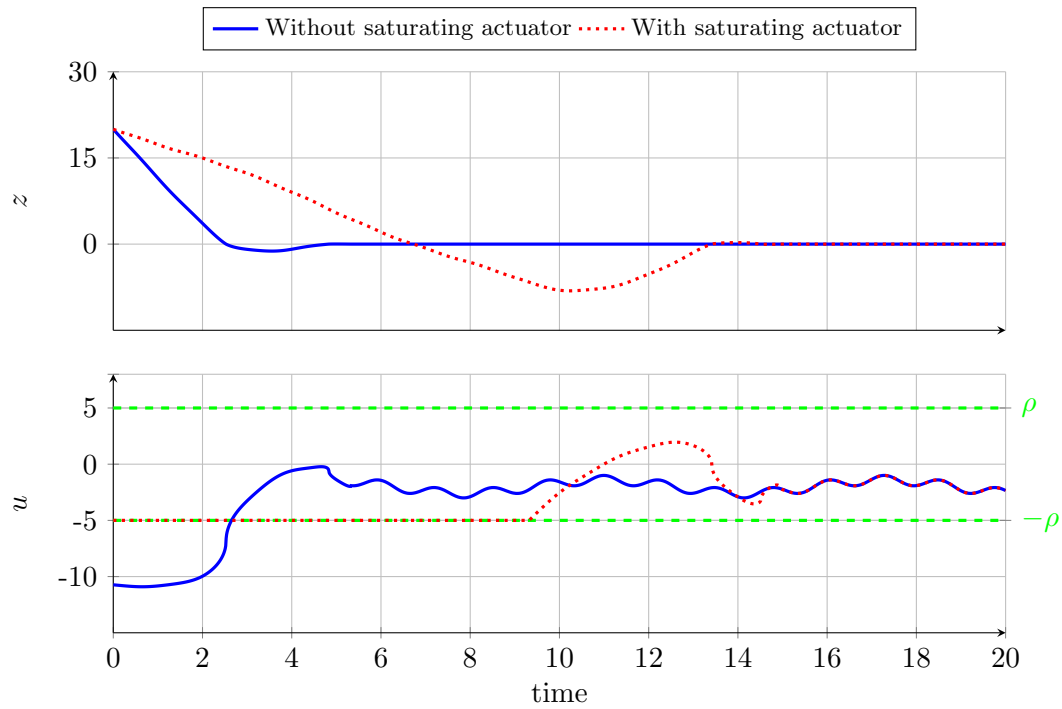


Figure 1.1.: The system output z and control input u simulated for the first-order system under the conventional super-twisting control without and with saturating actuator.

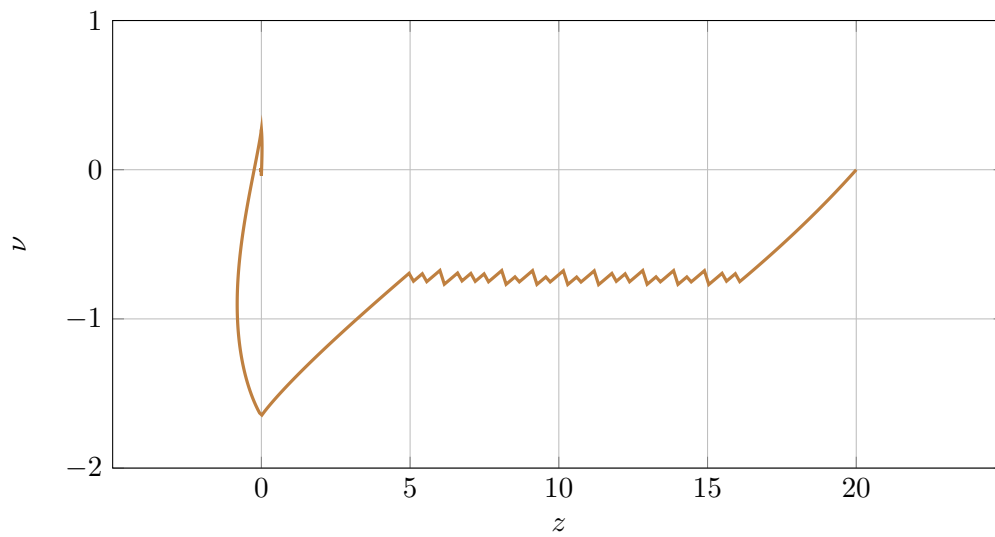


Figure 1.2.: The system trajectory of applying the original super-twisting approach given in (1.5) to the unperturbed case with saturating actuator.

1.2.2. Second-Order System

Take into consideration a system represented by

$$\frac{dz_1}{dt} = z_2, \quad (1.6a)$$

$$\frac{dz_2}{dt} = \text{sat}_\rho(u) + \bar{a}(t), \quad (1.6b)$$

$$y = z_1, \quad (1.6c)$$

where $z_1, z_2 \in \mathbb{R}$ are the state variables and y is the output of the system. Similar to that mentioned for the first-order system, the scalar control input u is restricted. The function \bar{a} denotes disturbances. The standard continuous twisting controller for this system is implemented as

$$u = -l_1 [z_1]^{\frac{1}{3}} - l_2 [z_2]^{\frac{1}{2}} + \nu, \quad (1.7a)$$

$$\frac{d\nu}{dt} = -l_3 [z_1]^0 - l_4 [z_2]^0, \quad (1.7b)$$

where the non-negative control parameters l_1, l_2, l_3 , and l_4 need to be chosen appropriately [Tor+17]. It is assumed that the system is affected by

$$\bar{a}(t) = 0.6 + 0.5 \sin(t) + 0.4 \sin(5t). \quad (1.8)$$

Since the Lipschitz constant of \bar{a} is $L_{\bar{a}} = 2.5$, the scaled gains $l_1 = 23.95$, $l_2 = 11.86$, $l_3 = 5.75$, and $l_4 = 2.75$ are selected as assigned in [Tor+17]. Considering the initial values $z_1(t = 0) = z_{1,0} = 80$, $z_2(t = 0) = z_{2,0} = -20$, and $\nu_0 = 0$, the numerical simulation is carried out using the same solver and sampling step size as employed for the conventional super-twisting control. The system performance without and with saturating actuator is shown in Figure 1.3. Similar to the first simulation example, in the case that the generated control signal is going beyond the actuator limits ($\rho = 10$), large overshoots and undershoots and a long settling time can be seen.

1.3. Study Objective and Contribution

First and second-order systems are considered in Part I and II of this thesis respectively. Detailed problem statements are given in the corresponding chapters. The objective is to design feedback control laws for different cases and scenarios of the systems such that

- the states of the systems tend to the origin despite the presence of disturbances and uncertainties;

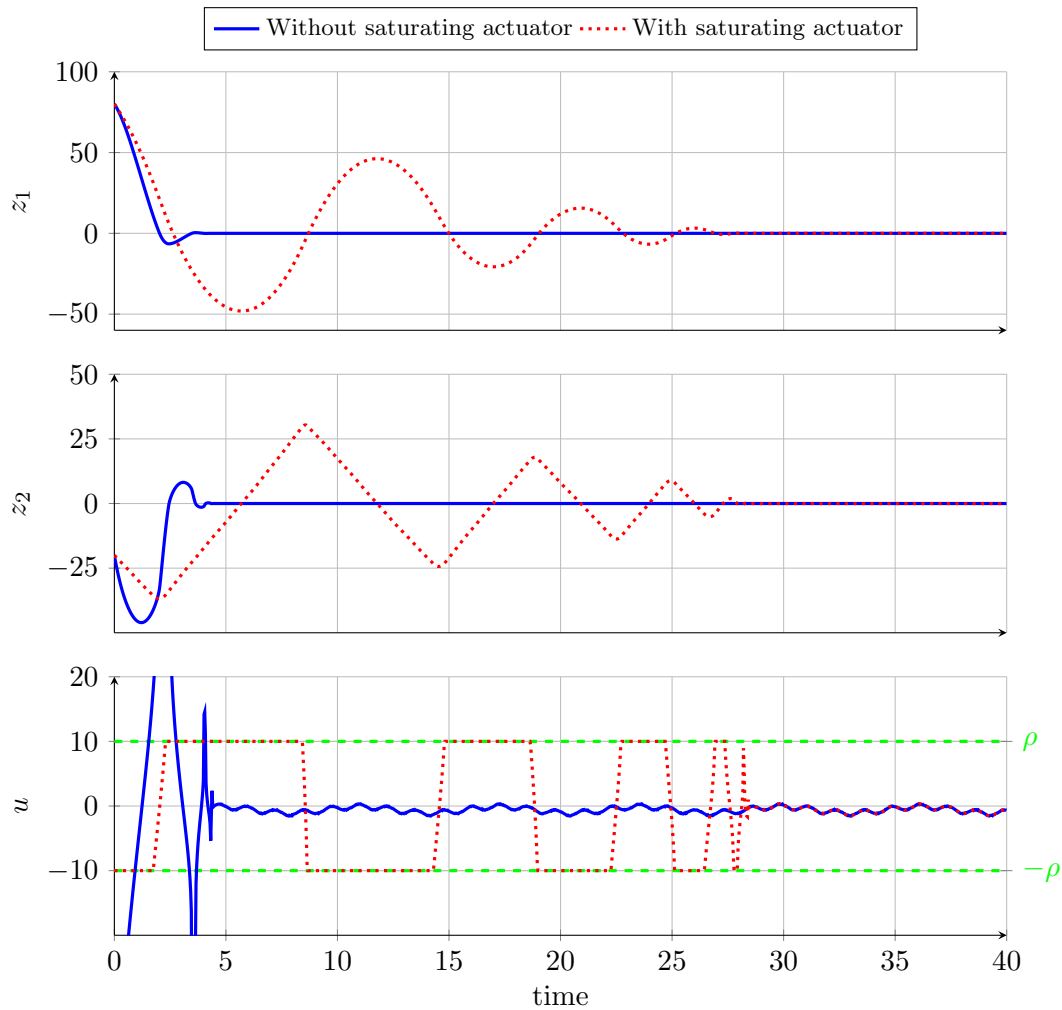


Figure 1.3.: Simulation response curves for applying the standard continuous twisting control to the second-order system without and with saturating actuator.

- either the control signal is continuous everywhere or it has a finite number of discontinuities;
- the windup effect is mitigated in the case that the absolute value of u is not confined to the saturation limit ρ .

The major contribution of this study is to introduce comprehensive higher-order sliding mode control strategies adopting anti-windup schemes. Non-redundant sliding mode control laws are presented in the sense that no disturbance estimator is employed. They are developed retaining the properties of the standard higher-order sliding mode algorithms and removing additional constraints imposed on the bound and class of perturbations and uncertainties. In the case that a state variable is not measurable, a sliding mode observer estimating the state is brought into play. The

research aims to introduce a control concept that can be extended for higher-order systems.

A portion of the material of this thesis has been presented within the publications:

M. A. Golkani et al. “Observer-based saturated output feedback control using twisting algorithm.” In: *14th International Workshop on Variable Structure Systems (VSS)*. June 2016, pp. 246–250. © 2016 IEEE.

M. A. Golkani et al. “A novel saturated super-twisting algorithm.” In: *Systems & Control Letters* 119 (2018), pp. 52–56. © 2018 Elsevier B.V.

M. A. Golkani et al. “Saturated continuous twisting algorithm.” In: *15th International Workshop on Variable Structure Systems (VSS)*. July 2018, pp. 138–143. © 2018 IEEE.

M. A. Golkani et al. “An anti-windup scheme for the super-twisting algorithm.” In: *58th Conference on Decision and Control (CDC)*. Dec. 2019, pp. 6947–6952. © 2019 IEEE.

M. A. Golkani et al. “Saturated feedback control using different higher-order sliding-mode algorithms.” In: *Variable-Structure Systems and Sliding-Mode Control: From Theory to Practice*. Vol. 271. Springer, 2020, pp. 125–148. (Reprinted/adapted by permission from Springer Nature © 2020).

1.4. Thesis Structure

The new version of the saturated super-twisting algorithm presented in [Gol+18a] is applied to the first-order system in Chapter 2. It is compact in the sense that switching from one algorithm to another one and the disturbance estimator are not used. However, this modification makes a fairly restrictive assumption on the bound and class of disturbances. In this chapter, the condition of the control gains laid down in [Gol+18a] is eased through a new proof. The system output z tends to the origin in a finite time and the continuous control signal remains within the given saturation bounds.

In order to enlarge the bound and class of addressed perturbations without using the estimator, as it is recorded in [Gol+19], an anti-windup strategy is incorporated in Chapter 3 into the design of a control law that is based on the super-twisting algorithm. It is applied to a first-order system affected by uncertainties and perturbations. Although the generated control signal may exceed the saturation limits, the windup effect is counteracted. The actuating signal is continuous everywhere and the global finite-time stability of the system origin is guaranteed.

The saturated continuous twisting algorithm presented in [Gol+18b; Gol+20] can be employed for the second-order system. Saturated and continuous control inputs and finite-time convergence of the system states z_1 and z_2 are ensured. It is illustrated in Chapter 4 that no estimator is required in the case that both the states are available for measurement and the first-order robust exact differentiator only needs to be used when the output is just measurable. Due to the fact that \bar{a} is just reconstructed here through the controller, this control law becomes non-redundant. Furthermore, in this chapter, the sufficient condition for the control parameters imposed in [Gol+18b] is relaxed by introducing the geometric proof provided in [Gol+20] for this algorithm.

In Chapter 5, having adopted the twisting algorithm as presented in [Gol+16; Gol+20], a Lipschitz continuous control signal with known maximum absolute value is introduced to the system, where the relative degree of the system with respect to the sliding function is one. Therefore, the second-order system states z_1 and z_2 drive to zero asymptotically. Since the time derivative of the sliding variable is incorporated into the control law design, estimate information of the time derivative of z_2 is required. It is noted that for the system dealt with in Chapter 4, this control law is redundant since both the estimator and controller reconstruct disturbances \bar{a} . However, it is shown in this chapter that it absolutely makes sense to use this algorithm for the second-order system with a multiplicative unknown.

In Chapter 6, having introduced new versions of the saturated continuous twisting algorithm, the restriction imposed on the class of disturbances by applying the approaches proposed in Chapters 4 and 5 is eased. Their permissible bound is also increased. It is explained that these new schemes should come into play when both of the system states are available. The states z_1 and z_2 of the system under the Lyapunov-based saturated continuous twisting control converge to the origin in a finite time. It is indicated that at most one switch from a suitable relay controller to the continuous twisting controller exists in this technique. As mentioned in this chapter, this concept can be adopted to controllers for systems of order more than two.

Part I.
First-Order System

2. Saturated Super-Twisting Algorithm

In this chapter, system (1.1) is taken into consideration. A saturated control approach based on the super-twisting algorithm is introduced, whose implementation enjoys the advantage of a simple structure. As a global remedy for such a system with saturating actuator, it contributes substantially to an improvement in the standard super-twisting performance in the case that the initial value of the system state is far away from the origin.

2.1. Problem Statement

Having considered system (1.1), the following assumption is made.

Assumption 2.1. *The function a is globally bounded and Lipschitz continuous with respect to time, i.e.*

$$|a(t)| \leq a_M < \rho \quad \text{and} \quad \left| \frac{da}{dt} \right| \leq L_a, \quad \forall t \geq 0, \quad (2.1)$$

where a_M and L_a are some known constants.

Remark 2.1. The inequality $a_M < \rho$ has to be satisfied in order to be able in principle to steer the system state z to zero through the saturated control signal (otherwise, $z = 0$ cannot be an equilibrium state of system (1.1) for every admissible function a).

In this chapter, it is aimed at designing a control law for the aforementioned system such that the system state z converges to zero in a finite time and the control signal u is continuous everywhere and bounded by

$$\sup |u| \leq \rho, \quad \forall t \geq 0. \quad (2.2)$$

2.2. Saturated Super-Twisting Control

Having adopted the super-twisting algorithm, the proposed saturated and continuous actuating signal is obtained through

$$u = -k_1 \text{sat}_\epsilon \left([z]^{\frac{1}{2}} \right) + \nu, \quad (2.3a)$$

$$\frac{d\nu}{dt} = -k_2 [z]^0 - k_3 \nu, \quad |\nu_0| \leq \frac{k_2}{k_3}, \quad (2.3b)$$

where the initial value ν_0 as well as positive constants k_1 , ϵ , k_2 , and k_3 need to be selected appropriately. Sufficient conditions for choosing the control gains are given later. As it is demonstrated in Figure 2.1, it becomes evident that

$$\left| \text{sat}_\epsilon \left([z]^{\frac{1}{2}} \right) \right| \leq \epsilon, \quad \forall z. \quad (2.4)$$

Lemma 2.1. *If the initial value ν_0 is selected such that $|\nu_0| \leq \nu_M = \frac{k_2}{k_3}$ holds, then the control signal u is bounded by*

$$|u(t)| \leq k_1 \epsilon + \nu_M, \quad \forall t \geq 0. \quad (2.5)$$

Proof. (2.3b) is a linear differential equation of ν with a bounded input. It can be represented as

$$\frac{d\nu}{dt} = \bar{k} - k_3 \nu, \quad (2.6)$$

where \bar{k} is a constant real value that belongs to the set $[-k_2, k_2]$. Its solution reads as

$$\nu(t) = \frac{\bar{k}}{k_3} + \left(\nu_0 - \frac{\bar{k}}{k_3} \right) e^{-k_3 t}. \quad (2.7)$$

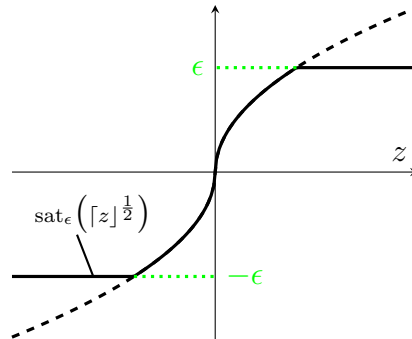


Figure 2.1.: The representation of the sat_ϵ function.

If $|\nu_0|$ is less than or equal to $\frac{k_2}{k_3}$, then $|\nu|$ is upper bounded by $\frac{k_2}{k_3}$. Therefore, the supremum of $|\nu|$ is

$$\sup |\nu| \leq \nu_M, \quad \forall t \geq 0, \quad (2.8)$$

where the condition $|\nu_0| \leq \nu_M$ is fulfilled. The upper bound of $|u|$ in (2.5) is derived easily from inequalities (2.4) and (2.8). \square

Hence, for any initial condition $z_0 \in \mathbb{R}$ and $|\nu_0| \leq \nu_M$, the continuous actuating signal remains within the given saturation bounds, i.e. $u \in [-\rho, \rho]$, if the control parameters are chosen such that

$$k_1\epsilon + \frac{k_2}{k_3} \leq \rho \quad (2.9)$$

is satisfied. Block diagrams of the conventional super-twisting control and the saturated version presented above are compared in Figure 2.2. It can be seen that in the proposed scheme, a saturation block and a feedback loop are added to the conventional algorithm in order to retain the control signal within the saturation bounds. It is noted that neither switching between two control strategies based on the saturation bound ρ (as introduced in [Lev93] and [FR09]) nor switching from one sliding mode algorithm to another one based on a predefined neighborhood of the origin (as proposed in [Cas+16b; Cas+16a]) is incorporated into the design.

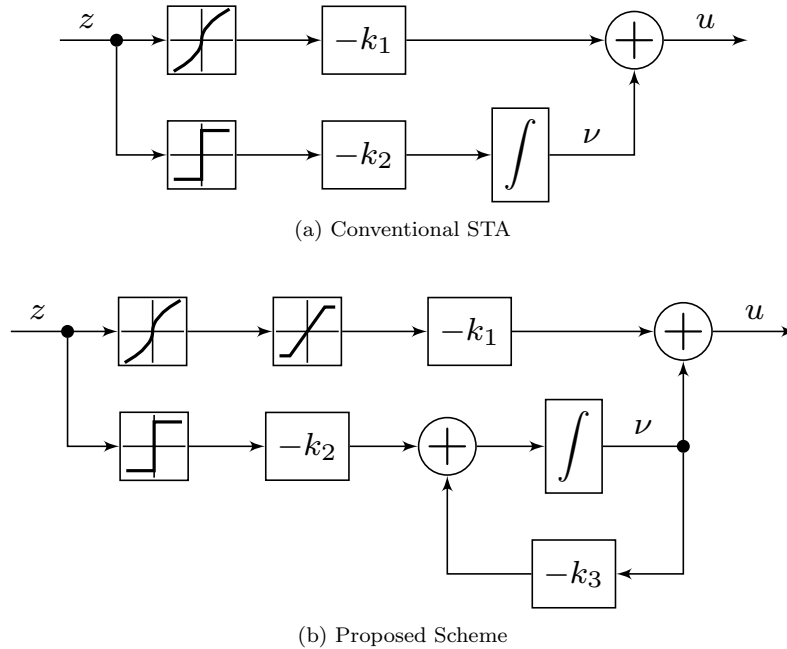


Figure 2.2.: Block diagrams of conventional super-twisting control (1.3) and the saturated version proposed in this chapter.

2. Saturated Super-Twisting Algorithm

Remark 2.2. Having applied the traditional first-order sliding mode control approach, a saturated and continuous control signal can be also obtained through

$$\frac{du}{dt} = -k [\sigma]^0 - \lambda u, \quad (2.10)$$

where k and λ are positive constants and the sliding function σ is defined as

$$\sigma = \frac{dz}{dt} + \lambda z. \quad (2.11)$$

Similar to that proved in the aforementioned lemma, it can be derived that $|u(t)| \leq \frac{k}{\lambda}$, $\forall t \geq 0$. Please note that the estimate information of the time derivative of z needs to be incorporated into the sliding function design. This makes the sliding mode control law for the considered system redundant since both the controller and estimator reconstruct disturbances a .

2.3. Stability Analysis

For system (1.1) under control law (2.3), the closed-loop dynamics is written as

$$\frac{dx_1}{dt} = -k_1 \text{sat}_\epsilon \left([x_1]^{\frac{1}{2}} \right) + x_2, \quad (2.12a)$$

$$\frac{dx_2}{dt} = -k_2 [x_1]^0 - k_3 x_2 + \phi(t), \quad (2.12b)$$

where a vector is defined as $\mathbf{x} = [x_1 \ x_2]^T = [z \ \nu + a]^T$. Suppose that (2.1) holds, then $\phi(t) = k_3 a + \frac{da}{dt}$ in the closed-loop system is bounded by

$$|\phi(t)| \leq \phi_M = k_3 a_M + L_a, \quad \forall t \geq 0. \quad (2.13)$$

For the perturbed system as well as the nominal system, i.e. $a = 0$, $\forall t \geq 0$, under the proposed control law, the finite-time convergence of the system state z is ensured in this section setting sufficient conditions for the gains. Different Lyapunov functions are employed here and the quite restrictive conditions imposed on the gains in the *perturbed case* in [Gol+18a] are relaxed by providing a novel proof.

2.3.1. Nominal Case

The stability properties of system (2.12) in the case that the system is not subject to perturbations and therefore $\phi(t) = 0$, $\forall t \geq 0$, are investigated in this subsection.

Proposition 2.1. *In the nominal case, the origin $\mathbf{x} = \mathbf{0}$ is globally finite-time stable and the control input does not exceed the saturation bounds (i.e. (2.2) is met) if the parameters k_1, ϵ, k_2 , and k_3 are chosen such that (2.9) is fulfilled.*

Proof. Consider the vector

$$\zeta = \begin{bmatrix} \zeta_1 & \zeta_2 \end{bmatrix}^T = \begin{bmatrix} |x_1|^{\frac{1}{2}} & x_2 \end{bmatrix}^T. \quad (2.14)$$

A strict and Lipschitz Lyapunov function candidate for system (2.12) without disturbances is introduced here as

$$V_n = \zeta_1^2 + \frac{1}{2k_2}\zeta_2^2 = |x_1| + \frac{1}{2k_2}x_2^2. \quad (2.15)$$

Remark 2.3. Since the sat_ϵ function and the linear term $-k_3x_2$ are incorporated into system (2.12), it is not possible any more to compute constant matrices for the Algebraic Lyapunov Equation as presented in [MO12].

The time derivative of the aforementioned Lyapunov function reads as

$$\frac{dV_n}{dt} = -k_1 \text{sat}_\epsilon \left(|x_1|^{\frac{1}{2}} \right) - \frac{k_3}{k_2} x_2^2. \quad (2.16)$$

It becomes evident that the globally positive definiteness of the radially unbounded function V_n as well as globally negative definiteness of $\frac{dV_n}{dt}$ (according to (2.4)) is guaranteed by the positive control parameters. Thus, the global asymptotic stability of the origin is achieved.

Lemma 2.2. *For closed-loop system (2.12), the conditions of the quasihomogeneity principle [Orl08, Theorem 4.2] are fulfilled. This is due to the fact that*

- *the right-hand side of differential equation (2.12) consists of a locally homogeneous piece-wise continuous function of degree $q_{\text{STA}} = -1$ with respect to dilation $r_{\text{STA}} = (2, 1)$;*
- *the components of the continuous function $\psi = -k_3x_2 + \phi(t)$ are globally bounded (according to the boundedness of ν , a , and $\frac{da}{dt}$);*
- *system (2.12) is globally asymptotically stable around the origin.*

Therefore, the convergence of the vector \mathbf{x} in a finite time is justified applying the aforementioned principle. \square

2.3.2. Perturbed Case

In this subsection, the stability analysis of system (2.12) in the presence of disturbances, i.e. $a \neq 0$ and thus $\phi(t) \neq 0$, is carried out. In order to show that the variables x_1 and x_2 tend to zero in a finite time, a Lyapunov function candidate, in which two quadratic functions are included, is considered in [Gol+18a] as

$$V_d = \zeta^T P \zeta + \mathbf{x}^T \tilde{P} \mathbf{x}, \quad (2.17)$$

$$P = \frac{1}{2} \begin{bmatrix} 6k_2 + k_1^2 & -k_1 \\ -k_1 & 1 \end{bmatrix}, \quad \tilde{P} = \frac{1}{2} \begin{bmatrix} k_3^2 & k_3 \\ k_3 & 2 \end{bmatrix}.$$

It is an absolutely continuous function of \mathbf{x} , radially unbounded and globally positive definite (if k_2 is positive).

Remark 2.4. It is noted that V_d is continuous but not locally Lipschitz due to the fact that ζ_1 is not Lipschitz at $x_1 = 0$. However, as it is explained in [MO12] by means of Zubov's theorem [Poz08, Theorem 20.2], it can be still employed as a Lyapunov function. Since V_d along the system trajectories $\varphi(t, \mathbf{x}_0)$, where $\mathbf{x}(t=0) = \mathbf{x}_0 \in \mathbb{R}^2$, is indeed an absolutely continuous function of time t , its time derivative is defined almost everywhere. Now, it needs to be shown that $V_d(\varphi(t, \mathbf{x}_0))$ decreases monotonically to zero, which is true if and only if $\frac{dV_d}{dt}$ is negative definite almost everywhere.

In the case that $|x_1|^{\frac{1}{2}} \leq \epsilon$, taking the time derivative of V_d along the trajectories of the system yields

$$\begin{aligned} \frac{dV_d}{dt} = & - \left(2k_1 k_2 + \frac{k_1^3}{2} \right) |x_1|^{\frac{1}{2}} + k_1^2 x_2 [x_1]^0 - \frac{k_1}{2} \frac{x_2^2}{|x_1|^{\frac{1}{2}}} + 3x_2 \phi(t) \\ & - k_1 [x_1]^{\frac{1}{2}} \phi(t) - k_1 k_3^2 |x_1|^{\frac{3}{2}} - 2k_3 x_2^2 - k_2 k_3 |x_1| + k_3 x_1 \phi(t). \end{aligned} \quad (2.18)$$

Considering the bound of perturbations in (2.13), it can be derived that

$$\frac{dV_d}{dt} \leq - \frac{1}{|x_1|^{\frac{1}{2}}} \zeta^T Q \zeta - k_1 k_3^2 |x_1|^{\frac{3}{2}} - 2k_3 x_2^2 - k_3 (k_2 - \phi_M) |x_1| \quad (2.19)$$

with

$$Q = \frac{1}{2} \begin{bmatrix} 4k_1 k_2 + k_1^3 - 2k_1 \phi_M & - (k_1^2 + 3\phi_M) \\ - (k_1^2 + 3\phi_M) & k_1 \end{bmatrix}.$$

Hence, $\frac{dV_d}{dt}$ is negative definite if $k_1 > 0$, $k_3 > 0$, and $k_2 > 2\phi_M + \left(\frac{3\phi_M}{2k_1}\right)^2$.

For $|x_1|^{\frac{1}{2}} > \epsilon$, (2.18) is rewritten as

$$\frac{dV_d}{dt} = W_{d1} + W_{d2} + W_{d3} \quad (2.20)$$

with

$$\begin{aligned} W_{d1} &= -k_2 k_3 |x_1| + k_1 k_3 x_2 [x_1]^{\frac{1}{2}} - 2k_3 x_2^2 + k_3 x_1 \phi(t), \\ W_{d2} &= -k_1 k_2 |x_1|^{\frac{1}{2}} + \left(\frac{k_1^2}{2} - \epsilon k_1 k_3 \right) x_2 [x_1]^0 + \frac{\epsilon k_1^2}{2} x_2 [x_1]^{-\frac{1}{2}} \\ &\quad - \frac{k_1}{2} \frac{x_2^2}{|x_1|^{\frac{1}{2}}} + 3x_2 \phi(t) - k_1 [x_1]^{\frac{1}{2}} \phi(t), \\ W_{d3} &= -\epsilon k_1 \left(3k_2 + \frac{k_1^2}{2} \right) + 2k_1 k_2 |x_1|^{\frac{1}{2}} - \epsilon k_1 k_3^2 |x_1|. \end{aligned}$$

It can be achieved that

$$W_{d1} \leq -\zeta^T \tilde{Q}_1 \zeta, \quad (2.21)$$

where

$$\tilde{Q}_1 = \begin{bmatrix} k_2 k_3 - k_3 \phi_M & -\frac{k_1 k_3}{2} \\ -\frac{k_1 k_3}{2} & 2k_3 \end{bmatrix}.$$

The matrix \tilde{Q}_1 is positive definite if $k_3 > 0$ and $k_2 > \phi_M + \frac{k_1^2}{8}$. For the case $|x_1|^{\frac{1}{2}} > \epsilon$, it can be shown that

$$\frac{\epsilon k_1^2}{2} x_2 [x_1]^{-\frac{1}{2}} \leq \frac{k_1^2}{2} |x_2|. \quad (2.22)$$

Therefore, having satisfied $\frac{k_1^2}{2} - \epsilon k_1 k_3 > 0$, it can be concluded that

$$W_{d2} \leq -\frac{1}{|x_1|^{\frac{1}{2}}} \zeta^T \tilde{Q}_2 \zeta, \quad (2.23)$$

where

$$\tilde{Q}_2 = \frac{1}{2} \begin{bmatrix} 2k_1 k_2 - 2k_1 \phi_M & -(k_1^2 + 3\phi_M) \\ -(k_1^2 + 3\phi_M) & k_1 \end{bmatrix}.$$

This matrix is positive definite if $k_1 > 0$ and $k_2 > 4\phi_M + \frac{9\phi_M^2}{2k_1^2} + \frac{k_1^2}{2}$. Based on Young's inequality [HLP52], it becomes evident that

$$2k_1 k_2 |x_1|^{\frac{1}{2}} \leq k_1 k_2 (|x_1| + 1). \quad (2.24)$$

2. Saturated Super-Twisting Algorithm

Thus, it can be written

$$W_{d3} \leq -\epsilon k_1 \left(3k_2 + \frac{k_1^2}{2} - \frac{k_2}{\epsilon} \right) - k_1 (\epsilon k_3^2 - k_2) |x_1|. \quad (2.25)$$

If $\epsilon > \frac{k_2}{k_3^2} + \frac{2k_2}{6k_2+k_1^2}$, then W_{d3} is negative definite.

Consequently, the globally negative definiteness of $\frac{dV_d}{dt}$ is ensured if the control parameters are selected as

$$\begin{aligned} k_1 &> 0, & k_2 &> 4\phi_M + \frac{9\phi_M^2}{2k_1^2} + \frac{k_1^2}{2}, \\ k_3 &> 0, & \epsilon &> \frac{2k_3}{k_1} + \frac{k_2}{k_3^2} + \frac{2k_2}{6k_2+k_1^2}. \end{aligned} \quad (2.26)$$

It is noted that (2.9) also needs to be satisfied to retain the control signal within the saturation bounds. This leads to rather restrictive conditions on the parameters, which limits the permissible bound of perturbations. According to (2.9) and (2.26), the inequality

$$\frac{8k_3k_1^2a_M + 9k_3^2a_M^2 + k_1^4}{2k_1^2} < k_2 < k_3\rho \quad (2.27)$$

needs to be fulfilled. Solving this inequality for k_3 gives

$$\frac{k_2}{\rho} < k_3 < \frac{k_1 \left(\sqrt{7k_1^2 + 18k_2} - 4k_1 \right)}{9a_M}. \quad (2.28)$$

Hence, the allowable bound of perturbations can be realized as

$$a_M < \frac{k_1 \left(\sqrt{7k_1^2 + 18k_2} - 4k_1 \right)}{9k_2} \rho. \quad (2.29)$$

It can be derived (e.g. numerically) that a_M has to be less than one sixth of the saturation bound ρ . In the following, this is relaxed to one third of ρ through a novel parameter setting for the controller.

Proposition 2.2. *There exist constants \tilde{k}_1 and \tilde{k}_2 such that for any positive real value ϕ_M , the choice of the control parameters as*

$$k_1 = \phi_M^{\frac{1}{2}} \tilde{k}_1, \quad k_2 = \phi_M \tilde{k}_2 \quad (2.30)$$

guarantees that if (2.9) and

$$k_1 \epsilon > \frac{k_2}{k_3} + a_M \quad (2.31)$$

are satisfied, then the origin $\mathbf{x} = \mathbf{0}$ is globally finite-time stable and the absolute value of the continuous control signal is bounded by ρ for all $t \geq 0$.

Remark 2.5. By solving the sum-of-squares problem formulated within the following proof using a MATLAB toolbox, e.g. SOSTOOLS [Pap+13], the values of \tilde{k}_1 and \tilde{k}_2 can be determined numerically. A valid choice is

$$\tilde{k}_1 = 2.2, \quad \tilde{k}_2 = 1.1. \quad (2.32)$$

Proof. In the case that $|x_1|^{\frac{1}{2}} > \epsilon$, (2.12a) reads as

$$\frac{dx_1}{dt} = -k_1 \epsilon [x_1]^0 + x_2. \quad (2.33)$$

Since x_2 is bounded (based on (2.8) and (2.1)) by

$$|x_2| \leq \nu_M + a_M, \quad \forall t \geq 0, \quad (2.34)$$

$|x_1|$ is decreasing if the control constants are selected as given in (2.31). After the finite time T , $|x_1|^{\frac{1}{2}} = \epsilon$ is satisfied, which leads to

$$\frac{dx_1}{dt} = -k_1 [x_1]^{\frac{1}{2}} + x_2, \quad (2.35a)$$

$$\frac{dx_2}{dt} = -k_2 [x_1]^0 - k_3 x_2 + \phi(t). \quad (2.35b)$$

In the following, it is shown that $|x_1|$ declines further. This guarantees the globally boundedness of $|z|^{\frac{1}{2}}$ by ϵ in the case that $|z_0|^{\frac{1}{2}} \leq \epsilon$. On the occasion $|x_1|^{\frac{1}{2}} = \epsilon$, taking the time derivative of $|x_1|$ along the trajectory of (2.35a) yields

$$\begin{aligned} \frac{d|x_1|}{dt} &= \frac{dx_1}{dt} [x_1]^0 = -k_1 |x_1|^{\frac{1}{2}} + x_2 [x_1]^0 \\ &\leq -k_1 \epsilon + |x_2|. \end{aligned} \quad (2.36)$$

Considering (2.34), if the sufficient condition (2.31) is met, then $\frac{d|x_1|}{dt}$ is negative definite. This implies that $|x_1|$ decreases and it can be inferred that $|x_1|^{\frac{1}{2}} \leq \epsilon$, $\forall t > T$.

The control gains k_1 and k_2 are scaled for all $\phi_M > 0$ as given in (2.30). This is justified by changing the coordinates in (2.35) as

$$\mathbf{x} = \phi_M \tilde{\mathbf{x}} = \phi_M \begin{bmatrix} \tilde{x}_1 & \tilde{x}_2 \end{bmatrix}^T. \quad (2.37)$$

The transformation gives

$$\frac{d\tilde{x}_1}{dt} = -\tilde{k}_1 [\tilde{x}_1]^{\frac{1}{2}} + \tilde{x}_2, \quad (2.38a)$$

$$\frac{d\tilde{x}_2}{dt} = -\tilde{k}_2 [\tilde{x}_1]^0 - k_3 \tilde{x}_2 + \frac{\phi(t)}{\phi_M}. \quad (2.38b)$$

2. Saturated Super-Twisting Algorithm

It is noted that $\frac{|\phi(t)|}{\phi_M}$ is less than or equal to one for all $t \geq 0$ (according to (2.13)). This is used to design a Lyapunov function in the following. Although system (2.38) is not a weighted homogeneous system (see e.g. [Lev05; Ber+14]) due to the presence of the linear term $-k_3\tilde{x}_2$, it is possible to ensure the asymptotic stability of the origin $\tilde{\mathbf{x}} = \mathbf{0}$ employing the Lyapunov function candidate

$$V(\tilde{\mathbf{x}}) = \alpha_1|\tilde{x}_1|^{\frac{3}{2}} - \alpha_2\tilde{x}_1\tilde{x}_2 + \alpha_3|\tilde{x}_2|^3. \quad (2.39)$$

This is the homogeneous generalized form function of degree three with the weights two and one considered in [SM14]. α_1 , α_2 , and α_3 are the coefficients and in order to guarantee the globally positive definiteness of V , both α_1 and α_3 need to be positive. It is differentiable and its time derivative along the trajectories of (2.38) reads as

$$\frac{dV}{dt} = -(W_1 + W_2) - 3\alpha_3k_3|\tilde{x}_2|^3, \quad (2.40)$$

with

$$W_1 = \beta_1|\tilde{x}_1| - \beta_2[\tilde{x}_1]^{\frac{1}{2}}\tilde{x}_2 + \beta_3[\tilde{x}_2]^2[\tilde{x}_1]^0 + \beta_4|\tilde{x}_2|^2, \quad (2.41a)$$

$$W_2 = \beta_5\tilde{x}_1 - \beta_6[\tilde{x}_2]^2. \quad (2.41b)$$

Both of the above discontinuous homogeneous functions are of degree two and their coefficients denote

$$\beta_1 = \frac{3}{2}\alpha_1\tilde{k}_1 - \alpha_2\tilde{k}_2, \quad \beta_2 = \frac{3}{2}\alpha_1 + \alpha_2\tilde{k}_1, \quad \beta_3 = 3\alpha_3\tilde{k}_2, \quad \beta_4 = \alpha_2, \quad (2.42a)$$

and

$$\beta_5 = \alpha_2 \frac{\left(-k_3\nu + \frac{da}{dt}\right)}{\phi_M}, \quad \beta_6 = 3\alpha_3 \frac{\phi(t)}{\phi_M}. \quad (2.42b)$$

It is noted that β_5 (according to (2.8) and (2.1)) as well as β_6 (as mentioned above) is bounded by some known constants. The extrema of β_5 are computed in Appendix A. A quadrant analysis, similar to that conducted in [SM14], is carried out in this appendix to determine conditions of the control gains and the coefficients of V such that V and $W_1 + W_2$ are globally positive definite. As a consequence, similar to the nominal case, the finite-time stability of the origin is guaranteed according to Lemma 2.2. \square

Remark 2.6. It is deduced from the conditions of the control parameters imposed in (2.30) that

$$k_2 > k_3a_M + L_a \quad (2.43)$$

needs to be fulfilled. Having also taken into consideration (2.31) and (2.9), it is concluded that perturbations with $a_M < \frac{\rho}{3}$ can be handled. It is also noted that L_a has to be a portion of the saturation limit ρ , which restricts the class of addressed disturbances. In the next chapter, a wider class of perturbations with a larger bound a_M close to ρ can be dealt with applying an anti-windup strategy instead of the saturated super-twisting algorithm.

2.4. Simulation Examples

In this section, it is indicated in simulation how the proposed control approach works in the nominal and perturbed cases. The achieved closed-loop performances are compared with the results obtained through the conventional super-twisting algorithm given in (1.3). The system under the saturated super-twisting control law presented in [Cas+16b; Cas+16a] is also simulated. This controller is implemented as

$$\begin{bmatrix} u \\ \frac{d\nu}{dt} \end{bmatrix} = \begin{cases} \begin{bmatrix} -\rho [z]^0 \\ 0 \end{bmatrix}, & \nu_0 = 0 & \text{if } s = 0 \\ \begin{bmatrix} -k_1 [z]^{\frac{1}{2}} + \nu \\ -k_2 [z]^0 \end{bmatrix}, & \nu(t = t_1) = \bar{\nu} & \text{if } s = 1, \end{cases} \quad (2.44)$$

where $\bar{\nu}$ is either set to zero (in [Cas+16b]) or to the negative value of disturbances estimation (in [Cas+16a]). The value of the binary variable s is determined by a dynamic switching law. It is set to zero and the relay controller is employed if the initial value z_0 is outside a neighborhood of the origin. After that the state enters a bound, one is assigned to s and the super-twisting algorithm is applied, which is maintained even if the state leaves the band. In order to assess the effectiveness of the proposed technique in this chapter, the constants k_1 and k_2 are left the same in implementation of control laws (2.3), (1.3), and (2.44).

2.4.1. Nominal Case

In this simulation case, assuming that $a = 0$, it is supposed the actuating signal remains bounded with $\rho = 5$. The positive control parameters of the proposed method are chosen as $k_1 = \epsilon = 2$ and $k_2 = k_3 = 1$ satisfying (2.9). The numerical simulation is carried out considering the initial values $z_0 = 20$ and $\nu_0 = 0$. The performances of the three algorithms are depicted in Figure 2.3. It can be clearly seen in the lower plot that the control signal of the scheme proposed in this chapter is continuous and bounded by the specification. The latter contributes substantially to alleviation

2. Saturated Super-Twisting Algorithm

of the windup effect as illustrated in the zoomed portion of the upper plot. It is also demonstrated that the output of the system under the proposed control law converges to the origin with a satisfactory speed, which is similar to the performance of the saturated super-twisting (with switching). Please note that the implementation of the proposed control technique is much easier since no switching between the algorithms takes place.

Control law (2.3) is also implemented with the same setting as that one made for the original super-twisting approach in the previous chapter. Their system trajectories are compared in Figure 2.4. It can be seen that undesirable oscillations are alleviated in the performance of the proposed technique.

2.4.2. Perturbed Case

In this scenario, it is assumed that the system is subject to disturbances $a(t)$ given in (1.4). The saturation bound $[-\rho, \rho]$ as well as the initial condition z_0 is the same as the previous example. It is noted that $a_M = 3$ is more than half of the given constant ρ . Therefore, as it is explained in [Cas+16a], information of the perturbation estimator

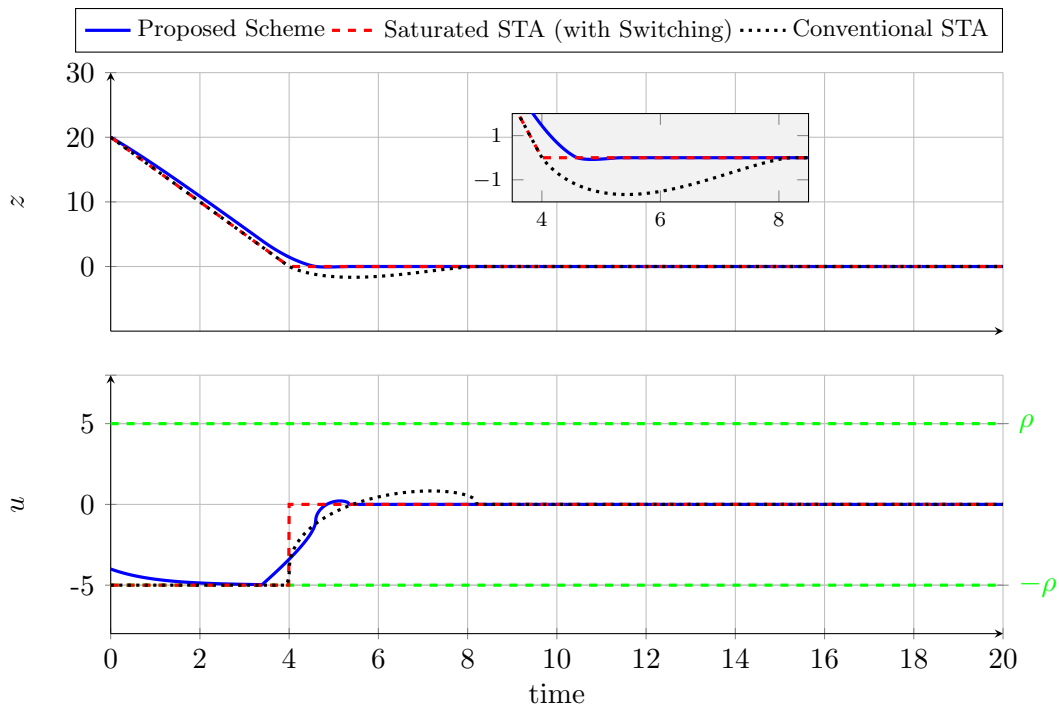


Figure 2.3.: Simulation response curves obtained through the unperturbed system under three different control laws (2.3), (2.44), and (1.3), which are labeled respectively with the Proposed Scheme, Saturated STA (with Switching), and Conventional STA.

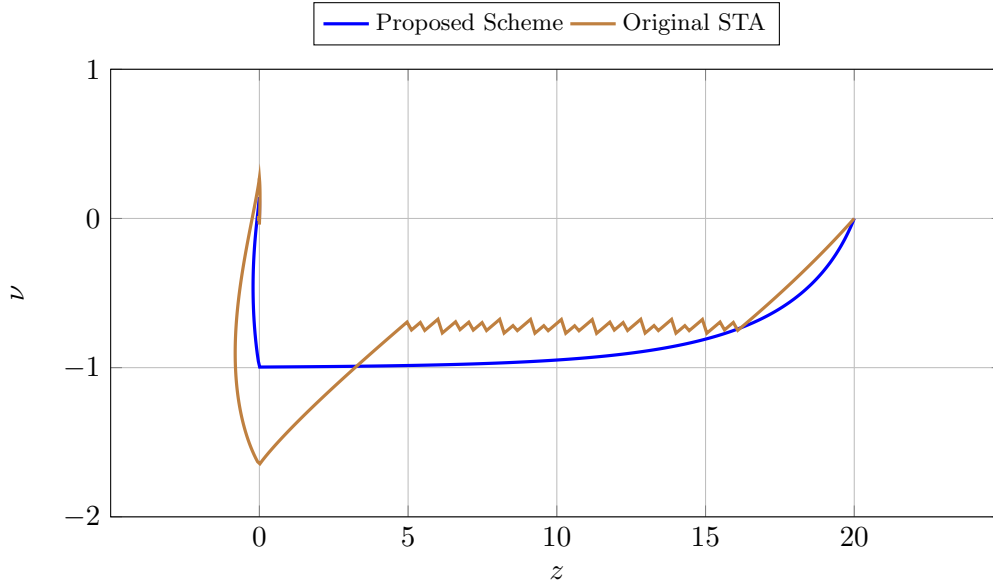


Figure 2.4.: System trajectories of applying the proposed technique and the original super-twisting algorithm presented respectively in (2.3) and (1.5) to the nominal case.

should be incorporated into the control law introduced in [Cas+16b]. The control gains $k_1 = 4$ and $k_2 = 9$ are selected based on the sufficient condition mentioned therein as

$$k_1 > 0, \quad k_2 > 3L_a + 2 \left(\frac{L_a}{k_1} \right)^2. \quad (2.45)$$

Furthermore, the estimator constants are well-tuned such that the estimation error tends to zero in a finite time faster than the convergence of the system state. Consequently, as it is indicated in the upper plot of Figure 2.5, the maximum rate of convergence is achieved (the dashed red line).

For the proposed approach, as it is given through the aforementioned proof, the permissible bound of disturbances is relaxed to just less than $\frac{\ell}{3}$. Although this is not satisfied in this example, the two other parameters $\epsilon = 0.1$ and $k_3 = 2$ are assigned such that (2.9) and (2.43) hold. In the next chapter, where the allowable bound and class of perturbations are enlarged, all sufficient conditions set for the corresponding stability analysis are met. Having implemented the proposed compact and non-redundant strategy (the integrator is initialized with $\nu_0 = 0$ and no information of perturbations is required), similar convergence to that one obtained through the saturated super-twisting (with estimator) is illustrated.

A large overshoot and long settling time can be seen in the performance of the conventional super-twisting. It is noted that the dotted black lines in the lower plots of Figure 2.3 and Figure 2.5 show the evolution of the control signals of this algorithm

2. Saturated Super-Twisting Algorithm

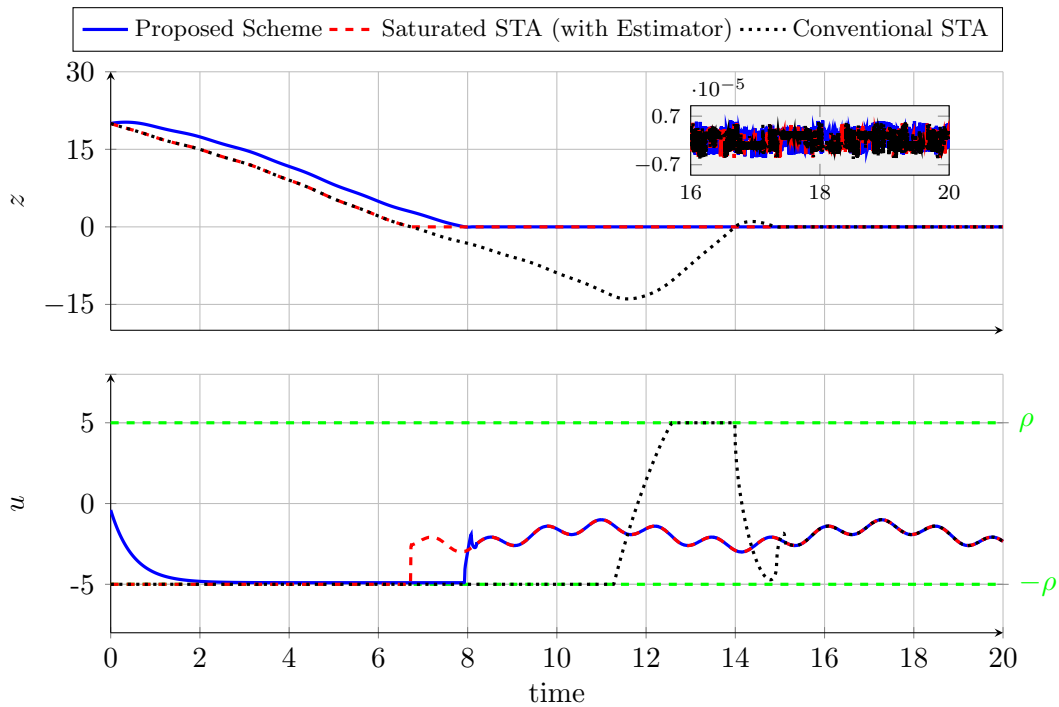


Figure 2.5.: Simulation results in the perturbed case comparing the proposed approach with the saturated super-twisting applying the disturbance estimator as presented in [Cas+16a] as well as the conventional super-twisting.

introduced to the systems through the saturating actuators, which are different from that ones generated by the controller. In contrast, the signals produced by the proposed control method and the conventional super-twisting with one switching are bounded by the saturation limits due to their structures.

3. An Anti-Windup Strategy for the Super-Twisting Algorithm

This chapter deals with a first-order system with uncertainties and disturbances. A comprehensive second-order sliding mode control strategy adopting an anti-windup scheme is introduced, in which the properties of the standard STA are retained and no additional constraints on the bound and class of perturbations are imposed.

3.1. Problem Statement

Consider a system represented by

$$\frac{dz}{dt} = b(t, z)\text{sat}_\rho(u) + a(t, z), \quad (3.1)$$

where a and b , which are the functions of time and state, represent the effect of uncertainties and disturbances.

Assumption 3.1. *The functions a and b are globally bounded and Lipschitz continuous with respect to time and state, i.e.*

$$|a(t, z)| \leq a_M, \quad \left| \frac{\partial a}{\partial t} \right| \leq L_a, \quad \left| \frac{\partial a}{\partial z} \right| \leq L_{a,z}, \quad \forall t \geq 0, \quad (3.2a)$$

$$0 < b_m \leq b(t, z) \leq 1, \quad \left| \frac{\partial b}{\partial t} \right| \leq L_b, \quad \left| \frac{\partial b}{\partial z} \right| \leq L_{b,z}, \quad \forall t \geq 0, \quad (3.2b)$$

where the constants a_M , L_a , $L_{a,z}$, b_m , L_b , and $L_{b,z}$ are known. The upper bound of $b(t, z)$ without loss of generality¹ is one. Furthermore, as it is explained in Remark 2.1, the inequality

$$\left| \frac{a(t, z)}{b(t, z)} \right| \leq \frac{a_M}{b_m} < \rho, \quad (3.3)$$

has to be fulfilled.

This chapter aims to design a control law for system (3.1) such that

¹For other known upper bounds, the proposed technique may still be applied.

3. An Anti-Windup Strategy for the Super-Twisting Algorithm

- the finite-time convergence of the system state z is achieved;
- the control signal u is continuous everywhere and in the case that the generated signal exceeds the saturation limits, the windup effect is counteracted.

3.2. Proposed Scheme

An anti-windup technique is incorporated into the standard super-twisting controller as

$$u = -k_1 [z]^{\frac{1}{2}} + \nu, \quad (3.4a)$$

$$\frac{d\nu}{dt} = -k_2 [z]^0 - k_3 \beta \nu, \quad |\nu_0| \leq \frac{k_2}{k_3}, \quad (3.4b)$$

where the initial value of the control law state variable ν_0 , similarly to the saturated super-twisting algorithm introduced in the previous chapter, is chosen appropriately. The value of the binary variable β is assigned as

$$\beta = \begin{cases} 1 & \text{if } |u| > \rho \\ 0 & \text{if } |u| \leq \rho. \end{cases}$$

It is shown later that at most, one switch in β from one to zero occurs therein if the control parameters k_1 , k_2 , and k_3 are selected appropriately. This implies that once the produced control signal satisfies $|u| \leq \rho$, the actuator saturation does not happen afterwards. Sufficient conditions for choosing the control parameters are given in the next section. Please note that, in contrast to (2.44), the introduced actuating signal is continuous everywhere due to the fact that the aforementioned switch lies in the same channel as the discontinuous element of the algorithm. Furthermore, in contrast with (1.5), the term $k_2 [z]^0$ exists in (3.4) for any value of u , which prevents high frequency switching on the saturation bounds. Therefore, similar to that illustrated in Figure 2.4, zigzag motions are also removed in the system trajectory of applying the scheme proposed in this chapter.

It is worth mentioning that, compared to the previous chapter, the control signal generated here does not remain within the bounds $\pm\rho$ if the initial value of z is very large. However, the proposed control scheme in this chapter enjoys the advantages that the windup effect is also alleviated and the standard STA is recovered close to the origin. The latter contributes significantly to an enlargement of the class of addressed disturbances in the sense that the limit ρ does *not* impose any constraint on the Lipschitz constant L_a (assuming $\frac{\partial a}{\partial z} = \frac{\partial b}{\partial z} = 0$). It is noted that, in comparison with [Cas+16b; Cas+16a], the implementation of control law (3.4) is relatively simpler since a switch is made if the absolute value of the control input is out of the bound

ρ rather than making a switch based on a predefined neighborhood of the origin. Moreover, perturbations with *any* bound a_M that is less than $b_m\rho$ can be handled here without using a disturbance estimator. A block diagram of the control approach introduced in this chapter is depicted in Figure 3.1.

3.3. Stability Analysis

Global finite-time stability properties of the closed-loop system are established in this section.

Proposition 3.1. *Suppose that Assumption 3.1 is satisfied. For system (3.1) under control law (3.4), the origin $z = 0$ is globally finite-time stable if the control parameters are selected such that*

$$\begin{aligned} k_1 &> 2\sqrt{\frac{k_2\rho}{b_m\rho - a_M}}, \quad k_2 > \frac{L_a + L_{a,z}(\rho + a_M) + (L_b + L_{b,z}(\rho + a_M))a_M}{b_m^2}, \\ \rho &\geq \frac{k_2}{k_3} \end{aligned} \quad (3.5)$$

holds.

Proof. In the case that $|u| > \rho$, the closed-loop dynamics reads as

$$\frac{dz}{dt} = \rho b [u]^0 + a, \quad (3.6a)$$

$$\frac{d\nu}{dt} = -k_2 [z]^0 - k_3\nu. \quad (3.6b)$$

As it is proved in Lemma 2.1, $|\nu|$ is bounded here by a calculable constant since (3.6b) is a linear differential equation with the state variable ν and the bounded input $[z]^0$. Having chosen ν_0 and the control gains as given in (3.4b) and (3.5) respectively, $|\nu| \leq \rho$ holds as long as $\beta = 1$. Thus, in this phase that the actuator is saturated, either $-k_1 [z]^{\frac{1}{2}}$ and ν are in the same sign or they have different signs with $k_1|z|^{\frac{1}{2}} > |\nu| + \rho$. Therefore,

$$[u]^0 = \left[-k_1 [z]^{\frac{1}{2}}\right]^0 = -[z]^0 \quad (3.7)$$

is fulfilled here, which implies that $|z|$ is decreasing while ν is bounded. After the finite time T ,

$$|z|^{\frac{1}{2}} \leq \frac{2\rho}{k_1} \quad (3.8)$$

3. An Anti-Windup Strategy for the Super-Twisting Algorithm

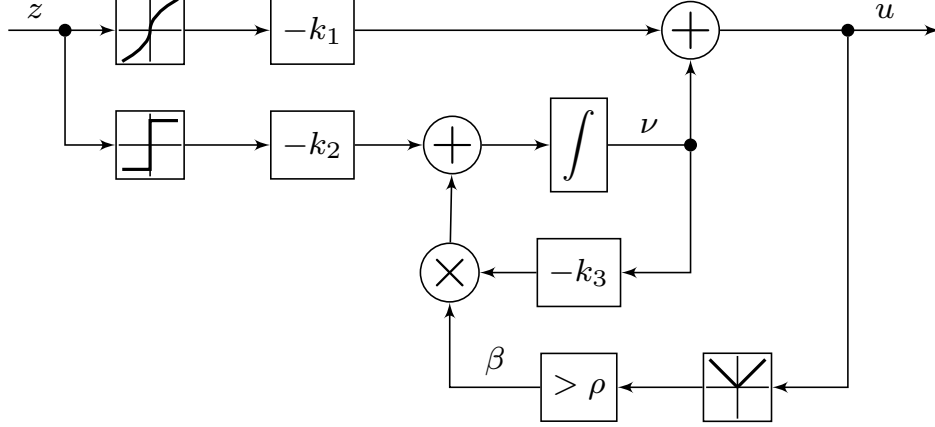


Figure 3.1.: Block diagram of proposed control law (3.4). It is noted that the output of the comparison block is one if its input is greater than the bound ρ . The output β is zero if $|u| \leq \rho$.

is satisfied, which leads to $|u| = \rho$ for the first time and a switch to $\beta = 0$. In the following, it is shown that the control signal remains within the limits afterwards, i.e. $|u(t)| \leq \rho, \forall t > T$.

On the occasion $|u| = \rho$, taking the time derivative of $|u|$ along the trajectory of system (3.1) yields

$$\begin{aligned} \frac{d|u|}{dt} &= \frac{du}{dt} [u]^0 = \left(-\frac{k_1}{2} |z|^{-\frac{1}{2}} \frac{dz}{dt} + \frac{d\nu}{dt} \right) [u]^0 \\ &= -\frac{k_1}{2} |z|^{-\frac{1}{2}} (b|u| + a [u]^0) - k_2 [z]^0 [u]^0. \end{aligned} \quad (3.9)$$

Considering (3.8) and Assumption 3.1, it can be derived that

$$\frac{d|u|}{dt} \leq -\frac{k_1^2 (b_m \rho - a_M)}{4\rho} + k_2. \quad (3.10)$$

If the sufficient conditions imposed in (3.5) are met, then $\frac{d|u|}{dt} < 0$ holds, which implies that $|u|$ decreases. Therefore, in order to guarantee the globally boundedness of $|u|$ by ρ , it needs to be indicated that (3.8) holds afterwards. To that end, it will be shown that (3.8) is maintained if $|u| \leq \rho$ is satisfied. Hence, violating either of these two inequalities requires the other one to be violated *before* and, since both hold at time instant T , neither can be violated.

To show that (3.8) is satisfied for $|u| \leq \rho$, consider the closed-loop dynamics, which

is written in this case as

$$\frac{dz}{d\tau} = -k_1 [z]^{\frac{1}{2}} + \omega, \quad (3.11a)$$

$$\frac{d\omega}{d\tau} = \frac{1}{b} \left(-k_2 [z]^0 + \delta \right), \quad (3.11b)$$

where time is scaled through $d\tau = bdt$, the auxiliary variable ω is defined as $\omega = \nu + \frac{a}{b}$, and δ reads as

$$\delta = \frac{d}{dt} \left(\frac{a(t, z)}{b(t, z)} \right) = \frac{\left(\frac{\partial a}{\partial t} + \frac{\partial a}{\partial z} \frac{dz}{dt} \right) b(t, z) - \left(\frac{\partial b}{\partial t} + \frac{\partial b}{\partial z} \frac{dz}{dt} \right) a(t, z)}{(b(t, z))^2}. \quad (3.12)$$

It can be verified that ν and z have the same sign if $|u| \leq \rho$ and $|\nu| > \rho$. Since $\frac{d\nu}{dt}$ has the opposite sign of ν in that case (according to (3.4b)), $|\nu|$ decreases. Having given that $|\nu| \leq \rho$ holds at $t = T$, it satisfies this bound for all time. Then, $|\omega|$ is bounded by 2ρ (according to (3.3)), and it can be inferred from (3.11a) that (3.8) is maintained.

In system (3.11), the asymptotic stability of the state vector $\zeta := \begin{bmatrix} z & \omega \end{bmatrix}^T$ can be ensured by using the Lyapunov function candidate considered in [SH17] as

$$V(\zeta) = \begin{cases} 2\sqrt{\omega^2 + 3\lambda^2 k_1^2 z} - \omega & \text{for } \zeta \in \mathcal{M}, \\ 2\sqrt{\omega^2 - 3\lambda^2 k_1^2 z} + \omega & \text{for } -\zeta \in \mathcal{M}, \\ 3|\omega| & \text{otherwise.} \end{cases} \quad (3.13)$$

The positive constant $\lambda < 1$ is chosen such that

$$k_1 > \frac{1}{\lambda} \sqrt{\frac{2k_2}{b_m}} \quad (3.14)$$

is met, and the set \mathcal{M} is defined as

$$\mathcal{M} = \{ \zeta \mid z \geq 0, \omega \leq \lambda k_1 \sqrt{z} \}. \quad (3.15)$$

The time derivative of V in the scenario of $\zeta \in \mathcal{M}$ along the trajectory of system (3.11) reads as

$$\frac{dV}{d\tau} = \frac{3\lambda^2 k_1^2 (-k_1 \sqrt{z} + \omega) - 2\omega \left(\frac{k_2 - \delta}{b} \right)}{\sqrt{\omega^2 + 3\lambda^2 k_1^2 z}} + \frac{k_2 - \delta}{b}. \quad (3.16)$$

It is noted that δ given in (3.12) as well as b is uniformly bounded since (3.2a) and (3.2b) hold and actuator is saturated when $|u| > \rho$ ($\frac{dz}{dt}$ is bounded). Hence, despite the presence of b and δ , $\frac{dV}{d\tau}$ is a homogeneous function (see e.g. [BB05]) of degree zero

3. An Anti-Windup Strategy for the Super-Twisting Algorithm

with respect to \sqrt{z} and ω . As it is done in [SH17], the performance of function (3.16) for z and ω such that $\omega^2 + 3\lambda^2 k_1^2 z = 1$ holds is assessed in the following. Having defined the function $g(\omega)$ as

$$g(\omega) = \frac{dV}{d\tau} \Big|_{\omega^2 + 3\lambda^2 k_1^2 z = 1} = -\lambda k_1^2 \sqrt{3 - 3\omega^2} + 3\lambda^2 k_1^2 \omega + \left(\frac{k_2 - \delta}{b} \right) (1 - 2\omega), \quad (3.17)$$

the second derivative of g with respect to ω in the interval $[-1, \frac{1}{2}]$ is

$$\frac{d^2 g}{d\omega^2} = \frac{\sqrt{3} \lambda k_1^2}{(1 - \omega^2)^{\frac{3}{2}}} \geq 0, \quad \forall \omega \in \left(-1, \frac{1}{2} \right]. \quad (3.18)$$

The local maximums of g that are on the border of the aforementioned interval are computed as

$$g(-1) = 3 \left(\frac{k_2 - \delta}{b} - \lambda^2 k_1^2 \right), \quad (3.19a)$$

$$g\left(\frac{1}{2}\right) = \frac{3\lambda(\lambda - 1)k_1^2}{2}. \quad (3.19b)$$

It is noted that if the constants k_1 and k_2 are selected as given in (3.5), the condition set on k_1 in (3.14) as well as $k_2 > |\delta|$ is fulfilled. Thus, $g(-1)$ is less than $3 \left(\frac{2k_2}{b_m} - \lambda^2 k_1^2 \right)$. From (3.14) and $0 < \lambda < 1$, it is derived that both $g(-1)$ and $g(\frac{1}{2})$ are negative. As a result of this negativeness, through homogeneity, it can be concluded that $\frac{dV}{d\tau} < 0$ holds in the entire set \mathcal{M} . The second scenario in (3.13), i.e. $-\zeta \in \mathcal{M}$, can be investigated symmetrically. In the third scenario, differentiating V with respect to τ and applying (3.11b) to that gives

$$\frac{dV}{d\tau} = \frac{3}{b} \left(-k_2 [z\omega]^0 + [\omega]^0 \delta \right). \quad (3.20)$$

As mentioned above, $|\delta|$ is less than the chosen parameter k_2 , which also results in the negative definiteness of $\frac{dV}{d\tau}$ in this scenario. Owing to that the time derivative of V along the trajectory of system (3.11) is upper bounded by a negative constant almost everywhere, the finite-time convergence of ζ is realized. This completes the global finite-time stability proof of the origin $z = 0$. \square

Remark 3.1. According to (3.5), it is achieved that

$$a_M < b_m \rho - \frac{4k_2 \rho}{k_1^2}. \quad (3.21)$$

It can be seen that having chosen $k_2 > |\delta|$, by assigning a larger value to k_1 , perturbations with a larger bound a_M close to $b_m \rho$ can be addressed. It becomes evident that in the case $b = 1$ is known, the allowable bound is enlarged to $a_M < \rho$. Please note that k_3 does not place any constraint on the permissible bound and class of disturbances.

3.4. Simulation Examples

In this section, it is demonstrated in simulation how the proposed control scheme comparing to the control strategies recorded in the literature and the previous chapter is able to deal with three different problem settings. Since uncertainties and multiplicative unknowns are not considered in [Cas+16b; Cas+16a] as well as Chapter 2, it is assumed that $\frac{\partial a}{\partial z} = 0$ and $b = 1$ is known in the first two cases. However, the bound of perturbations is enlarged from $a_M < \frac{\rho}{2}$ in the first case to $a_M = 0.9\rho$ in the second case. In the third case, the system is subject to disturbances and uncertainties, i.e. a and b are unknown functions of time and state. In all the cases, it is supposed that the actuating signal is saturated with $\rho = 5$.

In the first and second cases, the results obtained through the aforementioned versions of saturated STA are compared with the achieved closed-loop performance of the proposed technique in this chapter. The saturated version presented in [Cas+16b; Cas+16a] is given in (2.44). However, instead of satisfying (2.45), the control gains k_1 and k_2 are selected here as proposed in [SH19b] fulfilling

$$k_1 > 2\sqrt{k_2 - \sqrt{k_2^2 - L_a^2}}, \quad k_2 > L_a. \quad (3.22)$$

In Chapter 2, a novel stability analysis of the closed-loop system in the presence of perturbations is carried out to impose less restrictive conditions on the parameters. Nevertheless, the fairly restrictive conditions are still set and in the simulation example presented there, it is shown that controller (2.3) may be tuned satisfying (2.9) and necessary condition (2.43). Furthermore, in order to make a comparison, the system under the conventional super-twisting control law given in (1.3) is simulated in all the cases. The sufficient conditions for selecting the control constants set in [BCB18] are modified here as

$$k_1 > 1.8\sqrt{\frac{k_2 + \Gamma}{b_m}}, \quad k_2 > \Gamma = \frac{L_a + L_{a,z}(\rho + a_M) + (L_b + L_{b,z}(\rho + a_M))a_M}{b_m^2}. \quad (3.23)$$

3.4.1. First Case

In this simulation case, perturbations are represented as

$$a(t) = 1 + 0.6 \sin(t) + 0.8 \sin(5t). \quad (3.24)$$

As mentioned above, $b = 1$ holds in this case. Therefore, in the conditions of the proposed scheme as well as the conventional STA given in (3.5), (3.23), k_2 just needs

3. An Anti-Windup Strategy for the Super-Twisting Algorithm

to be greater than $L_a = 4.6$. The selected control constants are listed in Table 3.1. As laid down in (3.5), k_3 is chosen such that $\frac{k_2}{k_3} < \rho$ holds. It is noted that a larger value for k_3 contributes to that ν is retained closer to zero when the actuator is saturated. This leads to the actuating signal leaving the saturation a little bit earlier. Since disturbances are bounded with $a_M = 2.4 < \frac{\rho}{2}$, the saturated STA considered in [Cas+16b], in which the disturbance estimator is not incorporated, is employed in this case and its gains are set such that (3.22) holds. For the saturated version introduced in the previous chapter, having met (2.9) and (2.43), the parameters values are provided in Table 3.1.

For all the algorithms, the numerical simulation is carried out with the sampling step size of 1 ms and the initial values $z_0 = 30$ and $\nu_0 = 0$. Their performance is shown in Figure 3.2. It is revealed in the upper plot that the same rate of convergence is achieved by applying the approaches proposed in this chapter and in [Cas+16b]. The output of the system under the control law designed in Chapter 2 converges similarly. Please note that the implementation of the strategy introduced in [Cas+16b] is not as simple as the implementation of others. As it is illustrated in the zoomed portion of the plot, similar precision is obtained through all the algorithms. The evolution of the control signals introduced to the system through the saturating actuator is depicted in the lower plot. It is noted that for control laws (1.3) and (3.4), this is different from the generated control signal u , which is not bounded by the saturation limits. This results in a large overshoot and long settling time in the performance of the conventional STA. The proposed scheme, however, contributes significantly to the counteraction of the windup effect.

3.4.2. Second Case

In this scenario, b remains known, but the bound of disturbances given in (3.24) is increased as

$$a(t) = 3.1 + 0.6 \sin(t) + 0.8 \sin(5t). \quad (3.25)$$

Since L_a remains the same as last case, some of the control gains are left unchanged, see Table 3.1. However, $a_M = 4.5$ is close to the saturation bound ρ . Hence, having well-tuned the perturbation estimator constants such that the estimation error converges in a finite time faster than the convergence of the system output, information of the estimator is exploited in implementation of control law (2.44).

The simulation is initialized in this case with $z_0 = -30$ and $\nu_0 = 0$. As it is indicated in Figure 3.3, the saturated version of STA with the estimator as well as the proposed technique produces a similar satisfactory performance. In the zoomed portion of the upper plot, it is demonstrated that the output of the system under control law (2.3) does not converge with the same accuracy as those obtained through the other

Table 3.1.: Parameters of Applied Controllers

Controller	Parameter	Simulation Case		
		1 st	2 nd	3 rd
Anti-Windup Scheme	k_1	6.1	14	21.8
	k_2	4.7	4.7	14.2
	k_3	1	1	3
Conventional STA	k_1	5.5	5.5	12.4
	k_2	4.7	4.7	14.2
Saturated STA in [Cas+16b; Cas+16a]	k_1	4	4	—
	k_2	4.7	4.7	—
Saturated STA in Chapter 2	k_1	4	4	—
	k_2	10.7	10.7	—
	k_3	2.5	2.5	—
	ϵ	0.18	0.18	—

algorithms. This is due to the fact that in this approach, L_a needs to be a portion of the limit ρ and therefore there is no chance both inequalities (2.9) and (2.43) are satisfied in the case a_M is close to ρ . The values given in Table 3.1 for this controller in the second simulation case are assigned such that the absolute value of the control signal is confined to ρ .

3.4.3. Third Case

In this case, in addition to perturbations, uncertainties and multiplicative unknowns are taken into consideration as

$$a(t, z) = 1 + 0.6 \sin(t) + 0.4 \sin(5t) + 0.4 \cos(z), \quad (3.26a)$$

$$b(t, z) = 0.8 + 0.1 \sin(t) + 0.1 \cos(z). \quad (3.26b)$$

It is noted that $b(t, z)$ is lower bounded by $b_m = 0.6$ and therefore, $a(t, z)$ needs to be bounded by $a_M < 3$ (according to (3.3)). As mentioned before, this problem setting is not dealt with in [Cas+16b; Cas+16a] and the previous chapter. Thus, simulation response curves obtained through the system under control laws (3.4) and (1.3) are compared in this scenario. The selected control parameters are listed in Table 3.1. The simulation is carried out with the same initial condition as the last case. It can be clearly seen in Figure 3.4 that the windup effect is also mitigated in this performance of the proposed approach. The precision is different comparing to the result of the conventional STA due to the difference in the parameter values, but it is satisfactory in both the algorithms.

3. An Anti-Windup Strategy for the Super-Twisting Algorithm

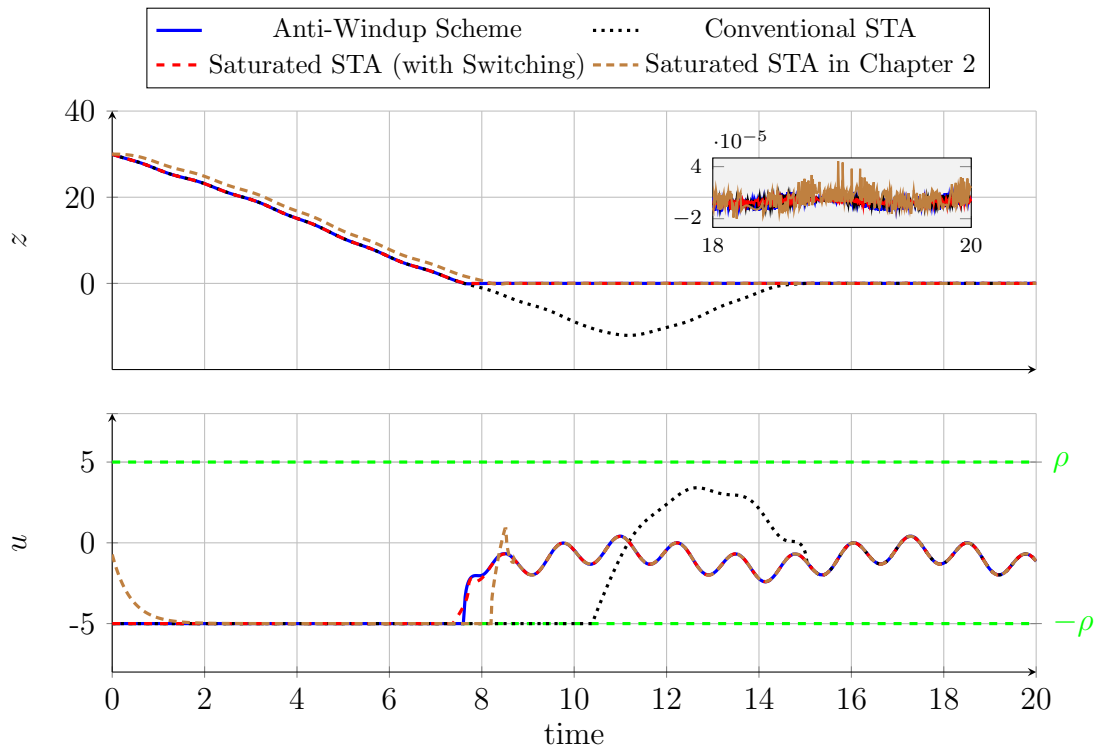


Figure 3.2.: Simulation response curves of the first case obtained through the system under four different control laws (3.4), (1.3), (2.44) with $\bar{\nu} = 0$, and (2.3), which are labeled respectively with Proposed Scheme, Conventional STA, Saturated STA in [Cas+16b], and Saturated STA presented in the previous chapter.

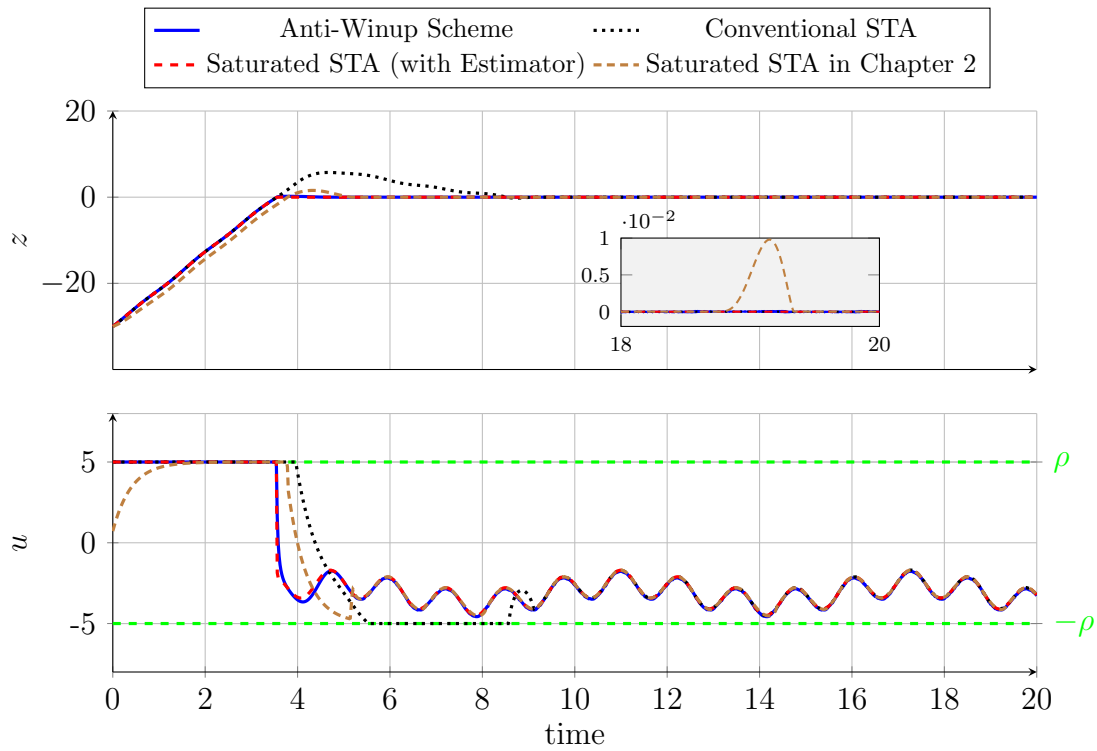


Figure 3.3.: Simulation results of the second case comparing the proposed approach with the conventional STA, the saturated STA applying the disturbance estimator as presented in [Cas+16a], as well as the saturated version of STA given in Chapter 2.

3. An Anti-Windup Strategy for the Super-Twisting Algorithm

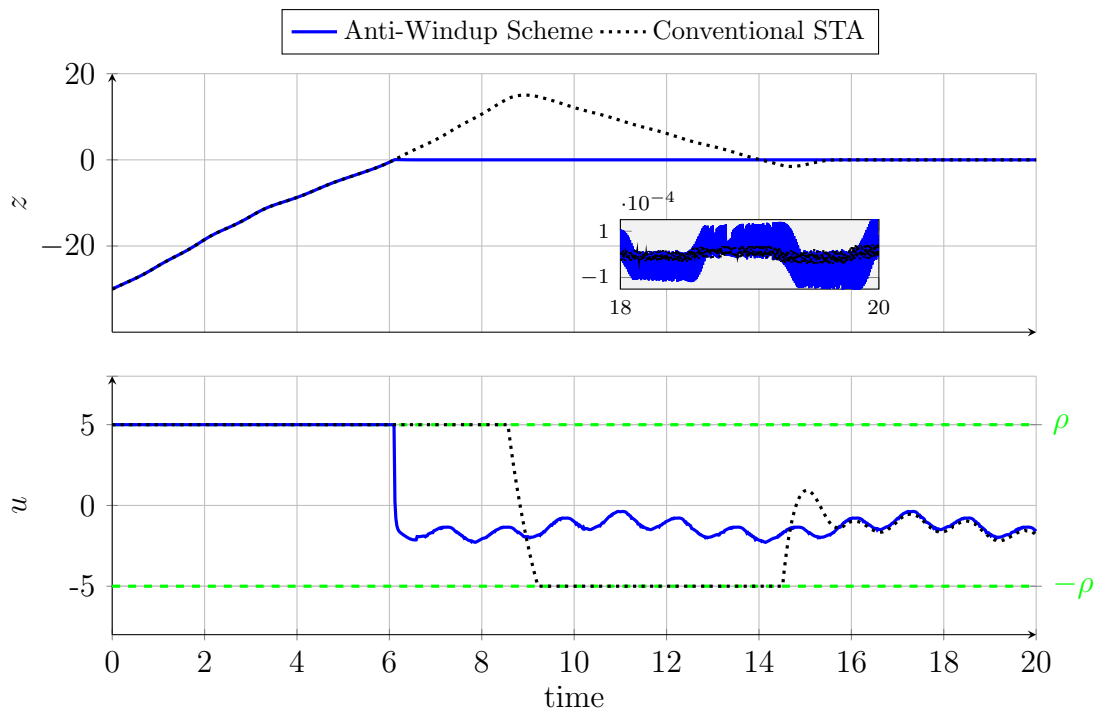


Figure 3.4.: The system output z and control input u simulated in the third case, where the system is affected by uncertainties and disturbances. The results obtained through the proposed approach and the conventional STA are compared since uncertainties and multiplicative unknowns are not addressed in [Cas+16b; Cas+16a] and the previous chapter.

Part II.
Second-Order System

4. Saturated Continuous Twisting Algorithm

In this chapter, system (1.6), which is also known as the perturbed double integrator system, is taken into consideration. Investigations of two scenarios are conducted:

- 4.i. Full State Information: it is assumed that the state z_2 as well as the system output y is available for measurement.
- 4.ii. Output Feedback Control: the output is just measurable and z_2 needs to be estimated.

For both of them, a saturated control scheme based on the continuous twisting algorithm is introduced. In the latter scenario, the first-order robust exact differentiator is used as a state observer.

4.1. Problem Statement

For system (1.6), the following assumption is made.

Assumption 4.1. *The function \bar{a} is globally bounded and Lipschitz continuous with respect to time, i.e.*

$$|\bar{a}(t)| \leq \bar{a}_M < \rho \quad \text{and} \quad \left| \frac{d\bar{a}}{dt} \right| \leq L_{\bar{a}}, \quad \forall t \geq 0, \quad (4.1)$$

where the constants \bar{a}_M and $L_{\bar{a}}$ are known. It is noted that the inequality $\bar{a}_M < \rho$ has to be satisfied due to the same reason as explained in Remark 2.1 (to ensure that $z_2 = 0$ is an equilibrium state of system (1.6) for every admissible function \bar{a}).

In this chapter, it is aimed at designing a control law for the aforementioned second-order system such that the system states z_1 and z_2 tend to the origin in a finite time and the control signal u is continuous everywhere and confined to the saturation bounds.

4. Saturated Continuous Twisting Algorithm

Remark 4.1. The objective cannot be achieved by applying the aforementioned saturated super-twisting algorithm and anti-windup strategy to this system. Let's define a sliding function as

$$\sigma = z_2 + \lambda z_1, \quad (4.2)$$

where λ is a positive constant. Its time derivative reads as

$$\frac{d\sigma}{dt} = u + \bar{a} + \lambda z_2. \quad (4.3)$$

If $\bar{a} + \lambda z_2$ is considered as perturbations and uncertainties, bounds of z_2 , which cannot be realized from a saturated control input, need to be known. In the case λz_2 is compensated through the saturated super-twisting control law as

$$u = -\lambda z_2 - k_1 \text{sat}_\epsilon \left([\sigma]^{\frac{1}{2}} \right) + \nu, \quad (4.4a)$$

$$\frac{d\nu}{dt} = -k_2 [\sigma]^0 - k_3 \nu, \quad |\nu_0| \leq \frac{k_2}{k_3}, \quad (4.4b)$$

the absolute value of the generated control signal is not bounded by a calculable constant anymore. If this term is incorporated into the controller designed in Chapter 3 as

$$u = -\lambda z_2 - k_1 [\sigma]^{\frac{1}{2}} + \nu, \quad (4.5a)$$

$$\frac{d\nu}{dt} = -k_2 [\sigma]^0 - k_3 \beta \nu, \quad |\nu_0| \leq \frac{k_2}{k_3}, \quad (4.5b)$$

the stability properties established therein may be violated. Exemplarily, in the case $|u| > \rho$, σ and u may have the same sign in contrast to that derived in (3.7).

4.2. Saturated Continuous Twisting Control

Full State Information: assuming that the states z_1 and z_2 are available, the proposed saturated and continuous control input is obtained through

$$u = -k_1 \text{sat}_{\epsilon_1} \left([z_1]^{\frac{1}{3}} \right) - k_2 \text{sat}_{\epsilon_2} \left([z_2]^{\frac{1}{2}} \right) + \nu, \quad (4.6a)$$

$$\frac{d\nu}{dt} = -k_3 [z_1]^0 - k_4 \nu, \quad |\nu_0| \leq \frac{k_3}{k_4}, \quad (4.6b)$$

where the initial value ν_0 as well as the positive constants k_1 , ϵ_1 , k_2 , ϵ_2 , k_3 , and k_4 need to be selected appropriately. Similar to that illustrated in Figure 2.1, it can be shown that

$$\begin{aligned} \left| \text{sat}_{\epsilon_1} \left([z_1]^{\frac{1}{3}} \right) \right| &\leq \epsilon_1, & \forall z_1, \\ \left| \text{sat}_{\epsilon_2} \left([z_2]^{\frac{1}{2}} \right) \right| &\leq \epsilon_2, & \forall z_2. \end{aligned} \quad (4.7)$$

Sufficient conditions for choosing the control parameters are given later in the next section. Block diagrams of the standard continuous twisting control and the saturated version for the Full State Information scenario are compared in Figure 4.1.

Remark 4.2. The term $\lceil z_2 \rceil^0$ within the continuous twisting algorithm presented in [Tor+17] is omitted in (4.6). This is due to the fact that it does not contribute to the stability of the origin of the closed-loop system.

Lemma 4.1. *If the initial value ν_0 is chosen such that $|\nu_0| \leq \nu_M$ is satisfied, where $\nu_M = \frac{k_3}{k_4}$, then the actuating signal u is bounded by*

$$|u(t)| \leq k_1 \epsilon_1 + k_2 \epsilon_2 + \nu_M, \quad \forall t \geq 0. \quad (4.8)$$

Proof. Similar to that proved in Lemma 2.1, It is derived that ν is bounded by

$$|\nu(t)| \leq \nu_M, \quad \forall t \geq 0, \quad (4.9)$$

where $|\nu_0| \leq \nu_M$ is met. The upper bound of $|u|$ in (4.8) is realized based on inequalities (4.7) and (4.9). \square

Output Feedback Control: If the state z_2 is not measurable, it is replaced in (4.6a) with its estimate \hat{z}_2 as

$$u = -k_1 \text{sat}_{\epsilon_1} \left(\lceil z_1 \rceil^{\frac{1}{3}} \right) - k_2 \text{sat}_{\epsilon_2} \left(\lceil \hat{z}_2 \rceil^{\frac{1}{2}} \right) + \nu, \quad (4.10a)$$

$$\frac{d\nu}{dt} = -k_3 \lceil z_1 \rceil^0 - k_4 \nu, \quad |\nu_0| \leq \nu_M. \quad (4.10b)$$

In [SMF18], the estimation obtained through the first-order as well as second-order RED is incorporated into the output feedback design of the continuous twisting algorithm. The closed-loops performances applying these two observers are compared therein and it is shown that under discrete-time measurements, the accuracy is improved in the case that the second-order RED is used. However, employing this order of the differentiator makes the continuous twisting control approach redundant since perturbations are reconstructed through the estimator as well as the controller. Therefore, for the saturated continuous twisting algorithm, the estimation is provided via a super-twisting observer designed as

$$e_1 = z_1 - \tilde{z}_1, \quad (4.11a)$$

$$\frac{d\tilde{z}_1}{dt} = \mu_1 \lceil e_1 \rceil^{\frac{1}{2}} + \hat{z}_2, \quad (4.11b)$$

$$\frac{d\hat{z}_2}{dt} = u + \mu_2 \lceil e_1 \rceil^0, \quad (4.11c)$$

where \tilde{z}_1 is an auxiliary variable and μ_1 and μ_2 are positive values to be chosen appropriately, see e.g. [Lev98; DFL05].

4. Saturated Continuous Twisting Algorithm

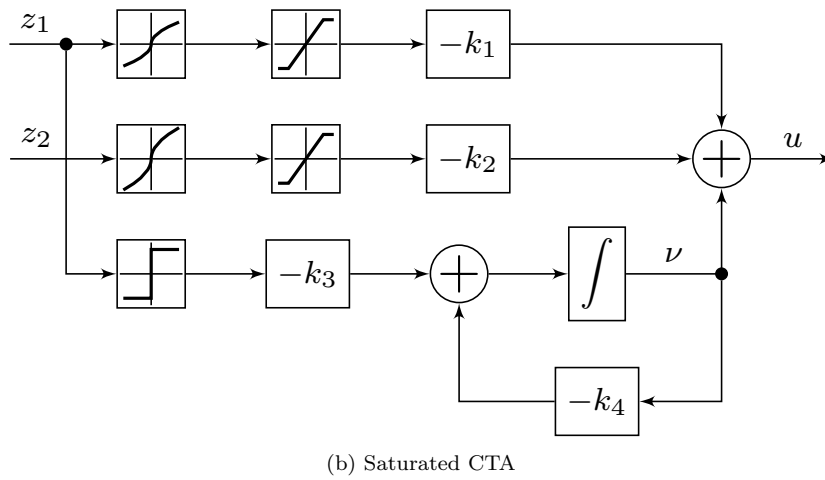
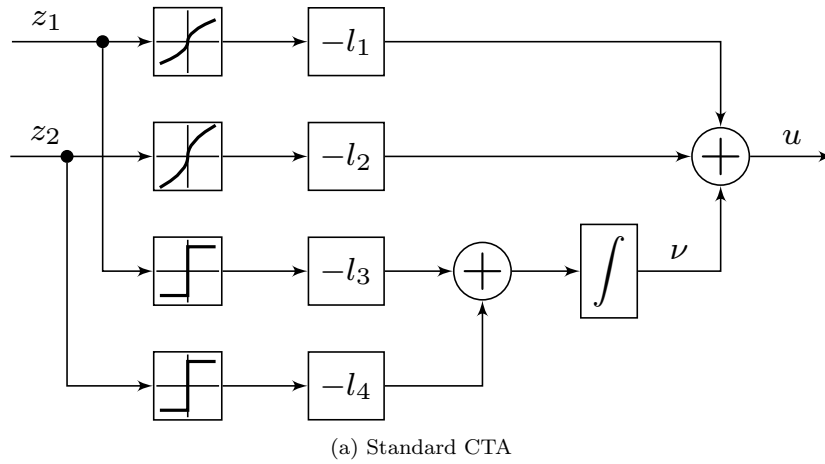


Figure 4.1.: Block diagrams of standard continuous twisting control (1.7) and the saturated version proposed in this chapter for the Full State Information scenario.

Remark 4.3. It is noted that the upper bound of the absolute value of the control input (4.10) remains the same as that one presented in Lemma 4.1.

4.3. Stability Analysis

For the closed loops, with and without observer, global finite-time stability properties are established in this section.

4.3.1. Full State Information

For system (1.6) under control law (4.6), the closed-loop dynamics reads as

$$\frac{dx_1}{dt} = x_2, \quad (4.12a)$$

$$\frac{dx_2}{dt} = -k_1 \text{sat}_{\epsilon_1} \left([x_1]^{\frac{1}{3}} \right) - k_2 \text{sat}_{\epsilon_2} \left([x_2]^{\frac{1}{2}} \right) + x_3, \quad (4.12b)$$

$$\frac{dx_3}{dt} = -k_3 [x_1]^0 - k_4 x_3 + \bar{\phi}(t), \quad (4.12c)$$

where the state vector is defined as

$$\mathbf{x} = [x_1 \quad x_2 \quad x_3]^T = [z_1 \quad z_2 \quad \nu + \bar{a}]^T. \quad (4.13)$$

Suppose that the inequalities given in (4.1) are fulfilled, then $\bar{\phi}(t) = k_4 \bar{a} + \frac{d\bar{a}}{dt}$ in the closed-loop system is bounded, i.e.

$$|\bar{\phi}(t)| \leq \bar{\phi}_M = k_4 \bar{a}_M + L_{\bar{a}}, \quad \forall t \geq 0. \quad (4.14)$$

Proposition 4.1. *There exist constants \bar{k}_1 , \bar{k}_2 , and \bar{k}_3 such that for any positive real value $\bar{\phi}_M$, choosing the control constants as*

$$k_1 = \bar{\phi}_M^{\frac{2}{3}} \bar{k}_1, \quad k_2 = \bar{\phi}_M^{\frac{1}{2}} \bar{k}_2, \quad k_3 = \bar{\phi}_M \bar{k}_3 \quad (4.15)$$

guarantees that if

$$\frac{1}{2} k_1 \epsilon_1 = k_2 \epsilon_2 > \frac{k_3}{k_4} + \bar{a}_M, \quad (4.16a)$$

$$\rho \geq k_1 \epsilon_1 + k_2 \epsilon_2 + \frac{k_3}{k_4} \quad (4.16b)$$

hold, then the origin $\mathbf{x} = \mathbf{0}$ is globally finite-time stable and the actuator is not saturated, i.e. $u \in [-\rho, \rho]$ for all $t \geq 0$.

Remark 4.4. Similar to Chapter 2, SOSTOOLS [Pap+13] can be employed to determine the values of \bar{k}_1 , \bar{k}_2 , and \bar{k}_3 . Having solved the sum-of-squares problem formulated within the following proof, they can be assigned as

$$\bar{k}_1 = 9, \quad \bar{k}_2 = 5, \quad \bar{k}_3 = 1.1. \quad (4.17)$$

4. Saturated Continuous Twisting Algorithm

Proof. The case $|x_1|^{\frac{1}{3}} \leq \epsilon_1$ and $|x_2|^{\frac{1}{2}} \leq \epsilon_2$ leads to the closed-loop system

$$\frac{dx_1}{dt} = x_2, \quad (4.18a)$$

$$\frac{dx_2}{dt} = -k_1 [x_1]^{\frac{1}{3}} - k_2 [x_2]^{\frac{1}{2}} + x_3, \quad (4.18b)$$

$$\frac{dx_3}{dt} = -k_3 [x_1]^0 - k_4 x_3 + \bar{\phi}(t). \quad (4.18c)$$

The control gains k_1 , k_2 and k_3 are scaled for all $\bar{\phi}_M > 0$ as given in (4.15). Changing the coordinates in (4.18) as

$$\mathbf{x} = \bar{\phi}_M \boldsymbol{\zeta} = \bar{\phi}_M \begin{bmatrix} \zeta_1 & \zeta_2 & \zeta_3 \end{bmatrix}^T \quad (4.19)$$

yields

$$\frac{d\zeta_1}{dt} = \zeta_2, \quad (4.20a)$$

$$\frac{d\zeta_2}{dt} = -\bar{k}_1 [\zeta_1]^{\frac{1}{3}} - \bar{k}_2 [\zeta_2]^{\frac{1}{2}} + \zeta_3, \quad (4.20b)$$

$$\frac{d\zeta_3}{dt} = -\bar{k}_3 [\zeta_1]^0 - k_4 \zeta_3 + \frac{\bar{\phi}(t)}{\bar{\phi}_M}. \quad (4.20c)$$

Similar to system (2.38), $\frac{|\bar{\phi}(t)|}{\bar{\phi}_M} \leq 1$ holds for all $t \geq 0$ (based on (4.14)) and system (4.20) is not a weighted homogeneous system (due to the presence of the linear term $-k_4 \zeta_3$). It is, however, possible to use the Lyapunov function candidate considered in [Tor+17] based on the homogeneous generalized form function as

$$V(\boldsymbol{\zeta}) = \alpha_1 |\zeta_1|^{\frac{5}{3}} + \alpha_2 \zeta_1 \zeta_2 + \alpha_3 |\zeta_2|^{\frac{5}{2}} + \alpha_4 \zeta_1 [\zeta_3]^2 - \alpha_5 \zeta_2 \zeta_3^3 + \alpha_6 |\zeta_3|^5, \quad (4.21)$$

where the coefficient vector is defined as $\boldsymbol{\alpha} = [\alpha_1 \ \cdots \ \alpha_6]^T \in \mathbb{R}^6$. It is differentiable and homogeneous of degree five with the weights $\mathbf{r} = [3 \ 2 \ 1]^T$. Taking the time derivative of V in (4.21) along the trajectories of system (4.20) gives

$$\frac{dV}{dt} = -(W_1 + W_2). \quad (4.22)$$

The function W_1 , which is similar to the derived function for the unperturbed case in [Tor+17], reads as

$$\begin{aligned} W_1(\boldsymbol{\zeta}) &= \beta_1 |\zeta_1|^{\frac{4}{3}} + \beta_2 \zeta_1 [\zeta_2]^{\frac{1}{2}} - \beta_3 [\zeta_1]^{\frac{2}{3}} \zeta_2 + \beta_4 [\zeta_1]^{\frac{1}{3}} [\zeta_2]^{\frac{3}{2}} + \beta_5 |\zeta_2|^2 \\ &\quad - \beta_6 \zeta_1 \zeta_3 + \beta_7 |\zeta_1| |\zeta_3| - \beta_8 [\zeta_1]^{\frac{1}{3}} \zeta_3^3 + \beta_9 [\zeta_1]^0 [\zeta_3]^4 - \beta_{10} [\zeta_2]^{\frac{3}{2}} \zeta_3 \\ &\quad - \beta_{11} \zeta_2 [\zeta_3]^2 - \beta_{12} [\zeta_2]^{\frac{1}{2}} \zeta_3^3 - \beta_{13} [\zeta_1]^0 \zeta_2 |\zeta_3|^2 + \beta_{14} |\zeta_3|^4, \end{aligned} \quad (4.23)$$

where the coefficients are

$$\begin{aligned}
 \beta_1 &= \alpha_2 \bar{k}_1, & \beta_2 &= \alpha_2 \bar{k}_2, & \beta_3 &= \frac{5}{3} \alpha_1, & \beta_4 &= \frac{5}{2} \alpha_3 \bar{k}_1, \\
 \beta_5 &= \frac{5}{2} \alpha_3 \bar{k}_2 - \alpha_2, & \beta_6 &= \alpha_2, & \beta_7 &= 2\alpha_4 \bar{k}_3, & \beta_8 &= \alpha_5 \bar{k}_1, \\
 \beta_9 &= 5\alpha_6 \bar{k}_3, & \beta_{10} &= \frac{5}{2} \alpha_3, & \beta_{11} &= \alpha_4, & \beta_{12} &= \alpha_5 \bar{k}_2, \\
 \beta_{13} &= 3\alpha_5 \bar{k}_3, & \beta_{14} &= \alpha_5.
 \end{aligned} \tag{4.24}$$

The function W_2 in (4.22) is written as

$$W_2(\zeta) = -\beta_{15} \zeta_1 |\zeta_3| + \beta_{16} \zeta_2 |\zeta_3|^2 - \beta_{17} [\zeta_3]^4, \tag{4.25}$$

where the coefficients denote

$$\begin{bmatrix} \beta_{15} & \beta_{16} & \beta_{17} \end{bmatrix}^T = \begin{bmatrix} 2\alpha_4 & 3\alpha_5 & 5\alpha_6 \end{bmatrix}^T \Xi, \tag{4.26}$$

with $\Xi = \frac{-k_4 \nu + \frac{d\bar{a}}{dt}}{\bar{\phi}_M}$. It is worth mentioning that both W_1 and W_2 are discontinuous homogeneous functions of degree four. Furthermore, the coefficients β_{15} , β_{16} , and β_{17} are bounded by some known constants (according to (4.9) and (4.1)). In order to determine conditions of the control parameters k_1 , k_2 , and k_3 and the coefficients α such that $W_1 + W_2$ as well as V is positive definite, a quadrant analysis as proposed in [SM14; Tor+17] is carried out in Appendix B. Please note that the other constants ϵ_1 , ϵ_2 , and k_4 do not play a role in the formulation of the sum-of-squares problem mentioned therein and they come into play in the following.

In the case that $|x_1|^{\frac{1}{3}} > \epsilon_1$ and $|x_2|^{\frac{1}{2}} > \epsilon_2$, (4.12a) and (4.12b) read as

$$\frac{dx_1}{dt} = x_2, \tag{4.27a}$$

$$\frac{dx_2}{dt} = -k_1 \epsilon_1 [x_1]^0 - k_2 \epsilon_2 [x_2]^0 + x_3. \tag{4.27b}$$

The twisting algorithm is recovered since the defined variable x_3 is bounded (according to (4.9) and (4.1)) by

$$|x_3| \leq \eta_M = \nu_M + \bar{a}_M, \quad \forall t \geq 0. \tag{4.28}$$

Having selected the control parameters ϵ_1 , ϵ_2 , and k_4 such that (4.16a) is satisfied, the states x_1 and x_2 drive to the origin (see e.g. [Sht+14]) and therefore the previous scenario or one of the following cases occurs.

For $|x_1|^{\frac{1}{3}} > \epsilon_1$ and $|x_2|^{\frac{1}{2}} \leq \epsilon_2$, the aforementioned closed-loop system is rewritten as

$$\frac{dx_1}{dt} = x_2, \tag{4.29a}$$

$$\frac{dx_2}{dt} = -k_1 \epsilon_1 [x_1]^0 - k_2 [x_2]^{\frac{1}{2}} + x_3, \tag{4.29b}$$

4. Saturated Continuous Twisting Algorithm

where (4.28) holds. If $|x_1|^{\frac{1}{3}} \leq \epsilon_1$ and $|x_2|^{\frac{1}{2}} > \epsilon_2$, having considered the boundedness of x_3 , the closed-loop system is represented as

$$\frac{dx_1}{dt} = x_2, \quad (4.30a)$$

$$\frac{dx_2}{dt} = -k_1 [x_1]^{\frac{1}{3}} - k_2 \epsilon_2 [x_2]^0 + x_3. \quad (4.30b)$$

For these two cases, the following local Lyapunov functions are introduced in [Gol+18b], which can guarantee the boundedness of the states. Therein, the proposed Lyapunov function candidate for (4.29) is

$$V_1(x_1, x_2) = k_1 \epsilon_1 |x_1| + \frac{1}{2} x_2^2 + \frac{k_2}{\epsilon_2} x_1 x_2 - x_1 x_3. \quad (4.31)$$

Since x_2 as well as x_3 is bounded in this case, this function is positive definite if (4.16a) is satisfied. Differentiating V_1 along the trajectories of (4.29) gives

$$\frac{dV_1}{dt} \leq -\frac{k_2}{\epsilon_2} |x_1| \left(k_1 \epsilon_1 + k_2 \epsilon_2 [x_1]^0 [x_2]^0 - \left(\eta_M + \frac{(2k_3 + L_{\bar{a}}) \epsilon_2}{k_2} \right) [x_1]^0 \right), \quad (4.32)$$

where $2k_3 + L_{\bar{a}}$ is the upper bound of $|\frac{dx_3}{dt}|$ in (4.12c). It can be seen that $\frac{dV_1}{dt}$ is globally negative semi-definite if

$$k_1 \epsilon_1 > k_2 \epsilon_2 + \eta_M + \frac{(2k_3 + L_{\bar{a}}) \epsilon_2}{k_2} \quad (4.33)$$

is fulfilled. Having compared the aforementioned condition with that one imposed in (4.16a), it is revealed that satisfying the relaxed sufficient condition set here in Proposition 4.1 does not result in the global negative semi-definiteness of $\frac{dV_1}{dt}$. A Lyapunov function candidate for (4.30) is presented in [Gol+18b] as

$$V_2(x_1, x_2) = |x_1|^{\frac{4}{3}} + \frac{2}{3k_1} x_2^2. \quad (4.34)$$

It becomes evident that the radially unbounded function V_2 is globally positive definite. Its time derivative along the trajectories of (4.30) yields

$$\frac{dV_2}{dt} \leq -\frac{4}{3k_1} |x_2| \left(k_2 \epsilon_2 - \eta_M [x_2]^0 \right). \quad (4.35)$$

If (4.16a) is met, the globally negative semi-definiteness of $\frac{dV_2}{dt}$ is ensured, which implies that x_2 is bounded.

The convergence of the states cannot be guaranteed through the Lyapunov functions V_1 and V_2 . However, it is derived intuitively from the aforementioned arguments that

the system trajectory in the corresponding cases cannot escape far away from the standard trajectory of the twisting algorithm. A mathematical explanation contributes here to the global stability proof of the closed-loop system origin. Intersections of a majorant curve with a straight line parallel to the axis $x_1 = 0$ drawn at $x_1 = \epsilon_1^3$ as well as straight lines parallel to the axis $x_2 = 0$ passing through $x_2 = \pm\epsilon_2^2$ for $x_1 > 0$ (see Figure 4.2) are computed. It is shown in the following that $|x_{2,M}| < |x_{2,0}|$ is always met if (4.16a) holds, which implies the states convergence. The majorant trajectory of (4.29) for $x_1 > 0$ is pointed out in Figure 4.2 by $x_{1,1}$, $x_{1,M}$, and $x_{1,2}$. It can be represented by

$$x_2 \frac{dx_2}{dx_1} = \begin{cases} -k_2 x_2^{\frac{1}{2}} - k_1 \epsilon_1 + \eta_M & \text{for } x_2 > 0, \\ k_2 (-x_2)^{\frac{1}{2}} - k_1 \epsilon_1 - \eta_M & \text{for } x_2 \leq 0, \end{cases} \quad (4.36)$$

where η_M is given in (4.28). The curve intersects the axis $x_2 = 0$ at the point $x_{1,M}$, which can be determined through the solution of (4.36) for $x_2 > 0$ based on $x_{1,1}$ (the intersection with $x_2 = \epsilon_2^2$) as

$$x_{1,M} = x_{1,1} - \frac{2(k_1 \epsilon_1 - \eta_M)^3 \ln(k_1 \epsilon_1 - \eta_M + k_2 \epsilon_2)}{k_2^4} + \frac{2(k_1 \epsilon_1 - \eta_M)^2 \epsilon_2}{k_2^3} - \frac{(k_1 \epsilon_1 - \eta_M) \epsilon_2^2}{k_2^2} + \frac{2\epsilon_2^3}{3k_2} + \frac{2(k_1 \epsilon_1 - \eta_M)^3 \ln(k_1 \epsilon_1 - \eta_M)}{k_2^4}. \quad (4.37)$$

Having calculated the solution of (4.36) for $x_2 \leq 0$, $x_{1,2}$ (the intersection with $x_2 = -\epsilon_2^2$) based on $x_{1,M}$ is derived as

$$x_{1,2} = x_{1,M} + \frac{2(k_1 \epsilon_1 + \eta_M)^3 \ln(k_1 \epsilon_1 + \eta_M - k_2 \epsilon_2)}{k_2^4} + \frac{2(k_1 \epsilon_1 + \eta_M)^2 \epsilon_2}{k_2^3} + \frac{(k_1 \epsilon_1 + \eta_M) \epsilon_2^2}{k_2^2} + \frac{2\epsilon_2^3}{3k_2} - \frac{2(k_1 \epsilon_1 + \eta_M)^3 \ln(k_1 \epsilon_1 + \eta_M)}{k_2^4}. \quad (4.38)$$

If the control parameters are selected as given in (4.16a), substituting (4.37) into (4.38) gives

$$x_{1,2} = x_{1,1} - \frac{1}{k_2^4} q \quad (4.39)$$

with

$$q = 2(k_1^3 \epsilon_1^3 + 3k_1 \epsilon_1 \eta_M^2) \ln(q_1) + 2(\eta_M^3 + 3k_1^2 \epsilon_1^2 \eta_M) \ln(q_2) - \frac{28}{24} k_1^3 \epsilon_1^3 - k_1 \epsilon_1 \eta_M^2 - \frac{1}{2} k_1^2 \epsilon_1^2 \eta_M.$$

4. Saturated Continuous Twisting Algorithm

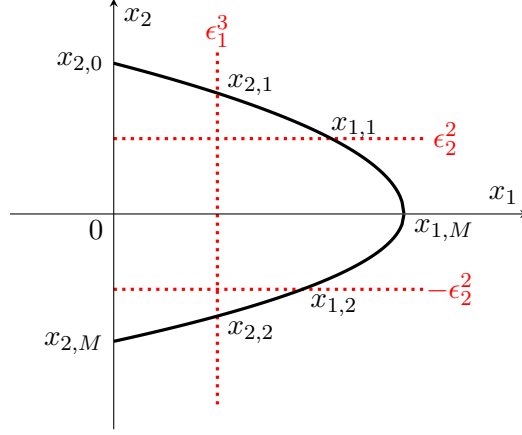


Figure 4.2.: A majorant trajectory for the saturated continuous twisting algorithm.

The bounds of q_1 and q_2 are obtained as

$$2.77 < q_1 = \frac{\left(\frac{3}{2}k_1\epsilon_1 - \eta_M\right) \left(k_1\epsilon_1 + \eta_M\right)}{\left(k_1\epsilon_1 - \eta_M\right) \left(\frac{1}{2}k_1\epsilon_1 + \eta_M\right)} < 3, \quad (4.40)$$

$$0.75 < q_2 = \frac{\left(k_1\epsilon_1 + \eta_M\right) \left(k_1\epsilon_1 - \eta_M\right)}{\left(\frac{1}{2}k_1\epsilon_1 + \eta_M\right) \left(\frac{3}{2}k_1\epsilon_1 - \eta_M\right)} < 1.34. \quad (4.41)$$

Therefore, the lower bound of q is calculated as

$$q > 0.83k_1^3\epsilon_1^3 + 5k_1\epsilon_1\eta_M^2 - 0.58\eta_M^3 - 2.24k_1^2\epsilon_1^2\eta_M > 0. \quad (4.42)$$

This implies that $x_{1,2}$ is smaller than $x_{1,1}$. The points $x_{2,1}$ and $x_{2,2}$ of intersection with $x_1 = \epsilon_1^3$ can be obtained through the majorant trajectory of the twisting algorithm realized in (4.27). For $x_1 > 0$, this differential equation is rewritten as

$$\frac{d^2x_1}{dt^2} = \begin{cases} -k_1\epsilon_1 - k_2\epsilon_2 + \eta_M & \text{for } x_2 > 0, \\ -k_1\epsilon_1 + k_2\epsilon_2 - \eta_M & \text{for } x_2 \leq 0, \end{cases} \quad (4.43)$$

where η_M , as mentioned above, is the upper bound of $|x_3|$. By solving (4.43), the aforementioned points are easily computed based on $x_{1,1}$ and $x_{1,2}$ as

$$x_{2,1}^2 = 2(x_{1,1} - \epsilon_1^3) \left(k_1\epsilon_1 + k_2\epsilon_2 - \eta_M\right) + \epsilon_2^4, \quad (4.44)$$

$$x_{2,2}^2 = 2(x_{1,2} - \epsilon_1^3) \left(k_1\epsilon_1 - k_2\epsilon_2 + \eta_M\right) + \epsilon_2^4. \quad (4.45)$$

Since $x_{1,2} < x_{1,1}$ holds, it can be concluded that $|x_{2,2}| < |x_{2,1}|$ is met if (4.16a) is satisfied. Finally, the majorant trajectory of (4.30) for $x_1 > 0$ needs to be considered

in order to determine the points $x_{2,0}$ and $x_{2,M}$. It can be denoted by

$$x_2 \frac{dx_2}{dx_1} = \begin{cases} -k_1 x_1^{\frac{1}{3}} - k_2 \epsilon_2 + \eta_M & \text{for } x_2 > 0, \\ -k_1 x_1^{\frac{1}{3}} + k_2 \epsilon_2 - \eta_M & \text{for } x_2 \leq 0, \end{cases} \quad (4.46)$$

where x_3 is replaced with its bounds η_M and $-\eta_M$. The curve intersections with the axis $x_1 = 0$ are achieved based on $x_{2,1}$ and $x_{2,2}$ through the solution of (4.46) for $x_2 > 0$ and $x_2 \leq 0$ respectively. They read as

$$x_{2,0}^2 = x_{2,1}^2 + 2 \left(\frac{3}{4} k_1 \epsilon_1 + k_2 \epsilon_2 - \eta_M \right) \epsilon_1^3, \quad (4.47)$$

$$x_{2,M}^2 = x_{2,2}^2 + 2 \left(\frac{3}{4} k_1 \epsilon_1 - k_2 \epsilon_2 + \eta_M \right) \epsilon_1^3. \quad (4.48)$$

Having fulfilled (4.16a), $|x_{2,M}| < |x_{2,0}|$ is guaranteed owing to that $|x_{2,2}|$ is smaller than $|x_{2,1}|$. It can be carried out similarly for the half-plane $x_1 \leq 0$.

This completes the global asymptotic stability proof of the origin $\mathbf{x} = \mathbf{0}$ in the Full State Information scenario. Similar to that mentioned in Lemma 2.2, the conditions of the quasihomogeneity principle are satisfied since

- the right-hand side of differential equation (4.12) consists of a locally homogeneous piece-wise continuous function of degree $q_{\text{CTA}} = -1$ with respect to dilation $r_{\text{CTA}} = (3, 2, 1)$;
- the components of the continuous function $-k_4 x_3 + \bar{\phi}(t)$ are globally bounded (according to the boundedness of ν , \bar{a} , and $\frac{d\bar{a}}{dt}$);
- system (4.12) is globally asymptotically stable around the origin.

Consequently, the finite-time convergence of the state vector \mathbf{x} is realized applying this principle. Furthermore, according to Lemma 4.1, it is ensured that the control input is bounded for any $z_{1,0}, z_{2,0} \in \mathbb{R}$. In order to retain it within the given saturation bounds $-\rho$ and ρ , it is sufficient that the control constants are chosen such that (4.16b) holds. \square

Remark 4.5. It is inferred from the conditions of the control gains laid down in (4.15) that

$$k_3 > k_4 \bar{a}_M + L_{\bar{a}} \quad (4.49)$$

needs to be satisfied. Having also considered (4.16), it is deduced that perturbations with $\bar{a}_M < \frac{\rho}{7}$ can be dealt with. Furthermore, disturbances, which change very fast, cannot be handled since $L_{\bar{a}}$ needs to be a portion of the saturation bound ρ . In Chapter 6, a wider class of perturbations with a larger bound \bar{a}_M is addressed applying a novel approach.

4.3.2. Output Feedback Control

In the following, the stability properties of the closed-loop system, in which the observer is incorporated into the design, are investigated.

Proposition 4.2. *Suppose that the assumptions about perturbations as given in (4.1) are satisfied. For system (1.6) under control law (4.10) employing observer (4.11), if the observer constants are selected such that*

$$\mu_1 = 1.5\sqrt{\bar{a}_M}, \quad \mu_2 = 1.1\bar{a}_M \quad (4.50)$$

hold and the control parameters are chosen such that Proposition 4.1 is fulfilled, then the origin of the closed-loop system $\mathbf{x} = \mathbf{0}$ is globally finite-time stable and the continuous actuating signal remains bounded by the given saturation limits $\pm\rho$.

Proof. Having considered observer dynamics (4.11) and defined the error variable $e_2 = z_2 - \hat{z}_2$, the overall closed-loop system using the mapping (4.13) is represented as

$$\frac{dx_1}{dt} = x_2, \quad (4.51a)$$

$$\frac{dx_2}{dt} = -k_1 \text{sat}_{\epsilon_1} \left([x_1]^{\frac{1}{3}} \right) - k_2 \text{sat}_{\epsilon_2} \left([x_2 - e_2]^{\frac{1}{2}} \right) + x_3, \quad (4.51b)$$

$$\frac{dx_3}{dt} = -k_3 [x_1]^0 - k_4 x_3 + \bar{\phi}(t), \quad (4.51c)$$

$$\frac{de_1}{dt} = -\mu_1 [e_1]^{\frac{1}{2}} + e_2, \quad (4.51d)$$

$$\frac{de_2}{dt} = -\mu_2 [e_1]^0 + \bar{a}(t). \quad (4.51e)$$

By taking into account the vector

$$\tilde{\mathbf{x}} = \begin{bmatrix} \tilde{x}_1 & \tilde{x}_2 & \tilde{x}_3 \end{bmatrix}^T = \begin{bmatrix} x_1 & x_2 - e_2 & x_3 \end{bmatrix}^T, \quad (4.52)$$

the subsystem in the variables x_1 , x_2 , and x_3 , i.e. (4.51a) to (4.51c), is rewritten as

$$\frac{d\tilde{x}_1}{dt} = \tilde{x}_2 + e_2, \quad (4.53a)$$

$$\frac{d\tilde{x}_2}{dt} = -k_1 \text{sat}_{\epsilon_1} \left([\tilde{x}_1]^{\frac{1}{3}} \right) - k_2 \text{sat}_{\epsilon_2} \left([\tilde{x}_2]^{\frac{1}{2}} \right) + \tilde{x}_3 - \frac{de_2}{dt}, \quad (4.53b)$$

$$\frac{d\tilde{x}_3}{dt} = -k_3 [\tilde{x}_1]^0 - k_4 \tilde{x}_3 + \bar{\phi}(t). \quad (4.53c)$$

A possible choice of the observer constants is that given in (4.50), see e.g. [Lev98]. As a result of choosing μ_1 and μ_2 properly, the observer errors e_1 and e_2 are bounded and converge to zero in the finite time T . It becomes evident that $\frac{de_2}{dt}$ is also bounded for all $t \geq 0$. A similar geometric approach as mentioned above can be used in order to show that, within cascaded system (4.51), subsystem (4.53) is input-to-state stable with respect to the input $\begin{bmatrix} e_2 & -\frac{de_2}{dt} & 0 \end{bmatrix}^T$. Therefore, it is ensured that the state vector $\tilde{\mathbf{x}}$ remains bounded for all $t \geq 0$. The finite-time convergence of the vector \mathbf{x} , for $t \geq T$, is guaranteed as it is proved for the Full State Information scenario. \square

4.4. Simulation Examples

In this section, it is shown in simulation how the saturated continuous twisting algorithm works in Full State Information and Output Feedback Control. The achieved performance is compared to the results obtained through the standard continuous twisting algorithm presented in (1.7). In both of the scenarios, similar to Chapter 1, it is supposed that the control input is saturated with $\rho = 10$ and the system is subject to perturbations $\bar{a}(t)$ given in (1.8). In order to assess the effectiveness of the proposed approach in this chapter, the constants k_1 , k_2 , and k_3 of control laws (4.6) and (4.10) are chosen as $k_1 = l_1$, $k_2 = l_2$, and $k_3 = l_3$. As it is explained in Remark 4.2, the term $[z_2]^0$ is omitted in saturated CTA. The three other parameters $\epsilon_1 = 0.1$, $\epsilon_2 = 0.39$, and $k_4 = 2$ are set such that (4.16b) and (4.49) are satisfied. The numerical simulation is carried out with the sampling step size of $T_s = 10^{-4}$ s and considering the same initial values as set in Chapter 1.

In the first simulation scenario, Full State Information, it is assumed that both of the system states are measurable and therefore the observer is not employed. In the simulation of Output Feedback Control, super-twisting observer (4.11) is incorporated. Since the addressed disturbances are bounded with $\bar{a}_M = 1.5$, the observer gains $\mu_1 = \mu_2 = 2$ are chosen. The performance of both of the algorithms, saturated CTA and standard CTA, for Output Feedback Control is depicted in Figure 4.3. It is revealed in Figure 4.4 that the observer errors tend to zero in a finite time. Since their convergence is much faster comparing to the convergence of the states, similar performance to that demonstrated in Figure 4.3 is achieved in the case of Full State Information.

It can be clearly seen in the lower plot of Figure 4.3 that due to the structure of the proposed control technique, the produced actuating signal is bounded by the saturation limit specification. It contributes significantly to the mitigation of the windup effect as illustrated in the plots of the states. Large overshoots and undershoots as well as a long settling time can be seen in the response curves of

4. Saturated Continuous Twisting Algorithm

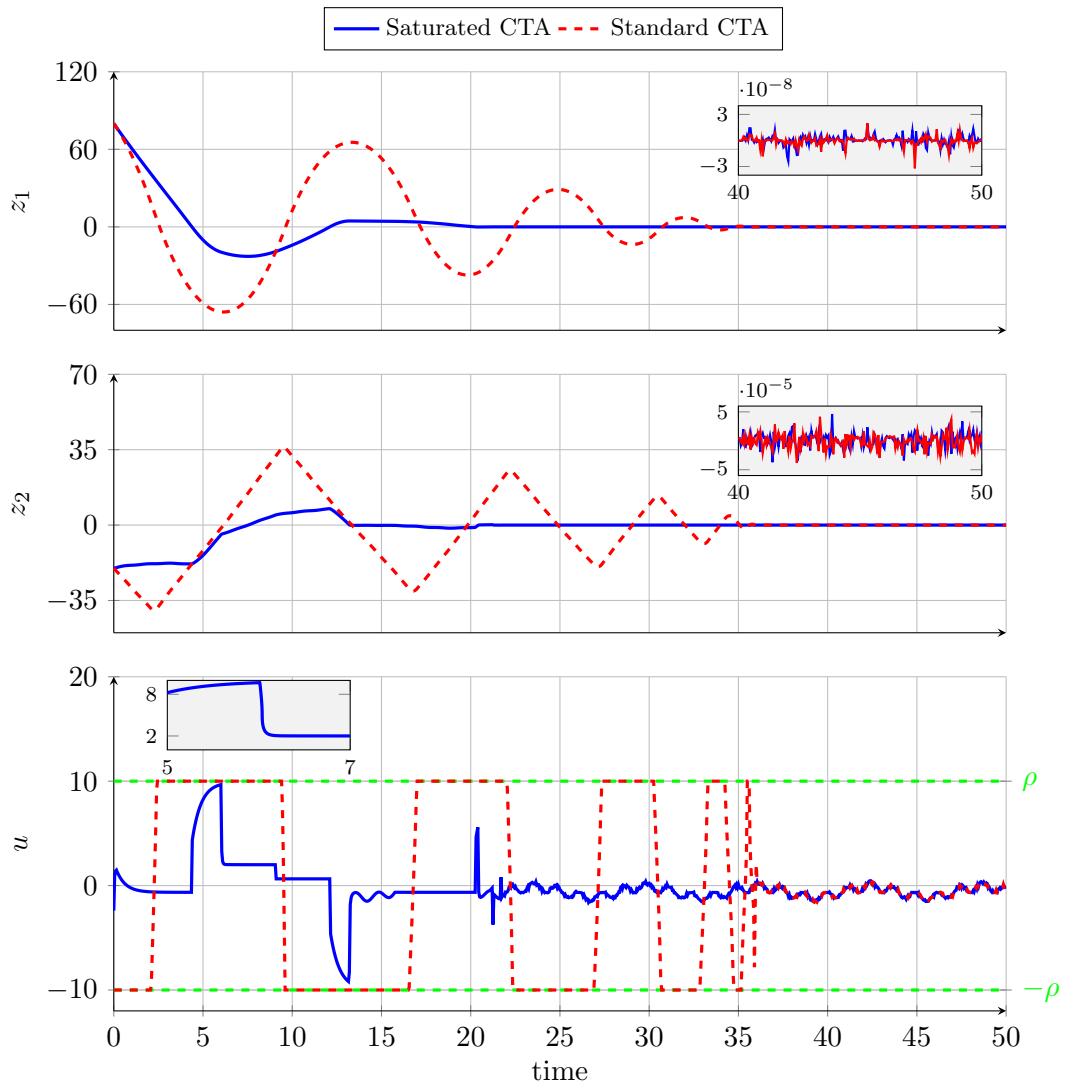


Figure 4.3.: Simulation response curves for Output Feedback Control comparing the proposed scheme with the standard continuous twisting algorithm. Similar results are obtained through the simulation of Full State Information.

standard CTA. As it is indicated in the zoomed portions of the upper and middle plots, for the system under saturated CTA, the finite-time convergence of the states is achieved with the same precision as that one obtained through the standard algorithm. Although the values of the constants ϵ_1 and ϵ_2 are small, it is shown in the zoomed portion of the lower plot that the controller of saturated CTA produces the continuous signal. It is noted that the control signal evolution of standard CTA introduced to the system through the saturating actuator is depicted in the aforementioned plot, which is different from that one generated by the controller.

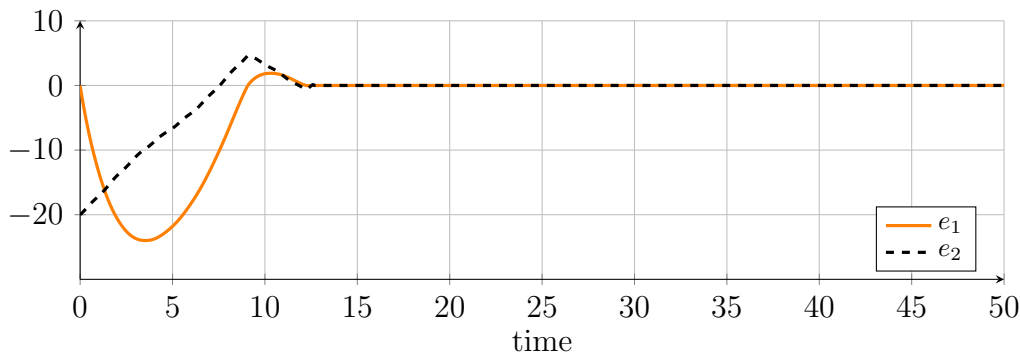


Figure 4.4.: Simulation results of the observer errors, which are unchanging as the algorithm of the controller differs.

4.5. Experimental Implementation

In this section, a system, which represents an ideal platform to test the saturated CTA as well as the standard CTA in a real-world application, is considered. Since only its output is available for measurement, the Output Feedback Control strategy is applied.

Hydraulic actuators provide a very high power-to-weight-ratio, modular design, high precision, and durability. They are widely used in industrial applications, which need high forces or torques (e.g. in heavy equipments such as earth moving or forestry machines). There is a strong trend nowadays towards fully or at least partially automating such working machines. Automation requires advanced low-level control strategies allowing precise control of the hydraulic actuators. However, uncertainties such as unknown load forces, external disturbances and changing operating conditions render the control design a rather challenging task.

The synthesis of position control systems of hydraulic cylinders can be divided into two steps. The first step aims to design a controller for the non-linear valve system, which, in most cases, relies on an exact linearization of the valve dynamics. Generally, the valve dynamics are completely known and the parameters, which remain constant during operation, are mostly available in data-sheets. In the second step, an outer loop controller is designed for the moving piston. This mechanical subsystem is subject to external forces and possibly time-varying plant parameters (e.g. due to changing masses of the load). Therefore, usually, a robust control strategy is essential.

A cascaded control structure is designed in [KR16] for the reference trajectory tracking of the piston rod of the hydraulic differential cylinder, which is subject to an unknown load force. The proposed control law is implemented on the test bench which is equipped with industrial hydraulic components. It consists of two coupled

hydraulic cylinders. One of these cylinders is regarded as the operating cylinder whilst the other one is used to apply certain load profiles (disturbances). For assessment purposes, a force sensor, which provides real-time measurements of the external load force, is installed at the test rig. The controller for the operating cylinder is composed of an inner loop, which aims to linearize the valve dynamics, and an outer loop. Here, saturated continuous twisting controller for reference trajectory tracking is applied to the outer loop. The first-order RED is implemented to estimate the unmeasured state variable. The inner control loop also requires full state information. Hence, the information of the observer is provided to both loops. It is noted that the load force in the outer piston position control loop is not reconstructed through the estimator.

4.5.1. System Model

A schematic diagram of a hydraulic differential cylinder is depicted in Figure 4.5. A general feature of a differential cylinder is that the effective piston cross sections have different areas. Due to this characteristic, depending on the direction, the cylinder moves at two different velocities at a constant flow rate Q_A and Q_B respectively. The control goal is to make that the position of the piston rod y tracks a certain reference profile despite the presence of unknown load force F_{ext} . The flows Q_A and Q_B are regulated by a servo valve. A hydraulic pump provides the valve with a considerable constant pressure, which is assumed to be independent of external load force. The pressure and the volume in the chambers A and B are denoted by p_A , p_B and V_A , V_B respectively.

A mathematical model describing the dynamics of the piston movement is derived by applying Newton's second law of motion as

$$m \frac{d^2 y}{dt^2} = F_h - F_r - F_{\text{ext}}, \quad (4.54)$$

where m is the total moving mass, i.e. the sum of the piston mass and the mass of the hydraulic medium, and F_r represents the friction force. The hydraulic force reads as

$$F_h = (p_A - \alpha_k p_B) A_k, \quad (4.55)$$

where A_k is the so-called piston ring surface and α_k denotes the ratio between the piston rod cross section and the piston ring surface. It is assumed that the valve is controlled and the closed-loop dynamics is described by an integrator, i.e.

$$\frac{dF_h}{dt} = u_h, \quad (4.56)$$

where u_h is considered as the input of the system.

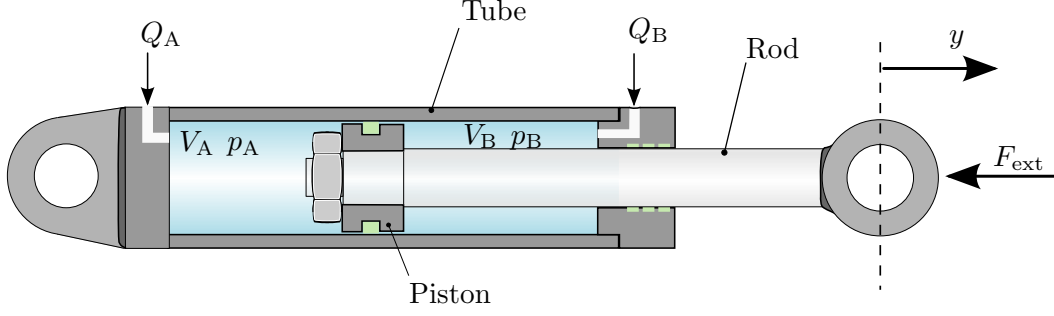


Figure 4.5.: A layout of the differential hydraulic cylinder.

4.5.2. Control Design

The control input is obtained through

$$u_h = k_0 (F_{h,d} - F_h), \quad (4.57)$$

where $F_{h,d}$ denotes the desired piston force and k_0 is a positive constant. Hence, an inner force control loop with closed-loop dynamics

$$\frac{dF_h}{k_0 dt} + F_h = F_{h,d} \quad (4.58)$$

is established. The choice $k_0 > 0$ ensures that the hydraulic force F_h asymptotically tracks a constant desired force $F_{h,d}$. Having applied the saturated continuous twisting control law, a bounded desired piston force is introduced as

$$F_{h,d} = u_{CTA} + F_r, \quad (4.59)$$

where u_{CTA} is identical to u given in (4.10) with $z_1 = y - y_d$ and $\hat{z}_2 = \frac{dy}{dt} - \frac{dy_d}{dt}$. It yields an outer feedback loop for reference trajectory tracking of the piston position and velocity. In the outer closed loop, x_3 reads as

$$x_3 = \nu - F_{ext} - m \frac{d^2 y_d}{dt^2}. \quad (4.60)$$

Please note that this control strategy does not require any information on the piston acceleration and external load. However, implementation of the outer control loop requires a model based estimation of the friction force F_r as well as estimation of the piston velocity $\frac{dy}{dt}$. In order to achieve a perfect tracking in principle, a smooth function of time t to be twice differentiable and slow enough such that its second time derivative is negligible is used as the reference position y_d (see Figure 4.6). As a consequence, $-F_{ext}$ is regarded as perturbations \bar{a} taken into consideration in (1.6).

4. Saturated Continuous Twisting Algorithm

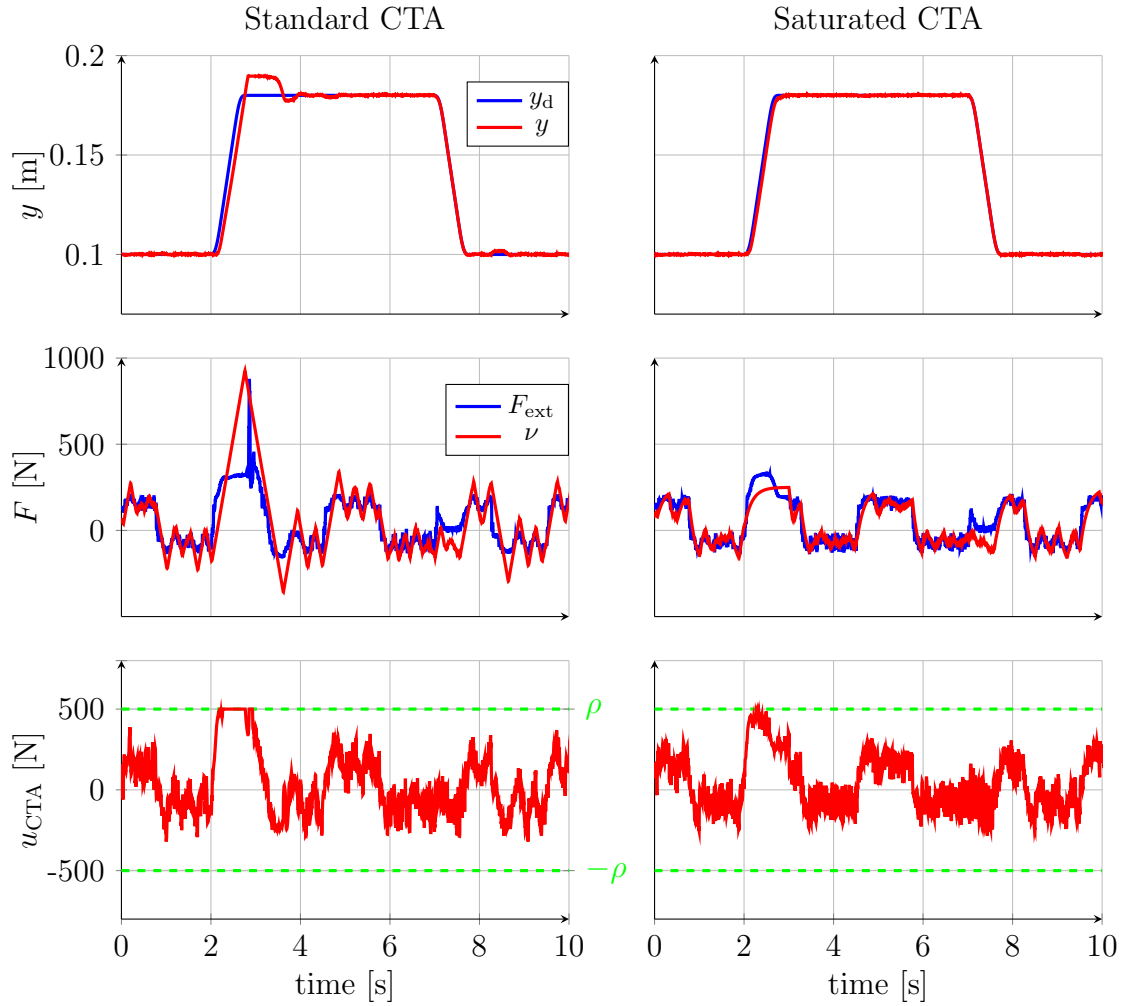


Figure 4.6.: Experimental response curves for Output Feedback Control comparing the proposed saturated continuous twisting algorithm with the standard one. The position, external force, and control input are illustrated.

The closed-loop performance using the saturated CTA is compared here with the result achieved through the standard CTA. The parameters of control law (1.7) are well tuned as

$$l_1 = 1000, \quad l_2 = 800, \quad l_3 = 1500, \quad l_4 = 0. \quad (4.61)$$

It is noted that by setting $l_4 = 0$, the term $[z_2]^0$ of the standard CTA is removed. Eliminating this term, which is not necessary for the stability of the closed-loop system origin (see e.g. [MMF17; MMF19]), reduces the windup effect. However, this cannot prevent the actuator from being saturated and thus, cannot remove the overshoot as shown in the corresponding response curves of the control input and piston position. In order to assess the effectiveness of the proposed saturated

CTA, the constants k_1 , k_2 , and k_3 are left the same as l_1 , l_2 , and l_3 respectively in implementation of control law (4.10). The three other control gains are selected in this case such that (4.16b) holds, where ρ is assumed to be 500N. They can be

$$k_4 = 6, \quad \epsilon_1 = 0.12, \quad \epsilon_2 = 0.16. \quad (4.62)$$

Furthermore, the state observer is tuned such that the estimation error tends to zero in a finite time faster than the convergence of the system state.

The performance of both of the algorithms is depicted in Figure 4.6. In the lower plot (right), it can be clearly seen that due to the structure of the saturated CTA, the produced actuating signal is bounded by the saturation limit specification. By contrast, the control input of standard CTA (left) introduced to the system is saturated through the actuator since the generated signal by the controller is got beyond the limit. As it is shown in the middle plots, both of the controllers can reconstruct the external force properly. A large overshoot is demonstrated in the response curve of piston position in the case of standard CTA. In contrast, the windup effect is significantly mitigated and a satisfactory performance is achieved in the case that saturated CTA is applied.

5. Saturated Feedback Control Using the Twisting Algorithm

This chapter deals with a second-order system affected by uncertainties and disturbances. The twisting algorithm is applied to the design of an observer-based control law. A Lipschitz continuous control signal, which remains within the saturation bounds, is provided.

5.1. Problem Statement

Consider a system described by

$$\frac{dz_1}{dt} = z_2, \quad (5.1a)$$

$$\frac{dz_2}{dt} = \bar{b}(t, z_2) \text{sat}_\rho(u) + \bar{a}(t, z_2), \quad (5.1b)$$

$$y = z_1, \quad (5.1c)$$

where \bar{a} and \bar{b} , which are the functions of time and state, denote uncertainties and disturbances.

Assumption 5.1. *The functions \bar{a} and \bar{b} are globally bounded and Lipschitz continuous with respect to time and state, i.e.*

$$|\bar{a}(t, z_2)| \leq \bar{a}_M, \quad \left| \frac{\partial \bar{a}}{\partial t} \right| \leq L_{\bar{a}}, \quad \left| \frac{\partial \bar{a}}{\partial z_2} \right| \leq L_{\bar{a}, z_2}, \quad \forall t \geq 0, \quad (5.2a)$$

$$0 < \bar{b}_m \leq \bar{b}(t, z_2) \leq 1, \quad \left| \frac{\partial \bar{b}}{\partial t} \right| \leq L_{\bar{b}}, \quad \left| \frac{\partial \bar{b}}{\partial z_2} \right| \leq L_{\bar{b}, z_2}, \quad \forall t \geq 0, \quad (5.2b)$$

where \bar{a}_M , $L_{\bar{a}}$, $L_{\bar{a}, z_2}$, \bar{b}_m , $L_{\bar{b}}$, and $L_{\bar{b}, z_2}$ are some known constants. The upper bound of $\bar{b}(t, z_2)$ without loss of generality¹ is one. As it is explained in the previous chapters, the inequality

$$\left| \frac{\bar{a}(t, z_2)}{\bar{b}(t, z_2)} \right| \leq \frac{\bar{a}_M}{\bar{b}_m} < \rho \quad (5.3)$$

¹For other known upper bounds, the proposed technique may still be applied.

has to be satisfied.

This chapter aims to design a control law for system (5.1) such that the system output y is insensitive to uncertainties and disturbances and the control signal u is continuous everywhere and bounded by the saturation limits.

Remark 5.1. Since z_2 can be regarded as the velocity of a mechanical system, addressing uncertainties depending on this state is important in many practical applications. Uncertainties depending on z_1 are not considered in the class of plant uncertainties here. This is due to that in such a case, z_2 appears in the time derivatives of \bar{a} and \bar{b} and therefore, bounds of z_2 , which cannot be realized from a saturated control input, need to be known.

Remark 5.2. If perturbations lie within a different channel from the control signal, they are called unmatched perturbations [ES98]. In order to tackle them, fairly restrictive assumptions have been made on them in [YLY13; DL17]. Bounded unmatched disturbances, whose time derivatives are also bounded, are dealt with in [EF10; FBF13; GSP14]. Having assumed the entire state vector is available for measurement, unmatched as well as matched perturbations are compensated using a high-order sliding mode differentiator in [Yan+14]. However, it can be shown that the problem is trivial if a second-order system is subject to matched disturbances and uncertainties $a_1(t, \xi_2)$ and unmatched perturbations $a_2(t)$ as

$$\frac{d\xi_1}{dt} = \xi_2 + a_2(t), \quad (5.4a)$$

$$\frac{d\xi_2}{dt} = \tilde{b}(t, \xi_2) \text{sat}_\rho(u) + a_1(t, \xi_2), \quad (5.4b)$$

$$y = \xi_1, \quad (5.4c)$$

where matched ones, similar to that given in (5.2a), are globally bounded and Lipschitz continuous as

$$|a_1(t, \xi_2)| \leq a_{1,M}, \quad \left| \frac{\partial a_1}{\partial t} \right| \leq L_{a_1}, \quad \left| \frac{\partial a_1}{\partial \xi_2} \right| \leq L_{a_1, \xi_2}, \quad \forall t \geq 0,$$

with the known constants $a_{1,M}$, L_{a_1} , and L_{a_1, ξ_2} . It is noted that in this case, unmatched disturbances can be a linearly growing function of time t satisfying

$$\left| \frac{da_2}{dt} \right| \leq L_{a_2}, \quad \left| \frac{d^2 a_2}{dt^2} \right| \leq \bar{L}_{a_2}, \quad \forall t \geq 0,$$

where the constants L_{a_2} and \bar{L}_{a_2} are also known. Please note that this system is neither strongly detectable nor strongly observable [Hau83] and therefore, there is

no chance to estimate ξ_2 and reconstruct $a_2(t)$ in the case that ξ_2 is unavailable for measurement. By applying the mapping $\begin{bmatrix} z_1 & z_2 \end{bmatrix}^T = \begin{bmatrix} \xi_1 & \xi_2 + a_2(t) \end{bmatrix}^T$ to system (5.4), system (5.1) is recovered, where $\bar{a}(t, z_2) = a_1(t, z_2 - a_2(t)) + \frac{da_2}{dt}$ and z_2 can be estimated using a robust exact differentiator. It becomes evident that \bar{a} and its derivatives with respect to time and z_2 are globally bounded. As a consequence, the systems with matched perturbations and uncertainties are dealt with in this study.

It becomes evident that in the case of system (5.1), there is no chance to reconstruct either \bar{a} or \bar{b} , or both using an RED. Furthermore, for the scenario of Output Feedback Control imagined in 4.ii, the super-twisting algorithm cannot be applied from the mathematical point of view, which is explained in the following.

5.1.1. Problem with Super-Twisting Controller

A super-twisting controller based on an observer using high-order sliding mode algorithm is introduced in [Cha+16] for the perturbed double integrator system (\bar{b} is assumed to be known and \bar{a} is just taken into account as a function of time). It is shown therein that the implementation of the standard super-twisting controller using the first-order RED as given in (4.11) to estimate z_2 does not have a mathematical justification. This is due to that, in the overall closed-loop system, the discontinuous element of this differentiator lies in the same channel as the continuous element of the controller and therefore, the second-order sliding mode does not exist. It is proposed therein that the estimation of z_2 should be obtained through a higher-order differentiator.

Having employed the second-order RED, a state observer for system (5.1) is introduced as

$$e_1 = z_1 - \tilde{z}_1, \quad (5.5a)$$

$$\frac{d\tilde{z}_1}{dt} = \mu_1 [e_1]^{\frac{2}{3}} + \hat{z}_2, \quad (5.5b)$$

$$\frac{d\hat{z}_2}{dt} = u + \mu_2 [e_1]^{\frac{1}{3}} + \tilde{z}_2, \quad (5.5c)$$

$$\frac{d\tilde{z}_2}{dt} = \mu_3 [e_1]^0, \quad (5.5d)$$

where \hat{z}_2 denotes the estimation of the state z_2 , \tilde{z}_1 and \tilde{z}_2 are auxiliary variables, and the positive values μ_1 , μ_2 , and μ_3 are observer constants to be chosen appropriately. It may be noted that $u + \hat{z}_2$ represents the estimate information of system's second channel (5.1b). By defining the error variables $e_2 = z_2 - \hat{z}_2$ and $\tilde{e}_2 = (\bar{b} - 1)u + \bar{a} - \tilde{z}_2$,

the error dynamics is written as

$$\frac{de_1}{dt} = -\mu_1 [e_1]^{\frac{2}{3}} + e_2, \quad (5.6a)$$

$$\frac{de_2}{dt} = -\mu_2 [e_1]^{\frac{1}{3}} + \tilde{e}_2, \quad (5.6b)$$

$$\frac{d\tilde{e}_2}{dt} = -\mu_3 [e_1]^0 + \psi, \quad (5.6c)$$

where ψ reads as

$$\psi = \left(\frac{\partial \bar{b}}{\partial t} + \frac{\partial \bar{b}}{\partial z_2} \frac{dz_2}{dt} \right) u + (\bar{b} - 1) \frac{du}{dt} + \frac{\partial \bar{a}}{\partial t} + \frac{\partial \bar{a}}{\partial z_2} \frac{dz_2}{dt}. \quad (5.7)$$

In order to achieve the convergence of $\mathbf{e} = [e_1 \ e_2 \ \tilde{e}_2]^T$ to zero in the finite time T , ψ needs to be globally bounded [Lev98].

The estimation of the state z_2 is incorporated into the sliding function definition as

$$\sigma_1 = \hat{z}_2 + \lambda z_1, \quad (5.8)$$

where λ is a positive constant value. A control law based on the super-twisting algorithm is designed as

$$u = -\lambda \hat{z}_2 - k_1 [\sigma_1]^{\frac{1}{2}} + \nu, \quad (5.9a)$$

$$\frac{d\nu}{dt} = -k_2 [\sigma_1]^0 - \mu_3 [e_1]^0, \quad (5.9b)$$

where control parameters $k_1 > 0$ and $k_2 > 0$ need to be selected appropriately. It is noted that the control signal u is continuous, but it is not Lipschitz continuous. Thus, ψ in (5.7) cannot be bounded for all $t \geq 0$ in the case \bar{b} is unknown. This leads to that

$$\forall T, \exists t > T : \mathbf{e} \neq \mathbf{0}. \quad (5.10)$$

Taking the time derivative of the sliding function σ_1 in (5.8) yields

$$\begin{aligned} \frac{d\sigma_1}{dt} &= u + \mu_2 [e_1]^{\frac{1}{3}} + \tilde{z}_2 + \lambda (\hat{z}_2 + e_2) \\ &= -k_1 [\sigma_1]^{\frac{1}{2}} - k_2 \int_0^t [\sigma_1]^0 dt + \mu_2 [e_1]^{\frac{1}{3}} + \lambda e_2. \end{aligned} \quad (5.11)$$

Consequently, in order to drive the system trajectories to the surface $\sigma_1 = 0$ and maintain the motion on that, the constants k_1 and k_2 need to be chosen based on upper bound of $|e|$. Moreover, from (5.10), it is derived that for $t > T$, \hat{z}_2 is not always equivalent to z_2 .

Furthermore, as it is pointed out in the previous chapter, for such a second-order system with saturating actuator (even if \bar{b} is known), the anti-windup scheme for the super-twisting control as well as the saturated super-twisting algorithm does not make a contribution. On this occasion, the twisting algorithm may be adopted to handle the problem. Providing a continuous control signal by using the twisting algorithm contributes significantly to avoidance of two dangerous chattering classes known as bounded and unbounded [Lev10]. In order to introduce this continuous control input to the system, a sliding function needs to be defined such that the relative degree of the system with respect to this function is one. Due to the fact that the time derivative of the sliding variable is included in the control law design, in the scenario of Full State Information considered in 4.i, the estimation of the time derivative of z_2 obtained through the first-order RED needs to be exploited to build up the controller. However, in the Output Feedback Control scenario imagined in 4.ii, estimates of z_2 and its time derivative obtained through the second-order RED mentioned in (5.5) need to be used. Please note that in this case, perturbations and uncertainties \bar{a} cannot be estimated and compensated in a controller. Therefore, this robust control technique becomes non-redundant. Since sliding functions and control laws will be similar in the aforementioned scenarios, the Output Feedback Control scenario is considered here.

5.2. Saturated Output Feedback Control

Having considered sliding function (5.8), the proposed saturated and Lipschitz continuous control input is obtained through

$$\frac{du}{dt} = -k \left([\sigma_1]^0 + \frac{1}{2} [\sigma_2]^0 \right) - \mu_3 [e_1]^0 - \lambda u, \quad u(t=0) = u_0, \quad (5.12)$$

where k is a positive constant to be selected and σ_2 is defined as

$$\sigma_2 = u + \tilde{z}_2 + \lambda \hat{z}_2. \quad (5.13)$$

It is noted that the high-order sliding mode observer also provides \tilde{z}_2 , which is included in σ_2 . In the following, it is outlined how the initial value u_0 of the control signal needs to be chosen. A block diagram of the control approach is depicted in Figure 5.1.

Lemma 5.1. *The supremum of the control signal absolute value is*

$$\sup |u(t)| \leq u_M = \frac{3k + 2\mu_3}{2\lambda}, \quad \forall t \geq 0, \quad (5.14)$$

where the initial value u_0 is selected such that $|u_0| \leq u_M$ holds.

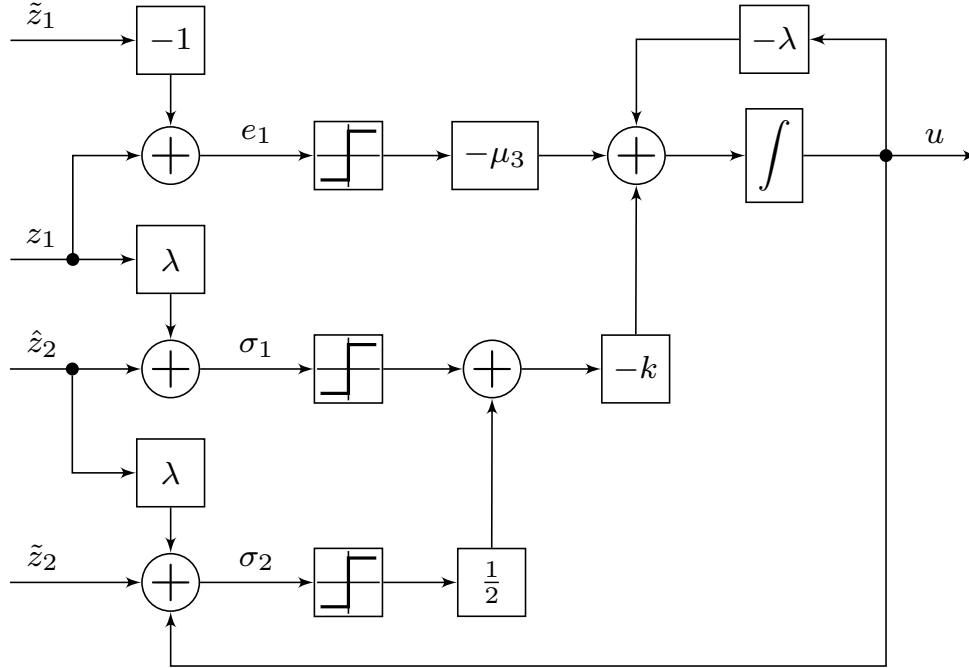


Figure 5.1.: Block diagram of proposed control law (5.12). Please note that \tilde{z}_1 and \tilde{z}_2 as well as \hat{z}_2 are provided by the second-order RED given in (5.5).

Proof. Similar to the proof of Lemma 2.1, (5.14) can be easily derived since (5.12) is a linear differential equation with the state variable u and a bounded input. \square

As a result of this lemma, the Lipschitz constant of the control input reads as

$$\left| \frac{du}{dt} \right| \leq \frac{3k}{2} + \mu_3 + \lambda u_M = 2\lambda u_M. \quad (5.15)$$

5.3. Stability Analysis

In the following, the stability properties of the closed-loop system, in which the observer error dynamics is considered, are investigated.

Proposition 5.1. *Suppose that Assumption 5.1 is fulfilled. For system (5.1) with any real values $z_{1,0}$ and $z_{2,0}$ under control law (5.12), the system states z_1 and z_2 tend to zero asymptotically and the continuous control signal remains within the given*

saturation bounds, i.e. $u \in [-\rho, \rho]$ for all $t \geq 0$, if the controller and observer gains are chosen such that

$$k > 2\lambda(u_M(1 - \bar{b}_m) + \bar{a}_M), \quad (5.16a)$$

$$\rho \geq u_M, \quad (5.16b)$$

$$\mu_1 = 2\psi_M^{\frac{1}{3}}, \quad \mu_2 = 1.5 \times \sqrt{2}\psi_M^{\frac{2}{3}}, \quad \mu_3 = 1.1\psi_M, \quad (5.16c)$$

with

$$\psi_M = \left(L_{\bar{b}} + L_{\bar{b},z_2}(u_M + \bar{a}_M) + 2\lambda(1 - \bar{b}_m) \right) u_M + L_{\bar{a}} + L_{\bar{a},z_2}(u_M + \bar{a}_M) \quad (5.16d)$$

hold.

Proof. Substituting (5.12), (5.5c), (5.5d), and (5.6b) into the time derivatives of σ_1 and σ_2 gives

$$\frac{d\sigma_1}{dt} = \sigma_2 + \mu_2 [e_1]^{\frac{1}{3}} + \lambda e_2, \quad (5.17a)$$

$$\frac{d\sigma_2}{dt} = -k \left([\sigma_1]^0 + \frac{1}{2} [\sigma_2]^0 \right) + \lambda \left((\bar{b} - 1) u + \bar{a} - \frac{de_2}{dt} \right). \quad (5.17b)$$

Having considered the boundedness of control input and its time derivative presented in (5.14) and (5.15), it can be concluded that the absolute value of ψ in (5.7) is globally bounded by the calculable constant value ψ_M . Hence, the observer error vector e converges to zero in the finite time T if the positive gains μ_1 , μ_2 , and μ_3 are chosen properly. As proposed in [LL14], they can be selected satisfying (5.16c). It becomes evident that e_1 , e_2 , and $\frac{de_2}{dt}$ are bounded for all $t \geq 0$. As proven in [Mor12, Theorem 5.1], within the overall closed-loop system considering (5.17) and (5.6), the trajectories of driven subsystem (5.17) cannot scape to infinity in a finite time. Therefore, for $t < T$, the states σ_1 and σ_2 cannot become unbounded and afterward, for $t \geq T$, their finite-time convergence is guaranteed if the control constants k and λ are selected such that the inequalities in (5.16) are satisfied. This implies asymptotic stability of the system states z_1 and z_2 . The boundedness of the actuating signal for any $z_{1,0}, z_{2,0} \in \mathbb{R}$ is justified applying Lemma 5.1. It becomes evident that its absolute value is bounded by the constant value ρ if $u_M \leq \rho$ is fulfilled. \square

Remark 5.3. A feasible region of the observer and controller gains μ_3 and k based on the inequalities given in (5.16) may be found numerically through a computer algebra software. In the case \bar{b} is known and \bar{a} is just a function of time, where the problem setting of the previous chapter is revisited, they can be tuned independently as

$$k > 2\lambda\bar{a}_M, \quad \mu_3 > L_{\bar{a}}. \quad (5.18)$$

Choosing them such that (5.16b) is fulfilled leads to a bounded control signal by a given ρ . Considering the aforementioned conditions, the permissible bound of perturbations derived in Remark 4.5 is relaxed here to $\bar{a}_M < \frac{\rho}{3}$. However, $L_{\bar{a}}$ still needs to be a portion of the saturation limit ρ and therefore, the class of addressed disturbances is left restricted. In the next chapter, this restriction is also eased. Furthermore, in the case that either \bar{b} is unknown or $\frac{\partial \bar{a}}{\partial z_2} \neq 0$ or both, the fairly restrictive assumptions made on the bound and class of perturbations and uncertainties by satisfying the conditions imposed in (5.16) are eased.

5.4. Simulation Examples

In this section, it is illustrated how the proposed control law is able to handle two different problem settings. In the first one, the simulation example of the previous chapter is revisited, i.e. it is assumed that \bar{b} is known and \bar{a} represents external disturbances and it does not depend on the system state variable. It is noted that, as mentioned earlier, for such a perturbed double integrator system, control law (5.12) is redundant and it is unnecessary for the application implementation. Nevertheless, it is applied in simulation to this system in order to make a comparison with the results achieved in the previous chapter. In the second case, the system is subject to both model uncertainties and perturbations, i.e. both unknown \bar{b} and \bar{a} are functions of time and z_2 . The observer and controller gains are selected based on bound specifications systematically.

5.4.1. Perturbed Double Integrator System

In this simulation case, $\bar{b} = 1$ and perturbations $\bar{a}(t)$ are denoted by the function given in (1.8). The absolute value of the control signal u is supposed to remain bounded by $\rho = 10$. As presented in (5.8), the sliding variable σ_1 is defined with $\lambda = 5$. In this example, the parameters k and μ_3 can be tuned satisfying (5.18) and (5.16b). Since the function \bar{a} is Lipschitz continuous with $L_{\bar{a}} = 2.5$, the parameters of the second-order RED, as mentioned in the above proof, can be e.g. $\mu_1 = 2.71$, $\mu_2 = 3.91$, and $\mu_3 = 2.75$. Now, considering the bound $\bar{a}_M = 1.5$ of disturbances, the control parameter $k = 31.5$ is selected such that the desired boundedness of the control signal is ensured.

The numerical simulation is carried out using the same solver and sampling step size as employed in the previous chapter. The initial condition of the system is left unchanged and the initial value of the control input is set to $u_0 = 0$. The results are compared in Figure 5.2 with the achieved closed-loop performance of the saturated continuous twisting algorithm in the Output Feedback Control scenario. As it is

proved above, having applied the twisting algorithm, the system states tend to zero asymptotically, whereas the states of the system under the saturated continuous twisting control converge in a finite time. However, as it can be seen in the zoomed portions of the upper and middle plots, similar precision is obtained through both the algorithms. This may be different by assigning another value to λ or realizing the saturated CTA with different discretization step size. The control signal evolution is illustrated in the lower plot. Both of the algorithms produce continuous signals, which are bounded by the saturation bound specification. The finite-time convergence of the error dynamics of the observer employed in this chapter is indicated in Figure 5.3. Please note that the errors convergence of the first-order RED, whose information is used for the saturated CTA in the case of Output Feedback Control, is shown in Figure 4.4. In the aforementioned approaches, the convergence of the observer errors is faster comparing to the convergence of the sliding variables (in the twisting algorithm-based control) or the convergence of the sates (in the saturated CTA).

5.4.2. System with Uncertainties and Disturbances

In this example, it is assumed that the system is affected by uncertainties as well as disturbances. They are represented as

$$\bar{a}(t, z_2) = 0.4 + 0.4 \sin(t) + 0.3 \sin(\sqrt{10}t) + 0.1 \cos(z_2), \quad (5.19a)$$

$$\bar{b}(t, z_2) = 0.95 + 0.03 \sin(2t) + 0.02 \cos(z_2). \quad (5.19b)$$

Inequalities (5.2a) and (5.2b) are satisfied with $\bar{a}_M = 1.2$, $L_{\bar{a}} = 1.35$, $L_{\bar{a}, z_2} = 0.1$, $\bar{b}_m = 0.9$, $L_{\bar{b}} = 0.06$, and $L_{\bar{b}, z_2} = 0.02$. The bound ρ and the constant λ are left unchanged. In contrast to the previous simulation case, the control and observer parameters k and μ_3 cannot be chosen independently any more, which leads to a more restrictive set of acceptable parameter pairs. Having considered the sufficient conditions imposed in (5.16), the parameter plan is realized using Mathematica, which is depicted in Figure 5.4. A suitable choice of the parameters is e.g. $k = 22.11$ and $\mu_3 = 16.83$, which makes the actuating signal bounded by $u_M = 10$. The observer gains $\mu_2 = 13.07$ and $\mu_1 = 4.96$ are selected appropriately as mentioned before.

The simulation is carried out with the same configuration and initial values as used in the previous example. Since this problem setting is not dealt with in [SMF18] and the previous chapter, the results of the system under control law (5.12) are revealed in Figure 5.5. As it can be seen in the upper and middle plots, the proposed control law is capable of driving the system states asymptotically to zero in the presence of perturbations and model uncertainties. It is noted that for the second-order RED also employed in this simulation case, similar performance to that demonstrated in Figure 5.3 is achieved.

5. Saturated Feedback Control Using the Twisting Algorithm

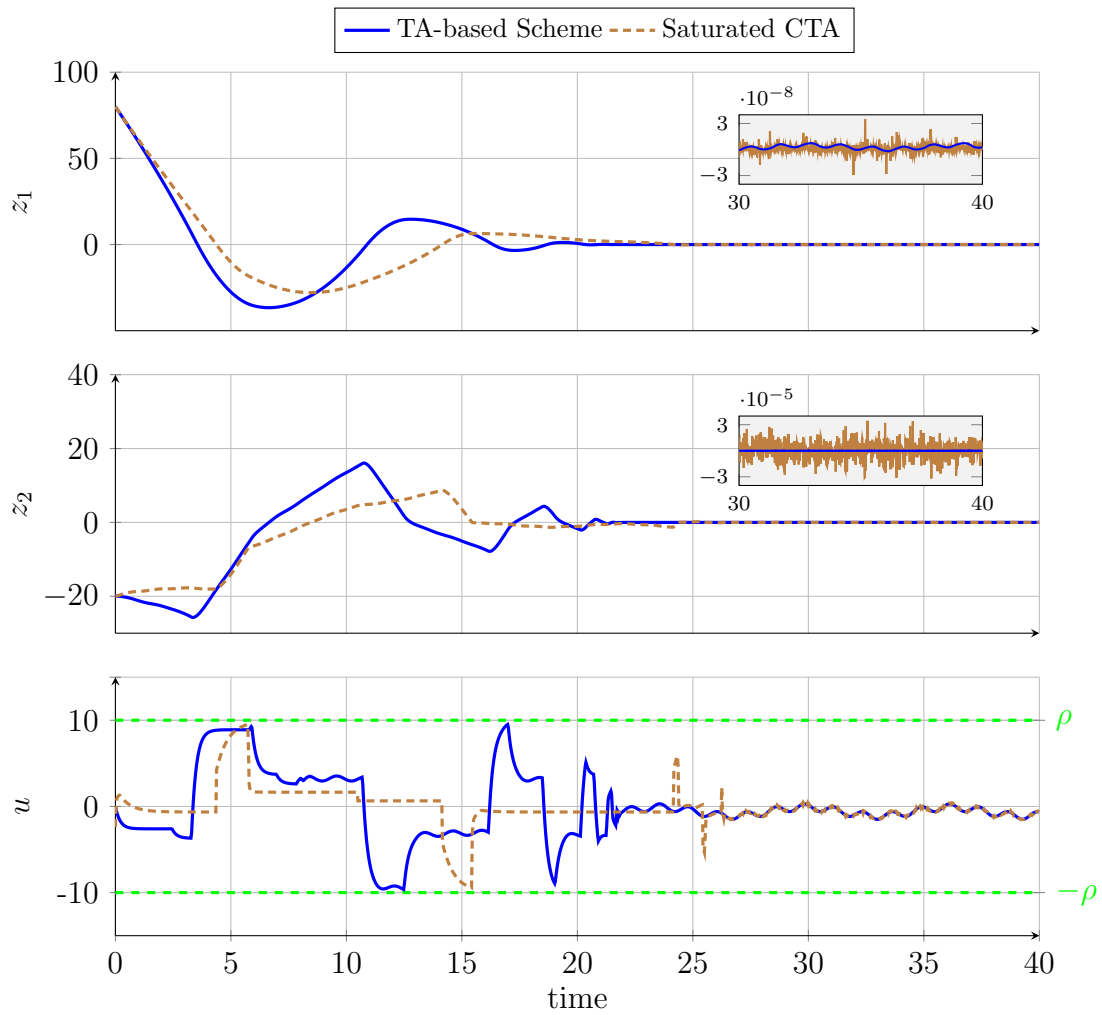


Figure 5.2.: Simulation results for the scenario of Output Feedback Control obtained through the second-order system with $\bar{b} = 1$ and $\frac{\partial \bar{a}}{\partial z_2} = 0$ under control laws (5.12) and (4.10).

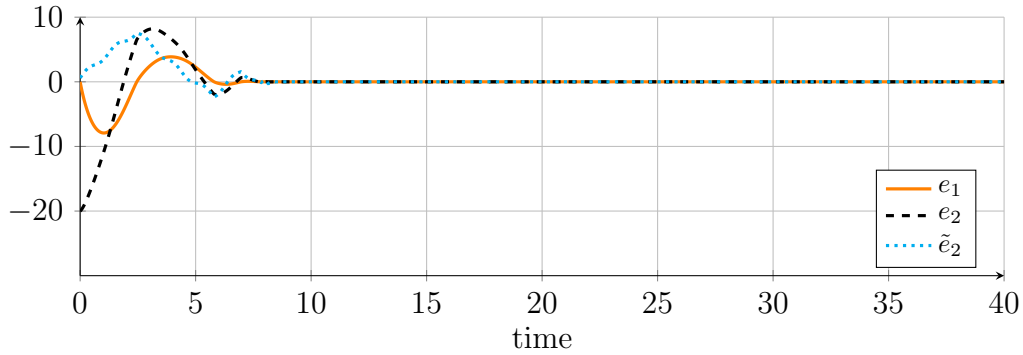


Figure 5.3.: Simulated errors of the second-order RED used for the case of perturbed double integrator system. Its information is incorporated into the twisting algorithm-based control law.

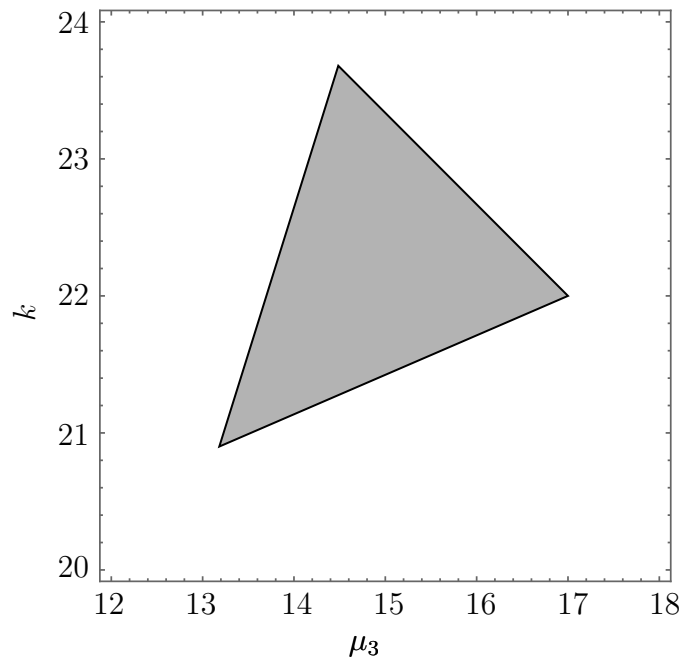


Figure 5.4.: Feasible parameter region for the system in the presence of uncertainties and disturbances denoted by (5.19) in the case that $\rho = 10$ and $\lambda = 5$.

5. Saturated Feedback Control Using the Twisting Algorithm

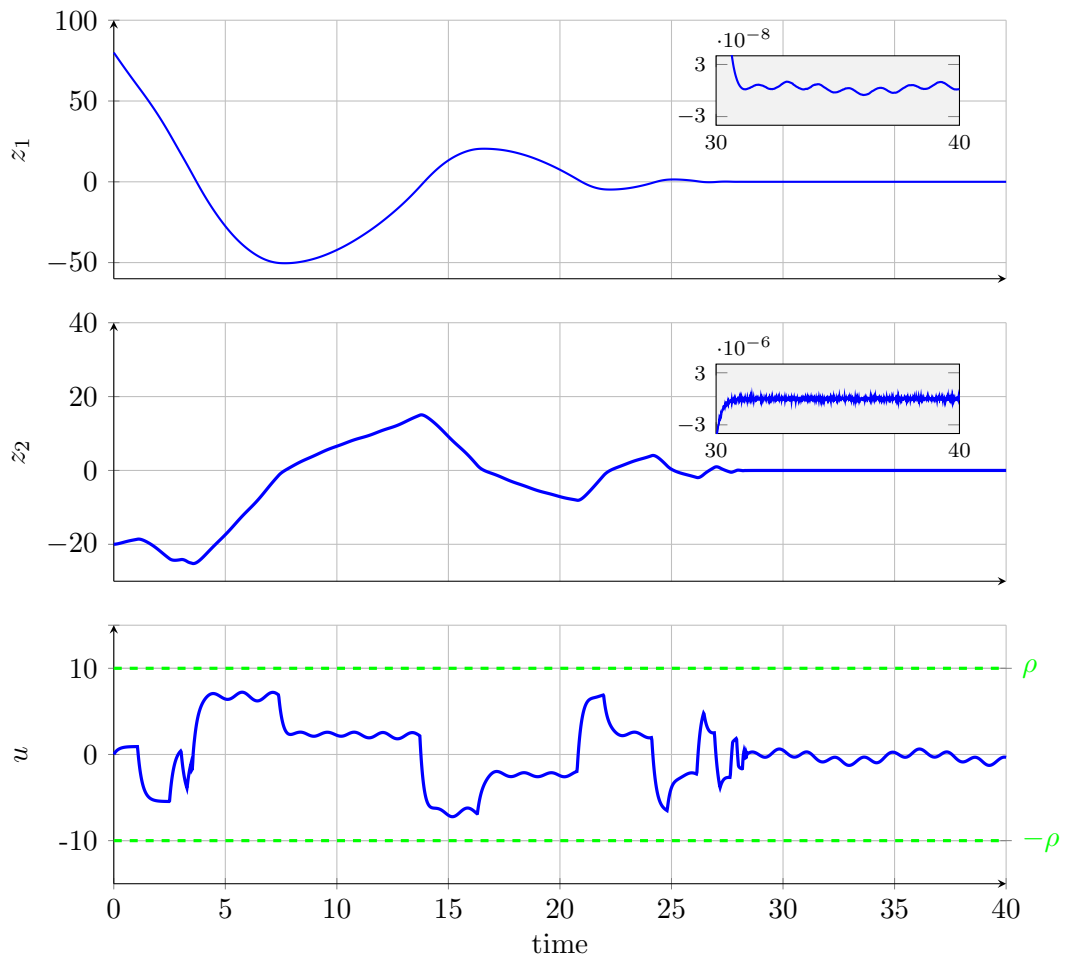


Figure 5.5.: Simulation response curves for the second-order system with uncertainties and perturbations under the saturated feedback control using the twisting algorithm. It is noted that uncertainties as well as multiplicative unknowns are not addressed in the standard and saturated CTA.

6. Lyapunov-based Saturated Continuous Twisting Algorithm

In this chapter, it is investigated how the permissible bound and class of perturbations \bar{a} addressed in the previous two chapters can be relaxed. The second-order systems, with and without considering uncertainties and multiplicative unknowns, are taken into account. It is aimed at designing control laws for systems (1.6) and (5.1) such that the system states converge to the origin in a finite time and the control signal belongs to the set $[-\rho, \rho]$ for all $t \geq 0$ and is continuous almost everywhere with a finite number of discontinuities. Having assumed both the states of the systems are available for measurement, new versions of the saturated continuous twisting algorithm are introduced.

6.1. Proposed Schemes

In the following, a novel Lyapunov-based saturated continuous twisting algorithm as well as a modification of the saturated continuous twisting control presented in Chapter 4 is proposed.

6.1.1. First Approach

The saturated continuous twisting control given in (4.6) is modified as

$$u = -k_1 \text{sat}_{\epsilon_1} \left(\lceil z_1 \rceil^{\frac{1}{3}} \right) - k_2 \text{sat}_{\epsilon_2} \left(\lceil z_2 \rceil^{\frac{1}{2}} \right) + \nu, \quad (6.1a)$$

$$\frac{d\nu}{dt} = \begin{cases} 0 & \text{if } t < T \\ -k_3 \lceil z_1 \rceil^0 & \text{if } t \geq T, \end{cases} \quad (6.1b)$$

where the initial value $\nu_0 = 0$ is assumed and T is

$$T = \inf \left\{ t \mid |z_1(t)|^{\frac{1}{3}} + |z_2(t)|^{\frac{1}{2}} \leq \gamma \right\}. \quad (6.2)$$

If the non-negative constant γ is chosen appropriately such that $\gamma \leq \min(\epsilon_1, \epsilon_2)$ holds, the controller produces a bounded signal until the states enter a neighborhood

of the origin. After that, the continuous twisting algorithm is recovered, which is maintained even if the states leave the neighborhood. Similar to that proved in Proposition 4.1, if either $z_{1,0}$ or $z_{2,0}$ or both are outside the bands, it can be shown that the states of the closed-loop system converge to domains in the vicinity of the origin. Having considered level sets of the Lyapunov function given in (4.21), the stability of the closed-loop system origin can be guaranteed in a similar way to that carried out in [Cas+16b]. Please note that here γ should not be selected too small close to zero (otherwise, in the presence of disturbances, there is no switch in (6.1b) and thus, the states do not tend to zero at all). This means a lower bound for γ also needs to be considered. In the next approach introduced in this chapter, this restriction is removed and a small non-negative value can be assigned to γ .

As a result of applying the above control law to system (1.6), the conditions imposed on the control gains in (4.16) are relaxed to

$$\frac{1}{2}k_1\epsilon_1 = k_2\epsilon_2 > \bar{a}_M, \quad (6.3a)$$

$$\rho \geq k_1\epsilon_1 + k_2\epsilon_2. \quad (6.3b)$$

Furthermore, there is no linear term in (6.1b) and k_3 just needs to be greater than the Lipschitz constant $L_{\bar{a}}$. Therefore, the allowable bound of disturbances is increased to

$$\bar{a}_M < \frac{\rho}{3} \quad (6.4)$$

and the restriction on the class of perturbations is relaxed as shown in the next section. Therein, a novel extension of the proof concept presented in [Cas+16b] is made utilizing a sum-of-squares based Lyapunov function. It is worth mentioning that, similar to the saturated continuous twisting algorithm given in Chapter 4, the introduced actuating signal here is continuous everywhere since the aforementioned switch is placed in the same channel as the discontinuous element of the control law.

6.1.2. Second Approach

The concept of the saturated super-twisting algorithm proposed in [Cas+16b] is modified here in order to be applicable to a second-order system affected by perturbations and uncertainties. The Lyapunov-based saturated continuous twisting

control law for system (5.1) reads as

$$\begin{bmatrix} u \\ \frac{d\nu}{dt} \end{bmatrix} = \begin{cases} \begin{bmatrix} -\frac{2}{3}\rho \left([z_1]^0 + \frac{1}{2} [z_2]^0 \right) \\ 0 \end{bmatrix} & \text{if } t < T \\ \begin{bmatrix} -k_1 [z_1]^{\frac{1}{3}} - k_2 [z_2]^{\frac{1}{2}} + \nu \\ -k_3 [z_1]^0 \end{bmatrix} & \text{if } t \geq T, \end{cases} \quad (6.5)$$

where, similar to the previous scheme, $\nu_0 = 0$ holds and T is the first time instant as defined in (6.2). It is given later how to choose the switching level parameter γ , which just needs to be a small enough non-negative constant in this technique. Furthermore, an appropriate choice of the positive gains k_1 , k_2 , and k_3 is made exemplarily, whose values can be scaled. Here, the relay controller based on the twisting algorithm is applied up to the time instant T and thereafter, the continuous twisting controller is employed. Thus, there is at most one switch between these two sliding mode algorithms and the number of discontinuities in the control signal is finite. A block diagram of this novel algorithm is shown in Figure 6.1. Lyapunov function candidate (4.21) is also used in the stability analysis of the closed-loop system, which is detailed in the next section. It can be seen, compared to the previous approach in this chapter, the same class of perturbations can be handled. The permissible bounds of disturbances for the cases with and without multiplicative unknowns are determined in the next section.

It is noted that for every initial condition of the system in the scenario of Output Feedback Control, the state z_2 in both of the above saturated control approaches cannot be replaced with its estimate \hat{z}_2 obtained through the first-order RED given in (4.11). This is explained later based on the following analysis.

6.2. Stability Analysis

Since the stability analyses of the above-mentioned schemes are similar and the condition of the control parameter γ is less restrictive in the latter one, stability properties of the closed loop of the Lyapunov-based saturated continuous twisting algorithm are established in the following. Investigation into the stability of the closed-loop system under the assumption of scenario 4.i is conducted.

Proposition 6.1. *Suppose that Assumption 5.1 and*

$$\frac{\bar{a}_M}{\bar{b}_m} < \kappa\rho \quad \text{with} \quad \kappa \leq \frac{1}{3} \quad (6.6)$$

6. Lyapunov-based Saturated Continuous Twisting Algorithm

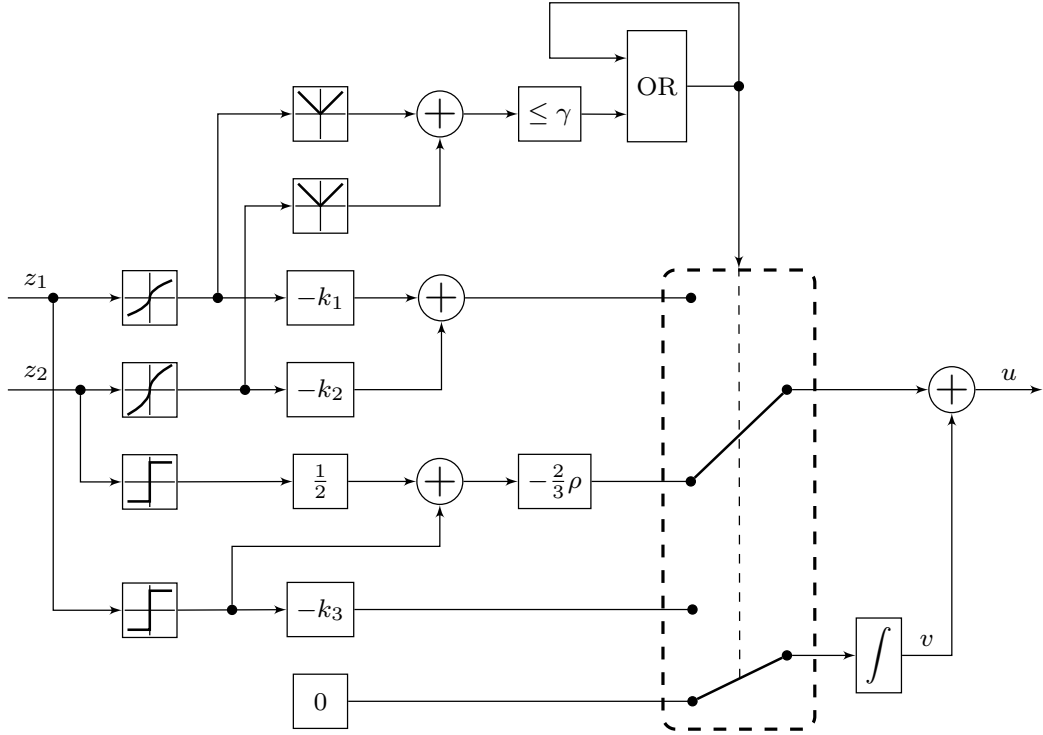


Figure 6.1.: Block diagram of proposed control law (6.5). It is noted that the output of the comparison block is one if its input is less than or equal to the constant γ and zero otherwise. The output of OR is initialized with zero and the switches are in the upper positions when this output is one.

are satisfied, where \bar{b}_m is greater than or equal to constant permissible lower bound $\kappa_{\bar{b}}$. Then there exist constants γ , \bar{k}_1 , \bar{k}_2 , \bar{k}_3 , $\bar{\delta}_1$, and $\bar{\delta}_2$ such that for all $\bar{\delta}_M \in \left[0, \bar{\delta}_1 \left(\rho - \frac{\bar{a}_M}{\bar{b}_m}\right)\right]$, where

$$\bar{\delta}_M = \frac{L_{\bar{a}} + (L_{\bar{a},z_2} + L_{\bar{b},z_2} \bar{a}_M) (\rho + \bar{a}_M) + L_{\bar{b}} \bar{a}_M}{\bar{b}_m^2}, \quad (6.7)$$

the choice of the control parameters as

$$k_1 = \mu^{\frac{2}{3}} \bar{k}_1, \quad k_2 = \mu^{\frac{1}{2}} \bar{k}_2, \quad k_3 = \mu \bar{k}_3 \quad (6.8a)$$

with

$$\mu = \max \left(\bar{\delta}_M, \bar{\delta}_2 \left(\rho + \frac{\bar{a}_M}{\bar{b}_m} \right) \right) \quad (6.8b)$$

guarantees that the origin of the closed-loop system (plant (5.1) under control law (6.5)) is globally finite-time stable.

Remark 6.1. In order to solve the sum-of-squares problem formulated within the following proof, YALMIP [Löf04] and SEDUMi [Stu99] are used here. The values of the constants γ , \bar{k}_1 , \bar{k}_2 , and \bar{k}_3 can be

$$\gamma = 0, \quad \bar{k}_1 = 10, \quad \bar{k}_2 = 5, \quad \bar{k}_3 = 1.1. \quad (6.9)$$

Furthermore, $\kappa_{\bar{b}} = 0.76$, $\bar{\delta}_2 = 0.09$, and different values of $\bar{\delta}_1$ as listed in Table 6.1 are determined numerically. Please note that $\bar{\delta}_1$ increases while κ decreases.

Proof. For $t < T$, the closed-loop dynamics is written as

$$\frac{dz_1}{dt} = z_2, \quad (6.10a)$$

$$\frac{dz_2}{dt} = -\frac{2}{3}\rho\bar{b} \left([z_1]^0 + \frac{1}{2} [z_2]^0 \right) + \bar{a}. \quad (6.10b)$$

The finite-time convergence of the states to zero is ensured if (6.6) holds. It is noted that in the case $\bar{b} = 1$, (6.4) is recovered, i.e. both of the aforementioned approaches can make the same relaxation of the permissible bound of \bar{a} . As a result of the states convergence, the switching condition given in (6.2) is met eventually.

For $t \geq T$, the closed-loop system can be represented by

$$\frac{dx_1}{d\tau} = \frac{x_2}{\bar{b}}, \quad (6.11a)$$

$$\frac{dx_2}{d\tau} = -k_1 [x_1]^{\frac{1}{3}} - k_2 [x_2]^{\frac{1}{2}} + x_3, \quad (6.11b)$$

$$\frac{dx_3}{d\tau} = \frac{1}{\bar{b}} \left(-k_3 [x_1]^0 + \bar{\delta} \right), \quad (6.11c)$$

where time is scaled through $d\tau = \bar{b}dt$, the state vector is defined as

$$\mathbf{x} = \begin{bmatrix} x_1 & x_2 & x_3 \end{bmatrix}^T = \begin{bmatrix} z_1 & z_2 & \nu + \frac{\bar{a}}{\bar{b}} \end{bmatrix}^T, \quad (6.12)$$

and $\bar{\delta}$ reads as

$$\bar{\delta} = \frac{d}{dt} \left(\frac{\bar{a}(t, z_2)}{\bar{b}(t, z_2)} \right) = \frac{\left(\frac{\partial \bar{a}}{\partial t} + \frac{\partial \bar{a}}{\partial z_2} \frac{dz_2}{dt} \right) \bar{b}(t, z_2) - \left(\frac{\partial \bar{b}}{\partial t} + \frac{\partial \bar{b}}{\partial z_2} \frac{dz_2}{dt} \right) \bar{a}(t, z_2)}{\bar{b}^2(t, z_2)}. \quad (6.13)$$

It is noted that, similar to that explained in Chapter 3, \bar{b} and $\bar{\delta}$ are uniformly bounded (due to that (5.2a) and (5.2b) are satisfied and $\frac{dz_2}{dt}$ is also bounded for all $t \geq 0$). It is realized that $|\bar{\delta}|$ is bounded by $\bar{\delta}_M$ defined in (6.7). The control gains k_1 , k_2 , and k_3

6. Lyapunov-based Saturated Continuous Twisting Algorithm

Table 6.1.: Permissible values of $\bar{\delta}_1$ for different values of κ in the case that the control parameters are chosen as given in (6.9).

	$\bar{\delta}_1$
$\frac{1}{4} \leq \kappa \leq \frac{1}{3}$	0.21
$\frac{1}{6} \leq \kappa < \frac{1}{4}$	0.27
$\frac{1}{12} \leq \kappa < \frac{1}{6}$	0.39
$0 \leq \kappa < \frac{1}{12}$	0.72

are scaled for all $\bar{\delta}_M$ as given in (6.8a). This is justified by changing the coordinates in (6.11) as

$$\mathbf{x} = \mu \boldsymbol{\zeta} = \mu \begin{bmatrix} \zeta_1 & \zeta_2 & \zeta_3 \end{bmatrix}^T. \quad (6.14)$$

The transformation yields

$$\frac{d\zeta_1}{d\tau} = \frac{\zeta_2}{\bar{b}}, \quad (6.15a)$$

$$\frac{d\zeta_2}{d\tau} = -\bar{k}_1 [\zeta_1]^{\frac{1}{3}} - \bar{k}_2 [\zeta_2]^{\frac{1}{2}} + \zeta_3, \quad (6.15b)$$

$$\frac{d\zeta_3}{d\tau} = -\frac{1}{\bar{b}} \left(\bar{k}_3 [\zeta_1]^0 + \frac{\bar{\delta}}{\mu} \right). \quad (6.15c)$$

Please note that $\frac{|\bar{\delta}|}{\mu} \leq 1$ holds (according to (6.8b)). This fact is used to design a Lyapunov function in the following. Even though unknown \bar{b} exists here, the Lyapunov function candidate considered in [Tor+17] can still be employed. Having taken the time derivative of the Lyapunov function given in (4.21) along the trajectories of system (6.15),

$$\frac{dV}{d\tau} = -(W_1 + W_2) \quad (6.16)$$

is derived. The functions W_1 and W_2 are the same as those written in (4.23) and (4.25) respectively, where their coefficients read as

$$\begin{aligned} \beta_1 &= \alpha_2 \bar{k}_1, & \beta_2 &= \alpha_2 \bar{k}_2, & \beta_3 &= \frac{5\alpha_1}{3\bar{b}}, & \beta_4 &= \frac{5}{2} \alpha_3 \bar{k}_1, \\ \beta_5 &= \frac{5}{2} \alpha_3 \bar{k}_2 - \frac{\alpha_2}{\bar{b}}, & \beta_6 &= \alpha_2, & \beta_7 &= \frac{2\alpha_4 \bar{k}_3}{\bar{b}}, & \beta_8 &= \alpha_5 \bar{k}_1, \\ \beta_9 &= \frac{5\alpha_6 \bar{k}_3}{\bar{b}}, & \beta_{10} &= \frac{5}{2} \alpha_3, & \beta_{11} &= \frac{\alpha_4}{\bar{b}}, & \beta_{12} &= \alpha_5 \bar{k}_2, \\ \beta_{13} &= \frac{3\alpha_5 \bar{k}_3}{\bar{b}}, & \beta_{14} &= \alpha_5, \end{aligned} \quad (6.17a)$$

and

$$\begin{bmatrix} \beta_{15} & \beta_{16} & \beta_{17} \end{bmatrix}^T = \begin{bmatrix} 2\alpha_4 & 3\alpha_5 & 5\alpha_6 \end{bmatrix}^T \frac{1}{\bar{b}} \begin{pmatrix} \bar{\delta} \\ \mu \end{pmatrix}. \quad (6.17b)$$

Conditions of the control parameters and the coefficients α are determined using a sum-of-squares optimization such that the positive definiteness of V and $W_1 + W_2$ and an inequality corresponding to level sets of the Lyapunov function V , which is given in the following, are satisfied. Considering the extrema of $\frac{\bar{\delta}}{\mu}$ mentioned above, the coefficients of W_2 can be denoted by the overlined letters as

$$\begin{bmatrix} \overline{\beta}_{15} & \overline{\beta}_{16} & \overline{\beta}_{17} \end{bmatrix}^T = \pm \frac{1}{\bar{b}} \begin{bmatrix} 2\alpha_4 & 3\alpha_5 & 5\alpha_6 \end{bmatrix}^T. \quad (6.18)$$

It is noted that for W_1 and W_2 , the upper and lower bounds of \bar{b} are taken into consideration in a quadrant analysis carried out in Appendix C.

In order to guarantee the stability of the combination of the aforementioned closed loops, it needs to be ensured that the control signal remains within the given saturation bounds for all $t \geq T$. This leads to the closed loop of the continuous twisting algorithm without input saturation from that point onward. To achieve that, level sets of V , which are of the form

$$\Omega_c = \{ \zeta \in \mathbb{R}^3 \mid V(\zeta) \leq c \}, \quad (6.19)$$

are considered. It is required to establish an invariant set in the space $(\zeta_1, \zeta_2, \frac{\nu}{\mu})$. Therein, the function $\frac{\bar{a}}{\mu\bar{b}}$ acts as an offset for the third coordinate and a displacement of the equilibrium point with the maximum amplitude of $\frac{\bar{a}M}{\mu\bar{b}m}$ is made along the $\frac{\nu}{\mu}$ -axis. Therefore, ζ_3 in $V(\zeta)$ can be replaced with $\frac{1}{\mu} \left(\nu + \frac{\bar{a}}{\bar{b}} \right)$, where $\frac{\nu}{\mu}$ can be represented by $\pm \frac{\rho}{\mu} + \bar{k}_1 [\zeta_1]^{\frac{1}{3}} + \bar{k}_2 [\zeta_2]^{\frac{1}{2}}$ (the planes, which are defined such that the control signal is on the border of the saturation limit). The largest level c_1 such that $|u| \leq \rho$ holds in the entire set Ω_{c_1} can be computed as

$$c_1 = \min_{\left| \frac{\bar{a}}{\bar{b}} \right| \leq \frac{\bar{a}M}{\bar{b}m}} \min_{\zeta} \left\{ V(\zeta) \mid \zeta_3 = \frac{\rho}{\mu} + \bar{k}_1 [\zeta_1]^{\frac{1}{3}} + \bar{k}_2 [\zeta_2]^{\frac{1}{2}} + \frac{\bar{a}}{\mu\bar{b}} \right\}. \quad (6.20)$$

Due to symmetry reasons, $u = \rho$ is only considered. The switching parameter γ needs to be selected such that the states z_1 and z_2 are within Ω_{c_1} at the switching time instant T . The smallest level c_2 for a given γ such that the states are contained in the set Ω_{c_2} at T can be calculated as

$$c_2 = \max_{\left| \frac{\bar{a}}{\bar{b}} \right| \leq \frac{\bar{a}M}{\bar{b}m}} \left\{ V \left(\zeta_1, \zeta_2, -\frac{\bar{a}}{\mu\bar{b}} \right) \mid \mu^{\frac{1}{3}} |\zeta_1|^{\frac{1}{3}} + \mu^{\frac{1}{2}} |\zeta_2|^{\frac{1}{2}} \leq \gamma \right\}. \quad (6.21)$$

6. Lyapunov-based Saturated Continuous Twisting Algorithm

It can be concluded that the states are in Ω_{c_1} after the switch if

$$c_2 \leq c_1 \quad (6.22)$$

is fulfilled. Through the aforementioned quadrant analysis conducted in Appendix C, allowable values of \bar{a}_M , \bar{b}_m , and $\bar{\delta}_M$ for the assigned control constants γ , \bar{k}_1 , \bar{k}_2 , and \bar{k}_3 and the given bound ρ are found such that V and $W_1 + W_2$ are positive definite and inequality (6.22) holds. It is noted that $\gamma = 0$ can be chosen here since the twisting algorithm can make that the states tend to the origin in a finite time. By this choice, as it is shown in therein, the least restrictive upper bound of $\frac{\bar{a}_M}{\bar{b}_m}$ is obtained. Having taken into consideration the permissible upper and lower bounds of μ , inequality (6.22) is satisfied for all values of $\bar{\delta}_M \geq 0$. \square

Remark 6.2. For every initial values of z_1 and z_2 , the estimate information \hat{z}_2 obtained through the super-twisting observer presented in (4.11) cannot be used instead of z_2 in the above proposed approaches. This becomes evident by considering the following counterexample. Let's imagine that $z_{1,0}$ is a small value close to zero and $z_{2,0}$ is far away from the origin. Since z_1 is available for measurement and z_2 is not, the initial values of the observer are set as $\begin{bmatrix} \tilde{z}_{1,0} & \hat{z}_{2,0} \end{bmatrix} = \begin{bmatrix} z_{1,0} & 0 \end{bmatrix}$. Having replaced $z_2(t)$ with $\hat{z}_2(t)$ in (6.2), the time instant T may be zero and therefore, the continuous twisting algorithm is recovered at the very beginning. However, in a finite time, \hat{z}_2 tends to z_2 , whose initial value is far away from zero and its absolute value may be still big enough to make that the generated control signal exceeds the saturation limits at a time instant greater than T . In other words, the aforementioned invariant set cannot be established since the error e_2 and its time derivative are added to closed loop (6.15). This problem is, however, trivial. Since the convergence time of the observer error dynamics can be estimated accurately (see e.g. [SHF18]), it is possible to employ a linear controller while the observer errors drive to zero and thereafter the proposed control techniques are brought into play.

Remark 6.3. It is worth mentioning that the proposed Lyapunov-based saturated continuous twisting algorithm does not work with every relay controller, i.e. a suitable one needs to be incorporated into the control law design. For instance, having applied the control algorithm with prescribed convergence law (see e.g. [Lev93; Sht+14]) as

$$u = -\rho \left[z_2 + \lambda \left[z_1 \right]^{\frac{1}{2}} \right]^0, \quad (6.23)$$

where λ is a positive constant, the system trajectory may reach the sliding manifold $z_2 + \lambda \left[z_1 \right]^{\frac{1}{2}} = 0$ before switching to the continuous twisting algorithm. This produces the chattering effect and thus, such a relay controller cannot be used.

Remark 6.4. For systems of order more than two, the concept of the Lyapunov-based saturated continuous twisting algorithm can be generalized if suitable relay controllers, e.g. extensions of the twisting algorithm, are built up. The continuous twisting algorithm for the higher-order systems (see [MMF17; MMF19]) can be employed for $t \geq T$ since a family of Lyapunov functions has been proposed for it. For the triple integrator system described by

$$\frac{dz_1}{dt} = z_2, \quad (6.24a)$$

$$\frac{dz_2}{dt} = z_3, \quad (6.24b)$$

$$\frac{dz_3}{dt} = u \quad (6.24c)$$

under the control law

$$u = -\rho_1 [z_1]^0 - \rho_2 [z_2]^0 - \rho_3 [z_3]^0, \quad (6.25)$$

it is shown in [SM13] that there is no set of the positive constants ρ_1 , ρ_2 , and ρ_3 such that the origin of the closed-loop system is globally asymptotically stable. It is, however, proved therein that for *almost every* initial condition, the system states can tend to the origin in a finite time. Investigations of the saturated algorithm that consists in switching from this relay controller to the continuous twisting controller for the third-order system should be conducted in the future.

6.3. Simulation Examples

In this section, comparing to the control strategies recorded in the literature and the previous two chapters, it is illustrated in simulation how the control approaches proposed in this chapter and particularly the Lyapunov-based saturated continuous twisting algorithm can handle two different problem settings (assuming both of the system states are available for measurement). Since uncertainties and multiplicative unknowns are not taken into consideration in [Tor+17] and Chapter 4, the simulation example considered in Chapters 1 and 4 is revisited in the first case. The simulation example of Subsection 5.4.2, where the system is subject to uncertainties and disturbances, is revisited in the second case. While the saturation limit $\rho = 10$ is left unchanged, the bounds of perturbations are enlarged here as given in the following.

In the first case, the result obtained through the saturated CTA presented in Chapter 4 is compared with the achieved closed-loop performances of the proposed schemes in this chapter. Furthermore, in order to make a comparison, the system under the standard continuous twisting control law given in (1.7) is simulated. In the second

case, the results achieved by applying the saturated feedback control presented in Chapter 5 and the Lyapunov-based saturated continuous twisting algorithm are compared.

6.3.1. First Case

In this simulation case, the bound of the function given in (1.8) is increased and perturbations are denoted by

$$\bar{a}(t) = 2.5 + 0.4 \sin(t) + 0.2 \sin(4t). \quad (6.26)$$

As mentioned above, $\frac{\partial \bar{a}}{\partial z_2} = 0$ and $\bar{b} = 1$ hold in this case. It is noted that \bar{a} and its time derivative are bounded by $\bar{a}_M = 3.1$ and $L_{\bar{a}} = 1.2$ respectively. Hence, the conditions laid down in Proposition 6.1 are met and the versions of the saturated CTA proposed in this chapter are able to handle these disturbances, whereas the saturated CTA introduced in Chapter 4 cannot deal with them. As assigned in [Tor+17], the scaled parameters $l_1 = 14.68$, $l_2 = 8.22$, $l_3 = 2.76$, and $l_4 = 1.32$ of the standard CTA given in (1.7) are chosen based on $L_{\bar{a}}$. Similar to Chapter 4, the effectiveness of the proposed schemes in this chapter as well as the saturated CTA is assessed by selecting the constants k_1 , k_2 , and k_3 of control laws (4.6), (6.1), and (6.5) the same as l_1 , l_2 , and l_3 respectively. For controller (4.6), there is no chance to tune ϵ_1 , ϵ_2 , and k_4 such that all inequalities given in (4.16) and (4.49) are satisfied. They are assigned as $\epsilon_1 = 0.39$, $\epsilon_2 = 0.34$, and $k_4 = 2$ to confine the control signal to $\pm\rho$. For controller (6.1), $\epsilon_1 = 0.45$ and $\epsilon_2 = 0.4$ are chosen to meet the conditions given in (6.3). For both of the control laws designed in this chapter, 0.3 is assigned to γ .

For all the algorithms, the numerical simulation is carried out with the sampling step size of 1 ms and the initial values $\begin{bmatrix} z_{1,0} & z_{2,0} \end{bmatrix} = \begin{bmatrix} 230 & -20 \end{bmatrix}$ and $\nu_0 = 0$. Their performance is illustrated in Figure 6.2. It is revealed in the upper and middle plots that the same rate of convergence is achieved by applying the strategies introduced in this chapter. They contribute substantially to the alleviation of the windup effect since their produced signals remain within the saturation bounds. The evolution of the control signals introduced to the system through the saturating actuator is demonstrated in the lower plot. Please note that only for control law (1.7), this is different from the generated control signal u , which is not bounded by the saturation limits. As explained before, this causes a long settling time and large overshoots and undershoots in the results of standard CTA. As it is shown in the zoomed portions of the state plots, similar precision is obtained through the Lyapunov-based saturated CTA, modified saturated CTA, and standard CTA. It can be seen that the states of the system under the control law proposed in Chapter 4 do not converge with the same accuracy as those achieved by the other algorithms. This is due to

that both inequalities (4.16b) and (4.49) cannot be fulfilled in this example, where the upper bound \bar{a}_M is close to $\frac{\rho}{3}$.

In the case $\gamma = 0.05$ is set, the performances of the new versions of the saturated CTA presented in this chapter are compared in Figure 6.3. As expected, the states of the perturbed system under control law (6.1) cannot tend to the origin with the same precision as that obtained through applying controller (6.5). This is explained earlier in this chapter that γ cannot be selected arbitrarily small in the modified saturated CTA.

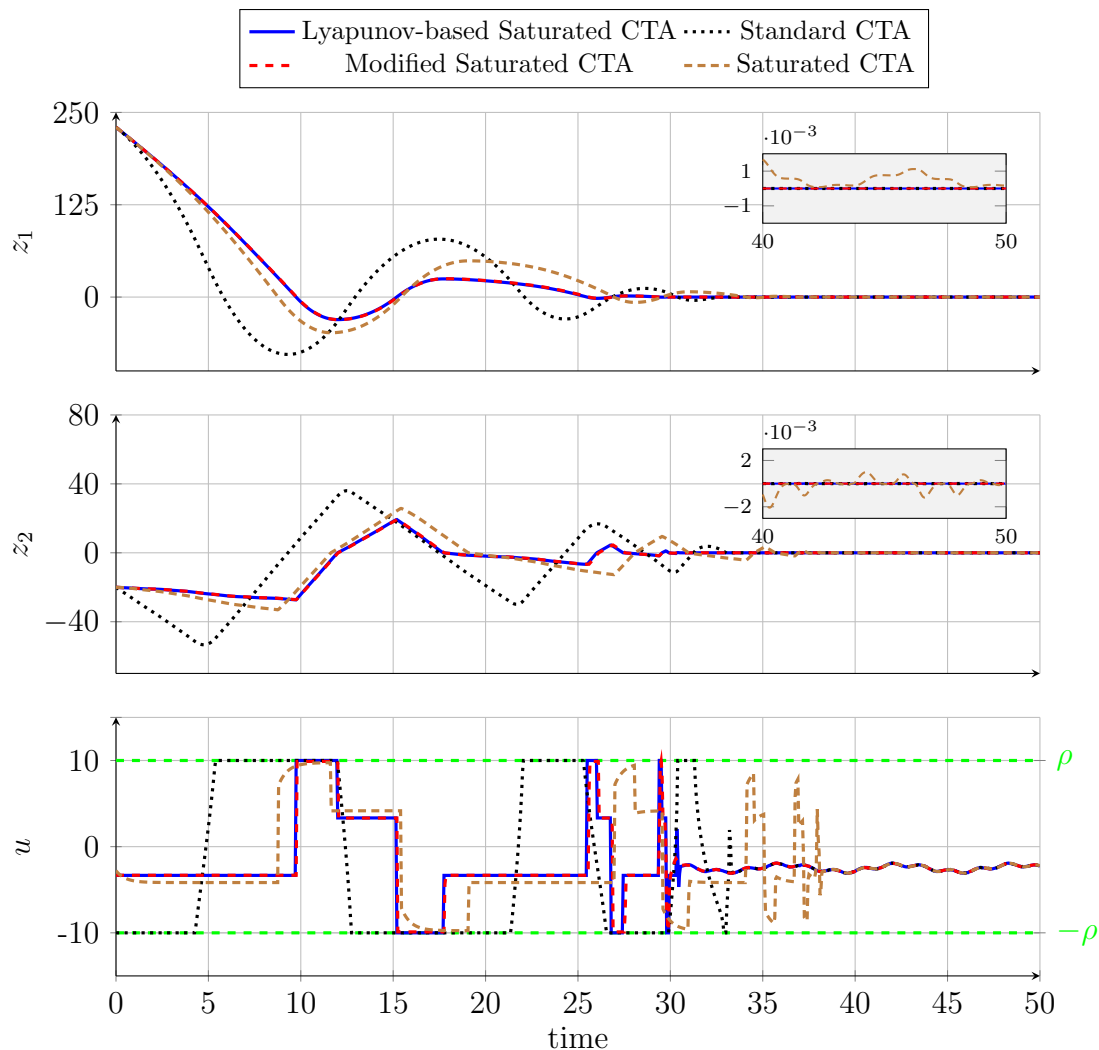


Figure 6.2.: Simulation response curves of the perturbed double integrator system under four control laws (6.5), (1.7), (6.1), and (4.6), which are labeled respectively with Lyapunov-based Saturated CTA, Standard CTA, Modified Saturated CTA, and Saturated CTA. It is noted that 0.3 is assigned to the switching level parameter γ .

6.3.2. Second Case

In this case, \bar{b} given in (5.19b) is left unchanged and \bar{a} given in (5.19a) is replaced with

$$\bar{a}(t, z_2) = 1.35 + 0.3 \sin(t) + 0.1 \sin(\sqrt{10}t) + 0.05 \cos(z_2). \quad (6.27)$$

It is noted that the conditions imposed in Proposition 6.1 are satisfied since $\bar{b}_m = 0.9$, $\bar{a}_M = 1.8$, and $\bar{\delta}_M = 2.15$. As mentioned before, this problem setting is not dealt with in [Tor+17] and Chapter 4. It is, however, addressed in the previous chapter. Since the Full State Information scenario is considered here, the estimate of the time derivative of z_2 , which is incorporated into the state feedback control using the twisting algorithm, can be obtained through the first-order RED. Thus, observer (5.5) is replaced with

$$e_2 = z_2 - \hat{z}_2, \quad (6.28a)$$

$$\frac{d\hat{z}_2}{dt} = u + \mu_1 [e_2]^{\frac{1}{2}} + \tilde{z}_2, \quad (6.28b)$$

$$\frac{d\tilde{z}_2}{dt} = \mu_2 [e_2]^0. \quad (6.28c)$$

In that case, twisting algorithm-based control law (5.12) is rewritten as

$$\frac{du}{dt} = -k \left([\sigma_1]^0 + \frac{1}{2} [\sigma_2]^0 \right) - \mu_2 [e_2]^0 - \lambda u, \quad (6.29a)$$

with

$$\sigma_1 = z_2 + \lambda z_1, \quad (6.29b)$$

$$\sigma_2 = u + \tilde{z}_2 + \lambda z_2. \quad (6.29c)$$

The observer gains $\mu_1 = 1.5\sqrt{\psi_M} = 5.65$ and $\mu_2 = 1.1\psi_M = 15.59$ are selected (ψ_M is the upper bound of the absolute value of ψ computed in (5.16d)). The same values as set in the previous chapter are assigned to λ and u_0 . In order to retain the control signal within the saturation limits, $k = 22.94$ is chosen such that $\rho \geq \frac{3k+2\mu_2}{2\lambda}$ is fulfilled. The parameters $k_1 = 16.66$, $k_2 = 7.33$, and $k_3 = 2.36$ of the Lyapunov-based saturated CTA are tuned as given in (6.8a). $\gamma = 0.05$ and $\nu_0 = 0$ are set in this simulation case.

For both of the algorithms, the numerical simulation is carried out with the same sampling interval and initial values as used in the previous case. The finite-time convergence of the error dynamics of the observer, whose information is exploited in implementation of control law (6.29), is indicated in Figure 6.4. Since \bar{a}_M is greater here comparing to the example taken in Subsection 5.4.2, there is no chance both inequalities (5.16a) and (5.16b) hold. Hence, as it is depicted in Figure 6.5, the convergence of the system states under the twisting algorithm-based control law is not as satisfactory as that achieved by the Lyapunov-based saturated CTA.

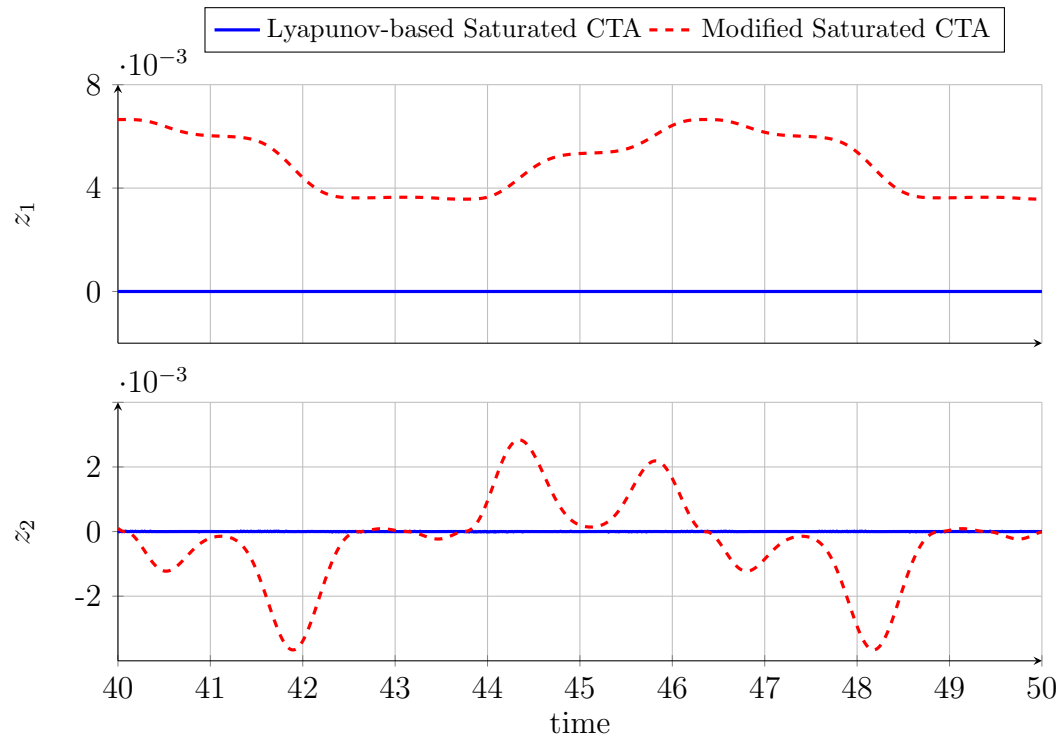


Figure 6.3.: Simulation results (zoomed portions of the state plots) for the perturbed system under the new versions of the saturated continuous twisting control designed in this chapter in the case $\gamma = 0.05$ is selected.

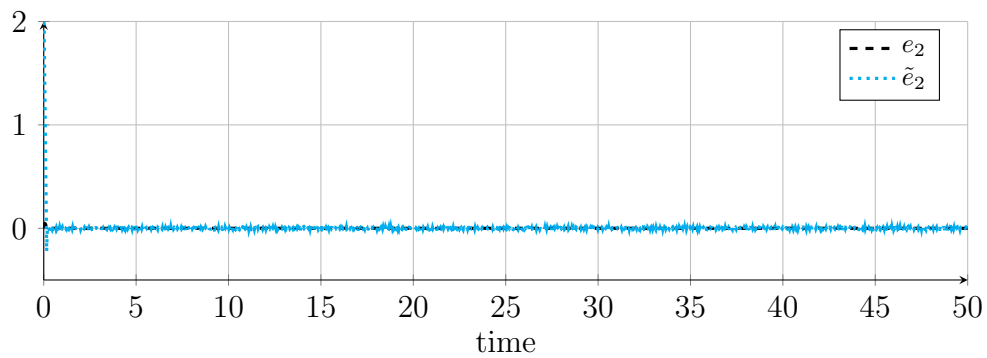


Figure 6.4.: Simulated errors of the first-order RED used for the case of system with disturbances and uncertainties. Since z_2 is assumed to be also available for measurement in this chapter, this observer is employed to provide \tilde{z}_2 for the twisting algorithm-based control law.

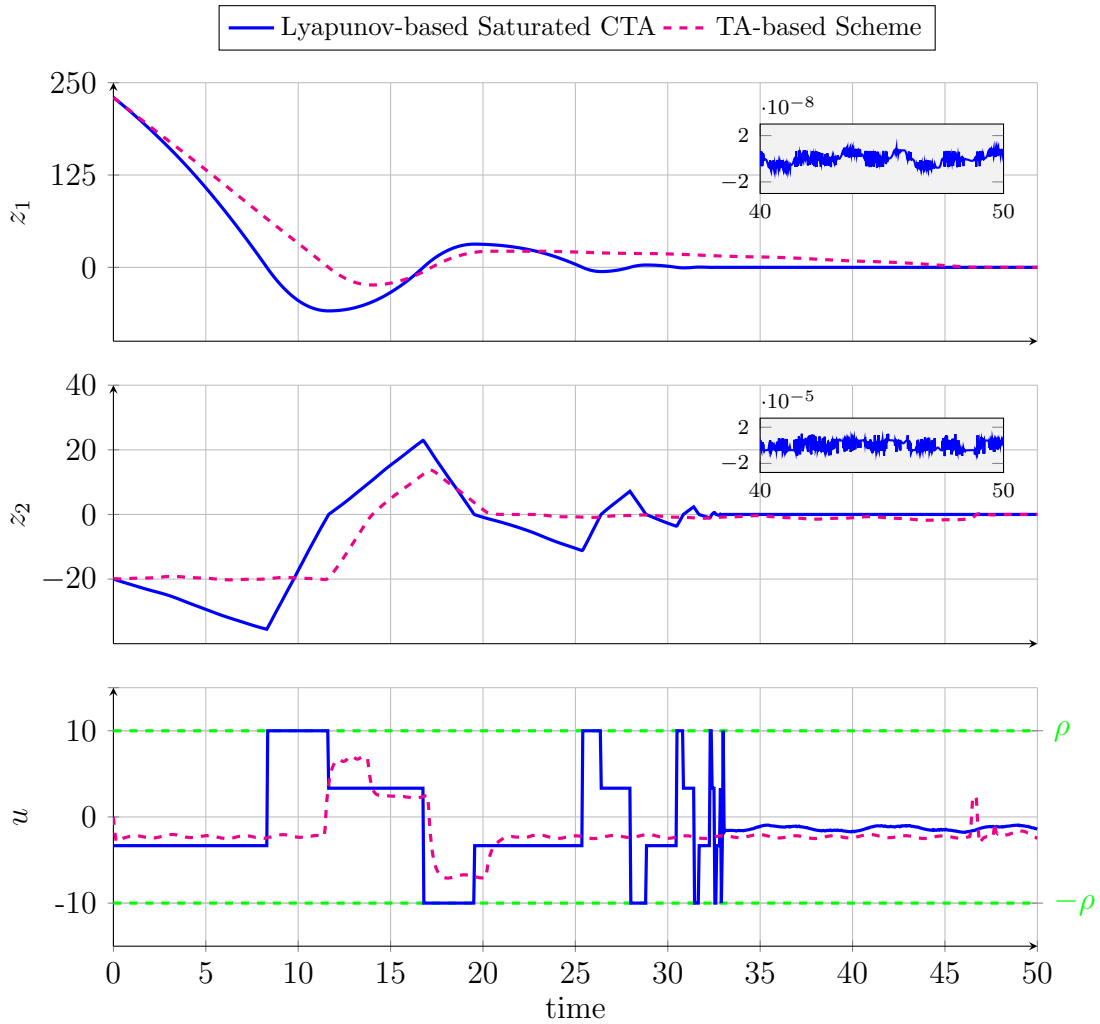


Figure 6.5.: Simulation response curves comparing the Lyapunov-based saturated continuous twisting algorithm introduced in this chapter with the twisting algorithm-based approach presented in the previous chapter. In this simulation case, the system is subject to disturbances and uncertainties.

6.4. Experimental Implementation

In order to test the Lyapunov-based saturated continuous twisting algorithm in a real-world application, it is applied to the hydraulic differential cylinder system described within Section 4.5. To compare the closed-loop performance with the results shown in Figure 4.6, the gains k_1 , k_2 , and k_3 of control law (6.5) are chosen respectively the same as l_1 , l_2 , and l_3 given in (4.61). Furthermore, 0.4 is assigned to γ . It is noted that the time derivative of z_1 needs to be estimated in this real-world system. Therefore, as proposed in Remark 6.2, having converged \hat{z}_2 to z_2 , the

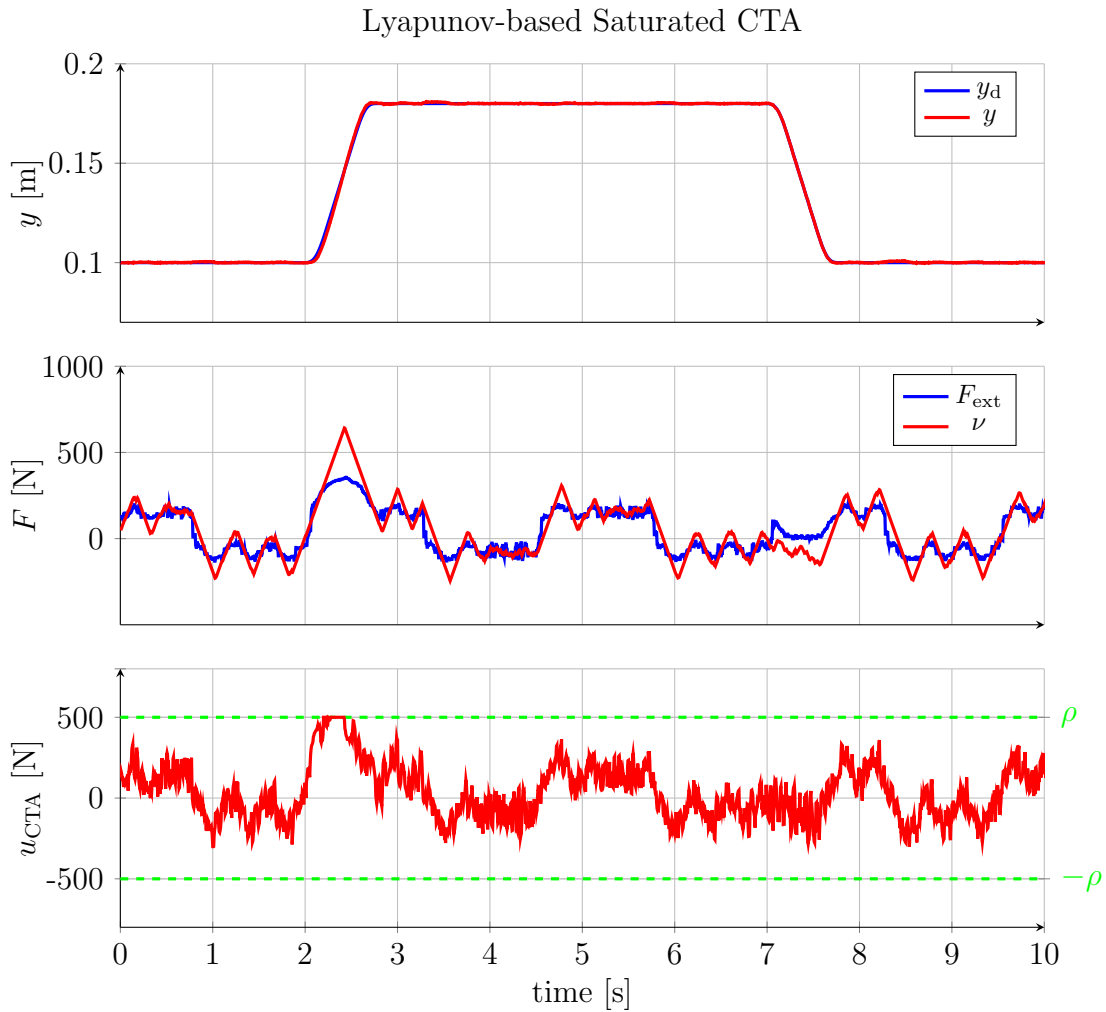


Figure 6.6.: Experimental performance of the proposed Lyapunov-based saturated continuous twisting algorithm (after converging the observer errors). The position, external force, and control input are depicted.

Lyapunov-based saturated CTA comes into play. The response curves are illustrated in Figure 6.6. It can be seen that, similar to the saturated CTA, the produced control signal remains within the saturation bounds (due to the structure of the algorithm). As a consequence, the windup effect is also alleviated here and a similar satisfactory performance is obtained through applying this new version of the saturated CTA.

7. Conclusion and Outlook

This thesis presents feedback control techniques for first and second-order systems affected by perturbations and uncertainties. Since the control inputs are introduced to the systems through saturating actuators, anti-windup strategies are incorporated into the design of the control laws.

Having applied the saturated super-twisting algorithm built up in this study to the first-order system, the global asymptotic stability of the closed-loop system origin is proved by means of different Lyapunov functions. Furthermore, the finite-time convergence is guaranteed based on the quasihomogeneity principle. In the case that the approach proposed in Chapter 3 is applied to this system, it is shown by means of a Lyapunov function that these closed-loop system states also converge to the origin in a finite time. For different problem settings in simulation, the performance of both the approaches indicates that the generated control signal is continuous everywhere and the windup effect is alleviated. However, in the latter, the standard super-twisting algorithm is recovered after a finite time. This results in that the class of addressed disturbances is not restricted by the saturation limit. Furthermore, without using a disturbance estimator, the latter scheme is able to reject perturbations and uncertainties with the maximum permissible bound that can be handled with the actuator limitation.

For both scenarios of the perturbed double integrator system, Full State Information and Output Feedback Control, the saturated continuous twisting algorithm is developed. A Lyapunov function and a geometric scheme are incorporated into the global asymptotic stability proof of the closed-loop system origin. The finite-time convergence is realized based on the quasihomogeneity principle again. In the case that the twisting algorithm-based control considered in Chapter 5 is employed, the sliding function drives to zero in a finite time. This implies that the system states tend to the origin asymptotically therein. Having applied the Lyapunov-based saturated continuous twisting algorithm introduced in Chapter 6, the global finite-time stability of the closed-loop system origin is guaranteed by means of a Lyapunov-based proof if both of the system states are available. Therefore, as proposed therein, this controller is used after the convergence of the observer errors. To provide required estimates in the above approaches, an appropriate order of the robust exact differentiator is adopted to the observer. The aforementioned controllers can be tuned such that the produced signals remain within the saturation bounds. This contributes greatly to mitigation of the windup effect, which is confirmed through the experimental studies

7. Conclusion and Outlook

on a hydraulic differential cylinder as well as numerical simulations. It is noted that the continuous twisting algorithm is recovered after a finite time in the last control technique. Hence, the bound and class of addressed perturbations and uncertainties are enlarged through that.

A list of problems of interest for future work is:

- investigating proper discretization schemes, which are applicable to the proposed saturated feedback control algorithms;
- carrying out the stability analysis of the closed-loop system, in which the extended version of the Lyapunov-based saturated continuous twisting algorithm, as mentioned in Remark 6.4, is applied to a perturbed third-order system;
- developing suitable relay controllers that can be incorporated into the extensions of the Lyapunov-based saturated continuous twisting algorithm for higher-order systems;
- designing non-redundant control laws based on robust higher-order sliding mode observers for such perturbed systems with saturating actuators.

Appendices

A. Quadrant Analysis for the Saturated Super-Twisting Algorithm

The functions V defined in (2.39) and W_1 and W_2 given in (2.41) are symmetric with respect to the origin. Therefore, the two sets

$$\mathcal{N}_1 = \{\tilde{x}_1, \tilde{x}_2 \geq 0\} \quad (\text{A.1a})$$

and

$$\mathcal{N}_2 = \{\tilde{x}_1 \geq 0, \tilde{x}_2 \leq 0\}, \quad (\text{A.1b})$$

out of four sets, only need to be considered. The coordinates are changed to $\tilde{\boldsymbol{\vartheta}} = [\tilde{\vartheta}_1 \ \tilde{\vartheta}_2]^\text{T}$ as

$$|\tilde{x}_1| = \tilde{\vartheta}_1^4, \quad |\tilde{x}_2| = \tilde{\vartheta}_2^2. \quad (\text{A.2})$$

Please note that the even numbers are assigned to the exponents in order to satisfy the quadrant constraints. For the above sets \mathcal{N}_1 and \mathcal{N}_2 , $V_1(\tilde{\boldsymbol{\vartheta}})$ and $V_2(\tilde{\boldsymbol{\vartheta}})$ are written respectively as

$$V_1(\tilde{\boldsymbol{\vartheta}}) = \alpha_1 \tilde{\vartheta}_1^6 - \alpha_2 \tilde{\vartheta}_1^4 \tilde{\vartheta}_2^2 + \alpha_3 \tilde{\vartheta}_2^6 \quad (\text{A.3a})$$

and

$$V_2(\tilde{\boldsymbol{\vartheta}}) = \alpha_1 \tilde{\vartheta}_1^6 + \alpha_2 \tilde{\vartheta}_1^4 \tilde{\vartheta}_2^2 + \alpha_3 \tilde{\vartheta}_2^6. \quad (\text{A.3b})$$

For the aforementioned quadrants, $W_1(\tilde{\boldsymbol{\vartheta}})$ is given as

$$W_{11}(\tilde{\boldsymbol{\vartheta}}) = \beta_1 \tilde{\vartheta}_1^4 - \beta_2 \tilde{\vartheta}_1^2 \tilde{\vartheta}_2^2 + (\beta_3 + \beta_4) \tilde{\vartheta}_2^4 \quad (\text{A.4a})$$

and

$$W_{12}(\tilde{\boldsymbol{\vartheta}}) = \beta_1 \tilde{\vartheta}_1^4 + \beta_2 \tilde{\vartheta}_1^2 \tilde{\vartheta}_2^2 + (-\beta_3 + \beta_4) \tilde{\vartheta}_2^4 \quad (\text{A.4b})$$

respectively.

The coefficients β_5 and β_6 given in (2.42b) are only subject to some bounded time-varying functions. In both the sets \mathcal{N}_1 and \mathcal{N}_2 , the maximum and minimum values of

A. Quadrant Analysis for the Saturated Super-Twisting Algorithm

β_6 are $\pm\bar{\beta}_6 = \pm 3\alpha_3$. In order to find the upper bound of $\Psi = \frac{-k_3\nu + \frac{da}{dt}}{\phi_M}$, the minimum value of ν needs to be realized. In the case $\tilde{x}_2 \geq 0$, $\nu \geq -a_M$ holds and thus, the maximum value of Ψ is one (based on (2.13)). Its lower bound is similarly calculated by setting the maximum value of ν , which is ν_M . As a result, the minimum value of $-k_3\nu + \frac{da}{dt}$ is $-k_2 - L_a$. Since $\frac{L_a}{\phi_M} \leq 1$ holds (according to (2.13)), the lower bound of Ψ considering (2.30) is $-\tilde{k}_2 - 1$. Hence, $W_2(\tilde{\boldsymbol{\vartheta}})$ for the set \mathcal{N}_1 reads as

$$\overline{W_{21}}(\tilde{\boldsymbol{\vartheta}}) = \bar{\beta}_5\tilde{\vartheta}_1^4 - \bar{\beta}_6\tilde{\vartheta}_2^4, \quad (\text{A.5a})$$

$$\underline{W_{21}}(\tilde{\boldsymbol{\vartheta}}) = -\tilde{\beta}_5\tilde{\vartheta}_1^4 + \bar{\beta}_6\tilde{\vartheta}_2^4, \quad (\text{A.5b})$$

where the coefficients $\bar{\beta}_5$ and $\tilde{\beta}_5$ are

$$\bar{\beta}_5 = \alpha_2, \quad \tilde{\beta}_5 = \alpha_2 \left(\tilde{k}_2 + 1 \right). \quad (\text{A.6})$$

For $\tilde{x}_2 \leq 0$, the upper bound of Ψ is $\tilde{k}_2 + 1$ since ν can be greater than or equal to $-\nu_M$. Its minimum value in this case is -1 due to the fact that $\nu \leq a_M$ holds therein. Therefore, $W_2(\tilde{\boldsymbol{\vartheta}})$ for the set \mathcal{N}_2 is

$$\overline{W_{22}}(\tilde{\boldsymbol{\vartheta}}) = \tilde{\beta}_5\tilde{\vartheta}_1^4 + \bar{\beta}_6\tilde{\vartheta}_2^4, \quad (\text{A.7a})$$

$$\underline{W_{22}}(\tilde{\boldsymbol{\vartheta}}) = -\bar{\beta}_5\tilde{\vartheta}_1^4 - \bar{\beta}_6\tilde{\vartheta}_2^4. \quad (\text{A.7b})$$

It becomes evident that to guarantee the functions V and $W_1 + W_2$ are positive definite, two polynomials for V and four polynomials for $W_1 + W_2$ need to be sum of squares at the same time. Please note that the positive definiteness of a function is ensured if the corresponding polynomials, after subtraction of positive polynomials with the same degree, are sum of squares (e.g. V is positive definite if $V_1(\tilde{\boldsymbol{\vartheta}}) - \Gamma$ and $V_2(\tilde{\boldsymbol{\vartheta}}) - \Gamma$ are sum of squares, where Γ is $c_\Gamma \left(\tilde{\vartheta}_1^6 + \tilde{\vartheta}_2^6 \right)$ with a small enough positive real constant c_Γ). Exemplarily, having selected the gains given in (2.32), the coefficients α_1 , α_2 , and α_3 obtained through SOSTOOLS [Pap+13] with $c_\Gamma = 0.001$ are

$$\alpha_1 = 2.32, \quad \alpha_2 = 1.13, \quad \alpha_3 = 0.17. \quad (\text{A.8})$$

B. Quadrant Analysis for the Saturated Continuous Twisting Algorithm

Since the functions V defined in (4.21) and W_1 and W_2 given in (4.23) and (4.25) are symmetric with respect to the origin, the following four sets out of eight sets only need to be considered:

$$\mathcal{M}_1 = \{\zeta_1, \zeta_2, \zeta_3 \geq 0\}, \quad (\text{B.1a})$$

$$\mathcal{M}_2 = \{\zeta_2, \zeta_3 \geq 0, \zeta_1 \leq 0\}, \quad (\text{B.1b})$$

$$\mathcal{M}_3 = \{\zeta_1, \zeta_3 \geq 0, \zeta_2 \leq 0\}, \quad (\text{B.1c})$$

$$\mathcal{M}_4 = \{\zeta_1, \zeta_2 \geq 0, \zeta_3 \leq 0\}. \quad (\text{B.1d})$$

Similar to that made for the saturated super-twisting control in the previous appendix, the coordinates are changed to $\boldsymbol{\vartheta} = [\vartheta_1 \ \vartheta_2 \ \vartheta_3]^T$ as

$$|\zeta_1| = \vartheta_1^6, \quad |\zeta_2| = \vartheta_2^4, \quad |\zeta_3| = \vartheta_3^2. \quad (\text{B.2})$$

The exponents are also even numbers here to fulfill the octant constraints. For the aforementioned sets $\mathcal{M}_1, \mathcal{M}_2, \mathcal{M}_3,$ and \mathcal{M}_4 , $V(\boldsymbol{\vartheta})$ is given as

$$V_1(\boldsymbol{\vartheta}) = \alpha_1 \vartheta_1^{10} + \alpha_2 \vartheta_1^6 \vartheta_2^4 + \alpha_3 \vartheta_2^{10} + \alpha_4 \vartheta_1^6 \vartheta_3^4 - \alpha_5 \vartheta_2^4 \vartheta_3^6 + \alpha_6 \vartheta_3^{10}, \quad (\text{B.3a})$$

$$V_2(\boldsymbol{\vartheta}) = \alpha_1 \vartheta_1^{10} - \alpha_2 \vartheta_1^6 \vartheta_2^4 + \alpha_3 \vartheta_2^{10} - \alpha_4 \vartheta_1^6 \vartheta_3^4 - \alpha_5 \vartheta_2^4 \vartheta_3^6 + \alpha_6 \vartheta_3^{10}, \quad (\text{B.3b})$$

$$V_3(\boldsymbol{\vartheta}) = \alpha_1 \vartheta_1^{10} - \alpha_2 \vartheta_1^6 \vartheta_2^4 + \alpha_3 \vartheta_2^{10} + \alpha_4 \vartheta_1^6 \vartheta_3^4 + \alpha_5 \vartheta_2^4 \vartheta_3^6 + \alpha_6 \vartheta_3^{10}, \quad (\text{B.3c})$$

$$V_4(\boldsymbol{\vartheta}) = \alpha_1 \vartheta_1^{10} + \alpha_2 \vartheta_1^6 \vartheta_2^4 + \alpha_3 \vartheta_2^{10} - \alpha_4 \vartheta_1^6 \vartheta_3^4 + \alpha_5 \vartheta_2^4 \vartheta_3^6 + \alpha_6 \vartheta_3^{10}, \quad (\text{B.3d})$$

respectively. For these sets, $W_1(\boldsymbol{\vartheta})$ is written as

$$W_{11}(\boldsymbol{\vartheta}) = \beta_1 \vartheta_1^8 + \beta_2 \vartheta_1^6 \vartheta_2^2 - \beta_3 \vartheta_1^4 \vartheta_2^4 + \beta_4 \vartheta_1^2 \vartheta_2^6 + \beta_5 \vartheta_2^8 - (\beta_6 - \beta_7) \vartheta_1^6 \vartheta_3^2 - \beta_8 \vartheta_1^2 \vartheta_3^6 - \beta_{10} \vartheta_2^6 \vartheta_3^2 - (\beta_{11} + \beta_{13}) \vartheta_2^4 \vartheta_3^4 - \beta_{12} \vartheta_2^2 \vartheta_3^6 + (\beta_9 + \beta_{14}) \vartheta_3^8, \quad (\text{B.4a})$$

$$W_{12}(\boldsymbol{\vartheta}) = \beta_1 \vartheta_1^8 - \beta_2 \vartheta_1^6 \vartheta_2^2 + \beta_3 \vartheta_1^4 \vartheta_2^4 - \beta_4 \vartheta_1^2 \vartheta_2^6 + \beta_5 \vartheta_2^8 + (\beta_6 + \beta_7) \vartheta_1^6 \vartheta_3^2 + \beta_8 \vartheta_1^2 \vartheta_3^6 - \beta_{10} \vartheta_2^6 \vartheta_3^2 - (\beta_{11} - \beta_{13}) \vartheta_2^4 \vartheta_3^4 - \beta_{12} \vartheta_2^2 \vartheta_3^6 - (\beta_9 - \beta_{14}) \vartheta_3^8, \quad (\text{B.4b})$$

$$W_{13}(\boldsymbol{\vartheta}) = \beta_1 \vartheta_1^8 - \beta_2 \vartheta_1^6 \vartheta_2^2 + \beta_3 \vartheta_1^4 \vartheta_2^4 - \beta_4 \vartheta_1^2 \vartheta_2^6 + \beta_5 \vartheta_2^8 - (\beta_6 - \beta_7) \vartheta_1^6 \vartheta_3^2 - \beta_8 \vartheta_1^2 \vartheta_3^6 + \beta_{10} \vartheta_2^6 \vartheta_3^2 + (\beta_{11} + \beta_{13}) \vartheta_2^4 \vartheta_3^4 + \beta_{12} \vartheta_2^2 \vartheta_3^6 + (\beta_9 + \beta_{14}) \vartheta_3^8, \quad (\text{B.4c})$$

$$W_{14}(\boldsymbol{\vartheta}) = \beta_1 \vartheta_1^8 + \beta_2 \vartheta_1^6 \vartheta_2^2 - \beta_3 \vartheta_1^4 \vartheta_2^4 + \beta_4 \vartheta_1^2 \vartheta_2^6 + \beta_5 \vartheta_2^8 + (\beta_6 + \beta_7) \vartheta_1^6 \vartheta_3^2 + \beta_8 \vartheta_1^2 \vartheta_3^6 + \beta_{10} \vartheta_2^6 \vartheta_3^2 + (\beta_{11} - \beta_{13}) \vartheta_2^4 \vartheta_3^4 + \beta_{12} \vartheta_2^2 \vartheta_3^6 - (\beta_9 - \beta_{14}) \vartheta_3^8, \quad (\text{B.4d})$$

B. Quadrant Analysis for the Saturated Continuous Twisting Algorithm

respectively.

For W_2 , as mentioned before, the coefficients given in (4.26) are bounded. The maximum and minimum values of Ξ are computed for every octant in the following. Since $\zeta_3 \geq 0$ holds in the sets \mathcal{M}_1 , \mathcal{M}_2 , and \mathcal{M}_3 , ν can be just greater than or equal to $-\bar{a}_M$ therein. Thus, in these sets, Ξ is upper bounded by one (based on (4.14)). It becomes evident that its lower bound can be obtained therein by setting $\nu = \nu_M$. As a result, the minimum value of $-k_4\nu + \frac{d\bar{a}}{dt}$ is $-k_3 - L_{\bar{a}}$. Since $\frac{L_{\bar{a}}}{\phi_M} \leq 1$ holds (according to (4.14)), the lower bound of Ξ considering (4.15) is $-\bar{k}_3 - 1$. In the set \mathcal{M}_4 , where x_3 is less than or equal to zero, the upper bound of Ξ is $\bar{k}_3 + 1$. This is achieved by setting $\nu = -\nu_M$. In order to calculate its lower bound therein, the upper bound of ν needs to be determined. Here, ν cannot be greater than \bar{a}_M and therefore, Ξ is lower bounded by -1 . Hence, $W_2(\boldsymbol{\vartheta})$ in the above-mentioned sets is

$$\overline{W_{21}}(\boldsymbol{\vartheta}) = -\bar{\beta}_{15}\vartheta_1^6\vartheta_3^2 + \bar{\beta}_{16}\vartheta_2^4\vartheta_3^4 - \bar{\beta}_{17}\vartheta_3^8, \quad (\text{B.5a})$$

$$W_{21}(\boldsymbol{\vartheta}) = \tilde{\beta}_{15}\vartheta_1^6\vartheta_3^2 - \tilde{\beta}_{16}\vartheta_2^4\vartheta_3^4 + \tilde{\beta}_{17}\vartheta_3^8, \quad (\text{B.5b})$$

$$\overline{W_{22}}(\boldsymbol{\vartheta}) = \bar{\beta}_{15}\vartheta_1^6\vartheta_3^2 + \bar{\beta}_{16}\vartheta_2^4\vartheta_3^4 - \bar{\beta}_{17}\vartheta_3^8, \quad (\text{B.5c})$$

$$W_{22}(\boldsymbol{\vartheta}) = -\tilde{\beta}_{15}\vartheta_1^6\vartheta_3^2 - \tilde{\beta}_{16}\vartheta_2^4\vartheta_3^4 + \tilde{\beta}_{17}\vartheta_3^8, \quad (\text{B.5d})$$

$$\overline{W_{23}}(\boldsymbol{\vartheta}) = -\bar{\beta}_{15}\vartheta_1^6\vartheta_3^2 - \bar{\beta}_{16}\vartheta_2^4\vartheta_3^4 - \bar{\beta}_{17}\vartheta_3^8, \quad (\text{B.5e})$$

$$W_{23}(\boldsymbol{\vartheta}) = \tilde{\beta}_{15}\vartheta_1^6\vartheta_3^2 + \tilde{\beta}_{16}\vartheta_2^4\vartheta_3^4 + \tilde{\beta}_{17}\vartheta_3^8, \quad (\text{B.5f})$$

$$\overline{W_{24}}(\boldsymbol{\vartheta}) = -\tilde{\beta}_{15}\vartheta_1^6\vartheta_3^2 + \tilde{\beta}_{16}\vartheta_2^4\vartheta_3^4 + \tilde{\beta}_{17}\vartheta_3^8, \quad (\text{B.5g})$$

$$W_{24}(\boldsymbol{\vartheta}) = \bar{\beta}_{15}\vartheta_1^6\vartheta_3^2 - \bar{\beta}_{16}\vartheta_2^4\vartheta_3^4 - \bar{\beta}_{17}\vartheta_3^8, \quad (\text{B.5h})$$

where the coefficients denote

$$\begin{bmatrix} \bar{\beta}_{15} & \bar{\beta}_{16} & \bar{\beta}_{17} \end{bmatrix}^T = \begin{bmatrix} 2\alpha_4 & 3\alpha_5 & 5\alpha_6 \end{bmatrix}^T \quad (\text{B.6a})$$

and

$$\begin{bmatrix} \tilde{\beta}_{15} & \tilde{\beta}_{16} & \tilde{\beta}_{17} \end{bmatrix}^T = \begin{bmatrix} 2\alpha_4 & 3\alpha_5 & 5\alpha_6 \end{bmatrix}^T (\bar{k}_3 + 1). \quad (\text{B.6b})$$

It can be concluded that four polynomials for the Lyapunov function and eight polynomials for its time derivative need to be sum of squares at the same time in order to ensure that V_1 and $W_1 + W_2$ are positive definite. Similar to that mentioned in the previous appendix, in order to ensure that a function is positive definite, the corresponding polynomials, from which positive polynomials with the same degree are deducted, need to be sum of squares. Exemplarily, in this case V is positive definite if $V_1(\boldsymbol{\vartheta}) - \Upsilon$, $V_2(\boldsymbol{\vartheta}) - \Upsilon$, $V_3(\boldsymbol{\vartheta}) - \Upsilon$, and $V_4(\boldsymbol{\vartheta}) - \Upsilon$ are sum of squares, where Υ is $c_\Upsilon (\vartheta_1^{10} + \vartheta_2^{10} + \vartheta_3^{10})$ with the small enough positive real constant c_Υ . If

the gains \bar{k}_1 , \bar{k}_2 , and \bar{k}_3 are selected as given in (4.17), the coefficients $\boldsymbol{\alpha}$ obtained through SOSTOOLS [Pap+13] with $c_\Upsilon = 0.001$ are

$$\begin{aligned} \alpha_1 &= 5370, & \alpha_2 &= 1189, & \alpha_3 &= 269.8, \\ \alpha_4 &= -118.1, & \alpha_5 &= 1.9, & \alpha_6 &= 0.16. \end{aligned} \tag{B.7}$$

C. Quadrant Analysis for the Lyapunov-based Saturated Continuous Twisting Algorithm

Since the same Lyapunov function as that one considered in the previous appendix is applied here, having transformed the coordinates as given in (B.2), $V(\boldsymbol{\vartheta})$ for the four sets considered in (B.1) is written as those given in (B.3). It is noted that unknown \bar{b} is also addressed through the Lyapunov-based saturated CTA and therefore, in each octant, two polynomials for $W_1(\boldsymbol{\vartheta})$ based on the upper and lower bounds of \bar{b} are taken into account. For the upper bound of \bar{b} , which is one (according to (5.2b)), the coefficients of the polynomials given in (B.4) are identical to those derived in (4.24). For the lower bound of \bar{b} , it is replaced with its permissible lower bound $\kappa_{\bar{b}}$ within the coefficients obtained in (6.17a) and therefore, the polynomials W_{11} , W_{12} , W_{13} , and W_{14} with the coefficients

$$\begin{aligned}
 \beta_1 &= \alpha_2 \bar{k}_1, & \beta_2 &= \alpha_2 \bar{k}_2, & \beta_3 &= \frac{5\alpha_1}{3\kappa_{\bar{b}}}, & \beta_4 &= \frac{5}{2}\alpha_3 \bar{k}_1, \\
 \beta_5 &= \frac{5}{2}\alpha_3 \bar{k}_2 - \frac{\alpha_2}{\kappa_{\bar{b}}}, & \beta_6 &= \alpha_2, & \beta_7 &= \frac{2\alpha_4 \bar{k}_3}{\kappa_{\bar{b}}}, & \beta_8 &= \alpha_5 \bar{k}_1, \\
 \beta_9 &= \frac{5\alpha_6 \bar{k}_3}{\kappa_{\bar{b}}}, & \beta_{10} &= \frac{5}{2}\alpha_3, & \beta_{11} &= \frac{\alpha_4}{\kappa_{\bar{b}}}, & \beta_{12} &= \alpha_5 \bar{k}_2, \\
 \beta_{13} &= \frac{3\alpha_5 \bar{k}_3}{\kappa_{\bar{b}}}, & \beta_{14} &= \alpha_5
 \end{aligned} \tag{C.1}$$

are considered. Investigation of allowable value of $\kappa_{\bar{b}}$ is conducted later.

In contrast to the previous appendix, for the sets \mathcal{M}_1 , \mathcal{M}_2 , \mathcal{M}_3 , and \mathcal{M}_4 , $W_2(\boldsymbol{\vartheta})$ is easily realized as

$$W_{21}(\boldsymbol{\vartheta}) = -\overline{\beta_{15}}\vartheta_1^6\vartheta_3^2 + \overline{\beta_{16}}\vartheta_2^4\vartheta_3^4 - \overline{\beta_{17}}\vartheta_3^8, \tag{C.2a}$$

$$W_{22}(\boldsymbol{\vartheta}) = \overline{\beta_{15}}\vartheta_1^6\vartheta_3^2 + \overline{\beta_{16}}\vartheta_2^4\vartheta_3^4 - \overline{\beta_{17}}\vartheta_3^8, \tag{C.2b}$$

$$W_{23}(\boldsymbol{\vartheta}) = -\overline{\beta_{15}}\vartheta_1^6\vartheta_3^2 - \overline{\beta_{16}}\vartheta_2^4\vartheta_3^4 - \overline{\beta_{17}}\vartheta_3^8, \tag{C.2c}$$

$$W_{24}(\boldsymbol{\vartheta}) = -\overline{\beta_{15}}\vartheta_1^6\vartheta_3^2 + \overline{\beta_{16}}\vartheta_2^4\vartheta_3^4 + \overline{\beta_{17}}\vartheta_3^8, \tag{C.2d}$$

respectively, where the coefficients are given in (6.18). This is due to that the continuous twisting algorithm is recovered after a finite time in this approach. Based

C. Quadrant Analysis for the Lyapunov-based Saturated Continuous Twisting Algorithm

on the upper and lower bounds of $\frac{\bar{\delta}}{\mu}$ and \bar{b} , four polynomials for $W_2(\boldsymbol{\vartheta})$ in each octant are derived. It can be seen that thus far to guarantee that V and $W_1 + W_2$ are positive definite, four polynomials for the Lyapunov function and 16 polynomials for its time derivative need to be sum of squares at the same time. It is explained in the previous appendices how a sum-of-squares problem should be formulated such that the positive definiteness of the functions is ensured. In the following, another seven polynomials are introduced, which also need to be sum of squares in order to ensure that the control signal is confined to the saturation limits for $t \geq T$.

Due to that the functions \bar{a} , \bar{b} , and $\bar{\delta}$ play a role in computing the levels c_1 and c_2 , it is also required to make a transformation as

$$\frac{1}{\mu} \left(\rho + \frac{\bar{a}}{\bar{b}} \right) = \vartheta_4^2. \quad (\text{C.3})$$

As given in (6.20), the largest level c_1 is realized in the case $\zeta_3 = \frac{\rho}{\mu} + \bar{k}_1 [\zeta_1]^{\frac{1}{3}} + \bar{k}_2 [\zeta_2]^{\frac{1}{2}} - \frac{\bar{a}}{\mu\bar{b}}$ holds. Therein, the function $V(\boldsymbol{\zeta})$ is represented by $V_\rho \left(\zeta_1, \zeta_2, \frac{\bar{a}}{\mu\bar{b}} \right)$ as

$$\begin{aligned} V_\rho \left(\zeta_1, \zeta_2, \frac{\bar{a}}{\mu\bar{b}} \right) &= \alpha_1 |\zeta_1|^{\frac{5}{3}} + \alpha_2 \zeta_1 \zeta_2 + \alpha_3 |\zeta_2|^{\frac{5}{2}} + \alpha_4 \zeta_1 \left[\frac{\rho}{\mu} + \bar{k}_1 [\zeta_1]^{\frac{1}{3}} + \bar{k}_2 [\zeta_2]^{\frac{1}{2}} + \frac{\bar{a}}{\mu\bar{b}} \right]^2 \\ &\quad - \alpha_5 \zeta_2 \left(\frac{\rho}{\mu} + \bar{k}_1 [\zeta_1]^{\frac{1}{3}} + \bar{k}_2 [\zeta_2]^{\frac{1}{2}} + \frac{\bar{a}}{\mu\bar{b}} \right)^3 \\ &\quad + \alpha_6 \left| \frac{\rho}{\mu} + \bar{k}_1 [\zeta_1]^{\frac{1}{3}} + \bar{k}_2 [\zeta_2]^{\frac{1}{2}} + \frac{\bar{a}}{\mu\bar{b}} \right|^5. \end{aligned} \quad (\text{C.4})$$

Having made the transformation of ζ_1 , ζ_2 , and $\frac{\bar{a}}{\mu\bar{b}}$ as given in (B.2) and (C.3), $V_\rho(\vartheta_1, \vartheta_2, \vartheta_4)$ for the set \mathcal{M}_1 is written as

$$\begin{aligned} V_{\rho,1}(\vartheta_1, \vartheta_2, \vartheta_4) &= \alpha_1 \vartheta_1^{10} + \alpha_2 \vartheta_1^6 \vartheta_2^4 + \alpha_3 \vartheta_2^{10} + \alpha_4 \vartheta_1^6 (\bar{k}_1 \vartheta_1^2 + \bar{k}_2 \vartheta_2^2 + \vartheta_4^2)^2 \\ &\quad - \alpha_5 \vartheta_2^4 (\bar{k}_1 \vartheta_1^2 + \bar{k}_2 \vartheta_2^2 + \vartheta_4^2)^3 + \alpha_6 (\bar{k}_1 \vartheta_1^2 + \bar{k}_2 \vartheta_2^2 + \vartheta_4^2)^5. \end{aligned} \quad (\text{C.5})$$

In each of the sets \mathcal{M}_2 and \mathcal{M}_3 , two polynomials based on sign of $\frac{\rho}{\mu} + \bar{k}_1 [\zeta_1]^{\frac{1}{3}} + \bar{k}_2 [\zeta_2]^{\frac{1}{2}} + \frac{\bar{a}}{\mu\bar{b}}$ are derived. For the set \mathcal{M}_2 , they are

$$\begin{aligned} V_{\rho,21}(\vartheta_1, \vartheta_2, \vartheta_4) &= \alpha_1 \vartheta_1^{10} - \alpha_2 \vartheta_1^6 \vartheta_2^4 + \alpha_3 \vartheta_2^{10} - \alpha_4 \vartheta_1^6 (-\bar{k}_1 \vartheta_1^2 + \bar{k}_2 \vartheta_2^2 + \vartheta_4^2)^2 \\ &\quad - \alpha_5 \vartheta_2^4 (-\bar{k}_1 \vartheta_1^2 + \bar{k}_2 \vartheta_2^2 + \vartheta_4^2)^3 + \alpha_6 (\bar{k}_1 \vartheta_1^2 + \bar{k}_2 \vartheta_2^2 + \vartheta_4^2)^5, \end{aligned} \quad (\text{C.6a})$$

$$\begin{aligned} V_{\rho,22}(\vartheta_1, \vartheta_2, \vartheta_4) &= \alpha_1 \vartheta_1^{10} - \alpha_2 \vartheta_1^6 \vartheta_2^4 + \alpha_3 \vartheta_2^{10} + \alpha_4 \vartheta_1^6 (-\bar{k}_1 \vartheta_1^2 + \bar{k}_2 \vartheta_2^2 + \vartheta_4^2)^2 \\ &\quad - \alpha_5 \vartheta_2^4 (-\bar{k}_1 \vartheta_1^2 + \bar{k}_2 \vartheta_2^2 + \vartheta_4^2)^3 + \alpha_6 (\bar{k}_1 \vartheta_1^2 + \bar{k}_2 \vartheta_2^2 + \vartheta_4^2)^5. \end{aligned} \quad (\text{C.6b})$$

In the set \mathcal{M}_3 , they read as

$$V_{\rho,31}(\vartheta_1, \vartheta_2, \vartheta_4) = \alpha_1 \vartheta_1^{10} - \alpha_2 \vartheta_1^6 \vartheta_2^4 + \alpha_3 \vartheta_2^{10} + \alpha_4 \vartheta_1^6 (\bar{k}_1 \vartheta_1^2 - \bar{k}_2 \vartheta_2^2 + \vartheta_4^2)^2 \\ + \alpha_5 \vartheta_2^4 (\bar{k}_1 \vartheta_1^2 - \bar{k}_2 \vartheta_2^2 + \vartheta_4^2)^3 + \alpha_6 (\bar{k}_1 \vartheta_1^2 + \bar{k}_2 \vartheta_2^2 + \vartheta_4^2)^5, \quad (\text{C.7a})$$

$$V_{\rho,32}(\vartheta_1, \vartheta_2, \vartheta_4) = \alpha_1 \vartheta_1^{10} - \alpha_2 \vartheta_1^6 \vartheta_2^4 + \alpha_3 \vartheta_2^{10} - \alpha_4 \vartheta_1^6 (\bar{k}_1 \vartheta_1^2 - \bar{k}_2 \vartheta_2^2 + \vartheta_4^2)^2 \\ + \alpha_5 \vartheta_2^4 (\bar{k}_1 \vartheta_1^2 - \bar{k}_2 \vartheta_2^2 + \vartheta_4^2)^3 + \alpha_6 (\bar{k}_1 \vartheta_1^2 + \bar{k}_2 \vartheta_2^2 + \vartheta_4^2)^5. \quad (\text{C.7b})$$

It is noted that the set \mathcal{M}_4 is disregarded in this case since ζ_3 is greater than or equal to zero for $\zeta_1, \zeta_2 \geq 0$ and $u = \rho$ (the upper bound of $|\frac{\bar{a}}{\bar{b}}|$ is a portion of ρ as given in (6.6)). According to (6.8b), ϑ_4^2 is constrained as

$$\vartheta_4^2 \in \left[\frac{\rho - \frac{\bar{a}_M}{\bar{b}_m}}{\bar{\delta}_1 \left(\rho - \frac{\bar{a}_M}{\bar{b}_m} \right)}, \frac{\rho + \frac{\bar{a}_M}{\bar{b}_m}}{\bar{\delta}_2 \left(\rho + \frac{\bar{a}_M}{\bar{b}_m} \right)} \right] = \left[\frac{1}{\bar{\delta}_1}, \frac{1}{\bar{\delta}_2} \right]. \quad (\text{C.8})$$

The sum-of-squares problem is formulated here such that the polynomials

$$V_{\rho,1} - S_1 - S_2 - c_1, \quad V_{\rho,21} - S_1 - S_2 - c_1, \quad V_{\rho,22} - S_1 - S_2 - c_1, \\ V_{\rho,31} - S_1 - S_2 - c_1, \quad V_{\rho,32} - S_1 - S_2 - c_1 \quad (\text{C.9})$$

are sum of squares, where S_1 and S_2 are

$$S_1 = \left(\vartheta_4^2 - \frac{1}{\bar{\delta}_1} \right) G_1(\vartheta_1, \vartheta_2, \vartheta_4), \quad (\text{C.10a})$$

$$S_2 = \left(\frac{1}{\bar{\delta}_2} - \vartheta_4^2 \right) G_2(\vartheta_1, \vartheta_2, \vartheta_4). \quad (\text{C.10b})$$

Please note that G_1 and G_2 are sum of squares themselves.

It can be considered that $\max \left(\mu^{\frac{1}{3}} |\zeta_1|^{\frac{1}{3}}, \mu^{\frac{1}{2}} |\zeta_2|^{\frac{1}{2}} \right) \leq \gamma$ holds in the case the switching condition $\mu^{\frac{1}{3}} |\zeta_1|^{\frac{1}{3}} + \mu^{\frac{1}{2}} |\zeta_2|^{\frac{1}{2}} \leq \gamma$ is met. Therefore, the smallest level c_2 presented in (6.21) can be computed through maximizing $V_\gamma \left(\frac{\bar{a}}{\mu \bar{b}} \right)$ written as

$$V_\gamma \left(\frac{\bar{a}}{\mu \bar{b}} \right) = \alpha_1 \frac{\gamma^5}{\mu^{\frac{5}{3}}} + \alpha_2 \frac{\gamma^5}{\mu^2} [\zeta_1]^0 [\zeta_2]^0 + \alpha_3 \frac{\gamma^5}{\mu^{\frac{5}{2}}} + \alpha_4 \frac{\gamma^3}{\mu} [\zeta_1]^0 \left[\frac{\bar{a}}{\mu \bar{b}} \right]^2 \\ - \alpha_5 \frac{\gamma^2}{\mu} [\zeta_2]^0 \left(\frac{\bar{a}}{\mu \bar{b}} \right)^3 + \alpha_6 \left| \frac{\bar{a}}{\mu \bar{b}} \right|^5. \quad (\text{C.11})$$

It can be seen that by setting $\gamma = 0$, V_γ decreases to its lowest value and hence, the maximum upper bound of $\frac{\bar{a}_M}{\bar{b}_m}$ for the given saturation limit ρ is realized. Based on (6.6) and (6.8b), it is derived that

$$c_2 = \alpha_6 \left(\frac{\bar{a}_M}{\mu \bar{b}_m} \right)^5 \leq \alpha_6 \left(\frac{1}{4\bar{\delta}_2} \right)^5. \quad (\text{C.12})$$

C. Quadrant Analysis for the Lyapunov-based Saturated Continuous Twisting Algorithm

To guarantee that inequality (6.22) is satisfied, this constraint is also integrated into the sum-of-squares problem. Allowable values of $\bar{\delta}_1$ and $\bar{\delta}_2$ for different values of κ as well as permissible value of $\kappa_{\bar{b}}$ are investigated such that feasible solutions for the coefficients $\boldsymbol{\alpha}$ and coefficients of G_1 and G_2 are achieved. Table 6.1 is provided. Exemplarily, for $\rho = 10$ and $\frac{\bar{a}_M}{b_m} = 3.3$, having chosen the constants given in (6.9), the coefficients $\boldsymbol{\alpha}$ obtained using YALMIP [Löf04] and SEDUMI [Stu99] with $c_\Upsilon = 10^{-6}$, $\bar{\delta}_1 = 0.21$, $\bar{\delta}_2 = 0.09$, and $\kappa_{\bar{b}} = 0.76$ are

$$\begin{aligned} \alpha_1 &= 106.4, & \alpha_2 &= 16.75, & \alpha_3 &= 4.952, \\ \alpha_4 &= -1.551, & \alpha_5 &= 0.014, & \alpha_6 &= 0.001. \end{aligned} \tag{C.13}$$

It is noted that, as mentioned before, the small positive real constant c_Υ is assigned to ensure the positive definiteness of V and $W_1 + W_2$.

Bibliography

- [BB05] S. P. Bhat and D. S. Bernstein. “Geometric homogeneity with applications to finite-time stability.” In: *Mathematics of Control, Signals and Systems* 17.2 (June 2005), pp. 101–127. DOI: 10.1007/s00498-005-0151-x (cit. on p. 31).
- [BCB18] A. K. Behera, A. Chalanga, and B. Bandyopadhyay. “A new geometric proof of super-twisting control with actuator saturation.” In: *Automatica* 87 (2018), pp. 437–441. DOI: 10.1016/j.automatica.2017.09.015 (cit. on pp. 2, 33).
- [Ber+14] E. Bernuau et al. “On homogeneity and its application in sliding mode control.” In: *Journal of the Franklin Institute* 351.4 (2014), pp. 1866–1901. DOI: 10.1016/j.jfranklin.2014.01.007 (cit. on p. 22).
- [Cas+16a] I. Castillo et al. “Saturated super-twisting algorithm based on perturbation estimator.” In: *55th Conference on Decision and Control (CDC)*. Dec. 2016, pp. 7325–7328. DOI: 10.1109/CDC.2016.7799400 (cit. on pp. 2, 3, 15, 23, 24, 26, 28, 33, 35, 37, 38).
- [Cas+16b] I. Castillo et al. “Saturated super-Twisting algorithm: Lyapunov based approach.” In: *14th International Workshop on Variable Structure Systems (VSS)*. June 2016, pp. 269–273. DOI: 10.1109/VSS.2016.7506928 (cit. on pp. 2, 3, 15, 23, 25, 28, 33–36, 38, 74).
- [Cha+16] A. Chalanga et al. “Implementation of super-twisting control: super-twisting and higher order sliding-mode observer-based approaches.” In: *IEEE Transactions on Industrial Electronics* 63.6 (June 2016), pp. 3677–3685. DOI: 10.1109/TIE.2016.2523913 (cit. on p. 63).
- [DFL05] J. Davila, L. Fridman, and A. Levant. “Second-order sliding-mode observer for mechanical systems.” In: *IEEE Transactions on Automatic Control* 50.11 (Nov. 2005), pp. 1785–1789. DOI: 10.1109/TAC.2005.858636 (cit. on p. 43).
- [DL17] S. Ding and S. Li. “Second-order sliding mode controller design subject to mismatched term.” In: *Automatica* 77 (2017), pp. 388–392. DOI: 10.1016/j.automatica.2016.07.038 (cit. on p. 62).

- [EF10] A. Estrada and L. Fridman. “Quasi-continuous HOSM control for systems with unmatched perturbations.” In: *Automatica* 46.11 (2010), pp. 1916–1919. DOI: 10.1016/j.automatica.2010.07.002 (cit. on p. 62).
- [ES98] C. Edwards and S. Spurgeon. *Sliding mode control: theory and applications*. CRC Press, 1998 (cit. on p. 62).
- [FBF13] A. Ferreira de Loza, F. J. Bejarano, and L. Fridman. “Unmatched uncertainties compensation based on high-order sliding mode observation.” In: *International Journal of Robust and Nonlinear Control* 23.7 (2013), pp. 754–764. DOI: 10.1002/rnc.2795 (cit. on p. 62).
- [FR09] A. Ferrara and M. Rubagotti. “A sub-optimal second order sliding mode controller for systems with saturating actuators.” In: *IEEE Transactions on Automatic Control* 54.5 (May 2009), pp. 1082–1087. DOI: 10.1109/TAC.2008.2010992 (cit. on pp. 2, 15).
- [Gol+16] M. A. Golkani et al. “Observer-based saturated output feedback control using twisting algorithm.” In: *14th International Workshop on Variable Structure Systems (VSS)*. June 2016, pp. 246–250. DOI: 10.1109/VSS.2016.7506924 (cit. on p. 9).
- [Gol+18a] M. A. Golkani et al. “A novel saturated super-twisting algorithm.” In: *Systems & Control Letters* 119 (2018), pp. 52–56. DOI: 10.1016/j.sysconle.2018.07.001 (cit. on pp. 8, 16, 18).
- [Gol+18b] M. A. Golkani et al. “Saturated continuous twisting algorithm.” In: *15th International Workshop on Variable Structure Systems (VSS)*. July 2018, pp. 138–143. DOI: 10.1109/VSS.2018.8460449 (cit. on pp. 9, 48).
- [Gol+19] M. A. Golkani et al. “An anti-windup scheme for the super-twisting algorithm.” In: *58th Conference on Decision and Control (CDC)*. Dec. 2019, pp. 6947–6952 (cit. on p. 8).
- [Gol+20] M. A. Golkani et al. “Saturated feedback control using different higher-order sliding-mode algorithms.” In: *Variable-Structure Systems and Sliding-Mode Control: From Theory to Practice*. Vol. 271. Springer International Publishing, 2020, pp. 125–148. DOI: 10.1007/978-3-030-36621-6_4 (cit. on p. 9).
- [GSP14] D. Ginoya, P. D. Shendge, and S. B. Phadke. “Sliding mode control for mismatched uncertain systems using an extended disturbance observer.” In: *IEEE Transactions on Industrial Electronics* 61.4 (Apr. 2014), pp. 1983–1992. DOI: 10.1109/TIE.2013.2271597 (cit. on p. 62).
- [Hau83] M.L.J. Hautus. “Strong detectability and observers.” In: *Linear Algebra and its Applications* 50 (1983), pp. 353–368. DOI: 10.1016/0024-3795(83)90061-7 (cit. on p. 62).

-
- [Hip06] P. Hippe. *Windup in control: its effects and their prevention*. Springer Science & Business Media, 2006 (cit. on p. 2).
- [HKH87] R. Hanus, M. Kinnaert, and J.-L. Henrotte. “Conditioning technique, a general anti-windup and bumpless transfer method.” In: *Automatica* 23.6 (1987), pp. 729–739. DOI: 10.1016/0005-1098(87)90029-X (cit. on p. 2).
- [HLP52] G. H. Hardy, J. E. Littlewood, and G. Pólya. *Inequalities*. Cambridge university press, 1952 (cit. on p. 19).
- [KR16] S. Koch and M. Reichhartinger. “Observer-based sliding mode control of hydraulic cylinders in the presence of unknown load forces.” In: *e & i Elektrotechnik und Informationstechnik* 133.6 (Sept. 2016), pp. 253–260. DOI: 10.1007/s00502-016-0418-6 (cit. on p. 55).
- [Lev05] A. Levant. “Homogeneity approach to high-order sliding mode design.” In: *Automatica* 41.5 (2005), pp. 823–830. DOI: 10.1016/j.automatica.2004.11.029 (cit. on p. 22).
- [Lev10] A. Levant. “Chattering analysis.” In: *IEEE Transactions on Automatic Control* 55.6 (June 2010), pp. 1380–1389. DOI: 10.1109/TAC.2010.2041973 (cit. on p. 65).
- [Lev93] A. Levant. “Sliding order and sliding accuracy in sliding mode control.” In: *International journal of control* 58.6 (1993), pp. 1247–1263. DOI: 10.1080/00207179308923053 (cit. on pp. 1, 2, 4, 15, 80).
- [Lev98] A. Levant. “Robust exact differentiation via sliding mode technique.” In: *Automatica* 34.3 (1998), pp. 379–384. DOI: 10.1016/S0005-1098(97)00209-4 (cit. on pp. 43, 53, 64).
- [Li+17] S. Li et al. *Advances in Variable Structure Systems and Sliding Mode Control—Theory and Applications*. Vol. 115. Springer, 2017 (cit. on p. 1).
- [LL14] M. Livne and A. Levant. “Proper discretization of homogeneous differentiators.” In: *Automatica* 50.8 (2014), pp. 2007–2014. DOI: 10.1016/j.automatica.2014.05.028 (cit. on p. 67).
- [Löf04] J. Löfberg. “YALMIP : A toolbox for modeling and optimization in MATLAB.” In: *IEEE International Symposium on Computer Aided Control Systems Design (CACSD)*. Taipei, Taiwan, 2004, pp. 284–289. DOI: 10.1109/CACSD.2004.1393890 (cit. on pp. 77, 102).
- [MMF17] J. Mendoza-Avila, J. A. Moreno, and L. Fridman. “An idea for Lyapunov function design for arbitrary order continuous twisting algorithms.” In: *56th Conference on Decision and Control (CDC)*. Dec. 2017, pp. 5426–5431. DOI: 10.1109/CDC.2017.8264462 (cit. on pp. 58, 81).

- [MMF19] J. Mendoza-Avila, J. A. Moreno, and L. Fridman. “Continuous twisting algorithm for third order systems.” In: *IEEE Transactions on Automatic Control* (2019). DOI: 10.1109/TAC.2019.2932690 (cit. on pp. 58, 81).
- [MO12] J. A. Moreno and M. Osorio. “Strict Lyapunov functions for the super-twisting algorithm.” In: *IEEE Transactions on Automatic Control* 57.4 (Apr. 2012), pp. 1035–1040. DOI: 10.1109/TAC.2012.2186179 (cit. on pp. 17, 18).
- [Mor12] J. A. Moreno. “A Lyapunov approach to output feedback control using second-order sliding modes.” In: *IMA Journal of Mathematical Control and Information* (2012), pp. 291–308. DOI: 10.1093/imamci/dnr036 (cit. on p. 67).
- [Orl08] Y. V. Orlov. *Discontinuous systems: Lyapunov analysis and robust synthesis under uncertainty conditions*. Springer Science & Business Media, 2008 (cit. on p. 17).
- [Pap+13] A. Papachristodoulou et al. *SOSTOOLS: Sum of squares optimization toolbox for MATLAB*. Available from <http://www.eng.ox.ac.uk/control/sostools> and <http://www.cds.caltech.edu/sostools>. 2013. URL: <http://arxiv.org/abs/1310.4716> (cit. on pp. 21, 45, 94, 97).
- [PF19] U. Pérez-Ventura and L. Fridman. “When is it reasonable to implement the discontinuous sliding-mode controllers instead of the continuous ones? Frequency domain criteria.” In: *International Journal of Robust and Nonlinear Control* 29.3 (2019), pp. 810–828. DOI: 10.1002/rnc.4347 (cit. on p. 1).
- [Poz08] A. S. Poznyak. *Advanced Mathematical Tools for Control Engineers: Deterministic Techniques*. Vol. 1. Elsevier, 2008 (cit. on p. 18).
- [PP09] A. Polyakov and A. Poznyak. “Lyapunov function design for finite-time convergence analysis: “Twisting” controller for second-order sliding mode realization.” In: *Automatica* 45.2 (2009), pp. 444–448. DOI: 10.1016/j.automatica.2008.07.013 (cit. on p. 1).
- [RGH15] M. Reichhartinger, M. A. Golkani, and M. Horn. “Experimental evaluation of observer-based throttle valve control using super-twisting algorithm.” In: *14th European Control Conference (ECC)*. July 2015, pp. 2144–2149. DOI: 10.1109/ECC.2015.7330857 (cit. on p. 1).
- [SH17] R. Seeber and M. Horn. “Stability proof for a well-established super-twisting parameter setting.” In: *Automatica* 84 (2017), pp. 241–243. DOI: 10.1016/j.automatica.2017.07.002 (cit. on pp. 4, 31, 32).

- [SH19a] R. Seeber and M. Horn. “Guaranteeing disturbance rejection and control signal continuity for the saturated super-twisting algorithm.” In: *IEEE Control Systems Letters* 3.3 (2019), pp. 715–720. DOI: 10.1109/LCSYS.2019.2917054 (cit. on p. 3).
- [SH19b] R. Seeber and M. Horn. “Optimal tuning of the saturated super-twisting algorithm.” In: *18th European Control Conference (ECC)*. June 2019, pp. 3606–3612. DOI: 10.23919/ECC.2019.8796271 (cit. on pp. 3, 33).
- [SHF18] R. Seeber, M. Horn, and L. Fridman. “A Novel method to estimate the reaching time of the super-twisting algorithm.” In: *IEEE Transactions on Automatic Control* 63.12 (Dec. 2018), pp. 4301–4308. DOI: 10.1109/TAC.2018.2812789 (cit. on p. 80).
- [Sht+14] Y. Shtessel et al. *Sliding mode control and observation*. Springer, 2014 (cit. on pp. 1, 47, 80).
- [SM13] T. Sánchez and J. A. Moreno. “On a sign controller for the triple integrator.” In: *52nd Conference on Decision and Control (CDC)*. Dec. 2013, pp. 3566–3571. DOI: 10.1109/CDC.2013.6760431 (cit. on p. 81).
- [SM14] T. Sánchez and J. A. Moreno. “A constructive Lyapunov function design method for a class of homogeneous systems.” In: *53rd Conference on Decision and Control (CDC)*. Dec. 2014, pp. 5500–5505. DOI: 10.1109/CDC.2014.7040249 (cit. on pp. 22, 47).
- [SMF18] T. Sánchez, J. A. Moreno, and L. M. Fridman. “Output feedback continuous twisting algorithm.” In: *Automatica* 96 (2018), pp. 298–305. DOI: 10.1016/j.automatica.2018.06.049 (cit. on pp. 43, 69).
- [Stu99] Jos F. Sturm. “Using SeDuMi 1.02, A Matlab toolbox for optimization over symmetric cones.” In: *Optimization Methods and Software* 11.1-4 (1999), pp. 625–653. DOI: 10.1080/10556789908805766 (cit. on pp. 77, 102).
- [Tor+17] V. Torres-González et al. “Design of continuous twisting algorithm.” In: *Automatica* 80 (2017), pp. 119–126. DOI: 10.1016/j.automatica.2017.02.035 (cit. on pp. 1, 6, 43, 46, 47, 78, 81, 82, 84).
- [Wan+14] Y. Wang et al. “Continuous nonsingular terminal sliding mode control with anti-windup compensation.” In: *40th Annual Conference of the IEEE Industrial Electronics Society (IECON)*. Oct. 2014, pp. 109–113. DOI: 10.1109/IECON.2014.7048485 (cit. on p. 2).
- [Yan+14] J. Yang et al. “High-Order mismatched disturbance compensation for motion control systems via a continuous dynamic sliding-mode approach.” In: *IEEE Transactions on Industrial Informatics* 10.1 (Feb. 2014), pp. 604–614. DOI: 10.1109/TII.2013.2279232 (cit. on p. 62).

- [YLY13] J. Yang, S. Li, and X. Yu. “Sliding-mode control for systems with mismatched uncertainties via a disturbance observer.” In: *IEEE Transactions on Industrial Electronics* 60.1 (Jan. 2013), pp. 160–169. DOI: 10.1109/TIE.2012.2183841 (cit. on p. 62).